

STUDIES ON STEEL FIBRE REINFORCED LIGHT
WEIGHT AGGREGATE CONCRETE SUBJECTED TO
COLD OCEAN ENVIRONMENT

CENTRE FOR NEWFOUNDLAND STUDIES

**TOTAL OF 10 PAGES ONLY
MAY BE XEROXED**

(Without Author's Permission)

YRAJAM GHEORGHE MUSTE, M.Eng.



STUDIES ON STEEL FIBRE REINFORCED LIGHT
WEIGHT AGGREGATE CONCRETE SUBJECTED TO
COLD OCEAN ENVIRONMENT

By

Traian Gheorghe Muste, M. Eng.

A thesis submitted to the School of Graduate
Studies in partial fulfillment of the
requirements for the degree of
Master of Engineering

Faculty of Engineering and Applied Science
Memorial University of Newfoundland

August 1988

St. John's

Newfoundland

Canada



National Library
of Canada

Bibliothèque nationale
du Canada

Canadian Theses Service Service des thèses canadiennes

Ottawa, Canada
K1A 0N4

The author has granted an irrevocable non-exclusive licence allowing the National Library of Canada to reproduce, loan, distribute or sell copies of his/her thesis by any means and in any form or format, making this thesis available to interested persons.

The author retains ownership of the copyright in his/her thesis. Neither the thesis nor substantial extracts from it may be printed or otherwise reproduced without his/her permission.

L'auteur a accordé une licence irrévocable et non exclusive permettant à la Bibliothèque nationale du Canada de reproduire, prêter, distribuer ou vendre des copies de sa thèse de quelque manière et sous quelque forme que ce soit pour mettre des exemplaires de cette thèse à la disposition des personnes intéressées.

L'auteur conserve la propriété du droit d'auteur qui protège sa thèse. Ni la thèse ni des extraits substantiels de celle-ci ne doivent être imprimés ou autrement reproduits sans son autorisation.

ISBN 0-315-59239-7

Canada

In memory of my Father

ABSTRACT

The present research, triggered by the potential development of offshore oil exploitation off Newfoundland coast, concludes a part of a research programme, at Memorial University, St. John's, Nfld, Canada, in which the use of lightweight aggregate concrete (LAC) and steel fibres reinforced lightweight aggregate concrete (SFRLAC) as structural materials for potential Arctic and sub-Arctic structures was investigated. The work was financed from NSERC Grant # 31176.

The thesis starts with the literature review and introduction in Chapter 1, and consists of two main parts. The first one, Chapters 2 and 3, presents a few relevant rheological and hardened state properties of lightweight aggregate concrete (LAC) and steel fibre reinforced lightweight aggregate concrete (SFRLAC); also in Chapter 2, the composition of concrete was determined to meet the specifications, and steel fibres were added by a trial-and-error method to obtain the most suitable SFRLAC. The second part, Chapters 4 to 6, includes the results of the theoretical and experimental analysis of the behaviour of the LAC and SFRLAC plates subjected to static loading. In Chapter 4, the design of the plates, based on the available semi-empirical methods is presented; in addition, a finite element computer code used in this work is introduced, and its

predictions are compared with the experimental results in Chapter 6. The laboratory experimental work is presented in Chapters 2, 3, 5 and 6.

The behaviour of the plates with regard to deformation, strain, cracking pattern, ultimate capacity, and modes of failure is given in Chapter 6; the effect of varying the shear and flexural reinforcement on the behaviour of the plates was also investigated. The comparison of theoretical predictions, as described in Chapter 4, using the actual properties of the concrete and reinforcement, with the experimental results is also given.

Throughout the thesis, one main purpose was to assess the suitability of the LAC and SFRLAC to cold ocean environment (COE), simulated under laboratory conditions. Another main purpose of the work was to assess the shear capacity of the plates, and to improve it. The shear capacity is calculated, as presented in Chapters 4 and 6, according to conventional and modified conventional reinforced concrete theory. The fibres contribution to the behaviour of the plates was also investigated.

It is concluded in Chapter 7, that LAC, and especially SFRLAC, are suitable structural materials for Arctic and sub-Arctic offshore structures, possessing suitable structural behaviour.

ACKNOWLEDGEMENTS

Many thanks to Dr. F. A. Aldrich for a good advice. Thanks are due to Dr. M. G. Andrews and to Dr. R. M. Hopkins for their encouragement. Thanks to Dr. T. R. Chari for understanding.

Thanks are due to my supervisor, Dr. A. S. J. Swamidas for his understanding and continuous support throughout this program. Thanks to C. Jebaraj.

Thanks to Dr. D. B. Muggeridge for his attention and encouragement.

Special thanks are due to Calvin, Austin and Ron for their support in the laboratory work.

The author remembers his Mother and Brother for their permanent thankworthy support; special thanks for a special reader.

TABLE OF CONTENTS

	Page
ABSTRACT.....	ii
ACKNOWLEDGMENTS.....	iv
TABLE OF CONTENTS.....	v
LIST OF FIGURES.....	viii
LIST OF TABLES.....	xiii
NOTATION.....	xv
 Chapter 1. LITERATURE REVIEW AND INTRODUCTION.....	 1
1.1. Concrete for Marine and Offshore Applications.....	 1
1.2. Lightweight Aggregate Concrete for Marine and Offshore Applications.....	 3
1.2.1. Properties of Interest to the Designer.....	 4
1.2.2. Previous Projects.....	7
1.3. Arctic Concrete Offshore Structures.....	9
1.4. Materials and Durability.....	12
1.5. Steel Fiber Reinforced Concrete in Marine and Offshore Applications.....	 18
1.5.1. Introduction.....	18
1.5.2. General Properties.....	21
1.5.3. Mechanical Properties of SFRC and SFRM Exposed to Marine Environment...	 28
1.5.4. Mix Design of SFRC.....	29
1.5.5. Applications.....	32

1.6. The Need of the Present Research and Rationale of Investigations.....	35
Chapter 2. PRODUCTION OF LAC AND SFRLAC.....	38
2.1. Mix Proportioning Criteria.....	38
2.2. Materials.....	43
2.3. Method of Proportioning; Mixing.....	49
2.3.1. LAC.....	49
2.3.2. SFRLAC.....	54
2.4. Placing and Curing.....	58
Chapter 3. CHARACTERISTICS AND PROPERTIES OF LAC AND SFRLAC.....	68
3.1. Introduction.....	68
3.2. Unit Weight (Density).....	68
3.3. Compressive Strength.....	70
3.4. Modulus of Elasticity.....	79
3.5. Tensile Strength - Flexural Strength.....	82
3.6. Absorption.....	89
Chapter 4. THEORETICAL STUDY: LAC AND SFRLAC PLATES.....	107
4.1. Plate Design.....	107
4.2. Mathematical Modelling and Computer Code.....	137
Chapter 5. EXPERIMENTAL STUDY: LAC AND SFRLAC PLATES.....	169
5.1. Test Set-up.....	169
5.2. Instrumentation.....	170
5.3. Methodology.....	171

Chapter 6. RESULTS: LAC AND SFRLAC PLATES.....	180
6.1. Introduction.....	180
6.2. Experimental Results and Discussions.....	182
6.3. Computation of the Ultimate Loading of the Plates.....	193
Chapter 7. CONCLUSIONS AND RECOMMENDATIONS.....	250
REFERENCES.....	258
APPENDIX A. Method of Proportionig LAC.....	270
APPENDIX B. Post-cracking Tensile Stress of SFRLAC...	279
APPENDIX C. Fibres Contribution to Flexural Resistance of the Plates.....	283
APPENDIX D. Calculation of the Punching Shear Strength of the Plates.....	288
APPENDIX E. Calculation of the Flexural and Shear Strengths of the Plates.....	298
APPENDIX F. Conversion Factors from English to SI Units.....	303

LIST OF FIGURES

		Page
Fig. 2.2-1	Granulometric curves of lightweight aggregates and sand	65
Fig. 2.3-1	Granulometric curves of concrete aggregates and domain of aggregates as per ASTM C 330	66
Fig. 2.3-2	Inverted slump cone test results	67
Fig. 3.2-1	The relationship between compressive strength and unit weight (density)	101
Fig. 3.3-1	Variation of compressive strength of concrete cylinders with age	102
Fig. 3.3-2	Compressive strength vs. axial strain - typical stress-strain curves for SFRLAC and LAC cylinders	103
Fig. 3.4-1	Dependence of modulus of elasticity on the age of the cylinder	104
Fig. 3.5-1	Representative LAC load-central deflection Curves obtained in flexural test	105
Fig. 3.5-2	Representative SFRLAC load-central deflection curves obtained in flexural test	106
Fig. 4.1-1	Bottom reinforcement - 10 #10 bars/m	153
Fig. 4.1-2	Top reinforcement	154
Fig. 4.1-3	Assumed yield-line mechanism	155
Fig. 4.1-4	Bottom plate reinforcement - 6 #10 bars/unit width	156
Fig. 4.1-5	Shear reinforcement: vertical stirrups	157
Fig. 4.1-6	Shear reinforcement: single & double shear head	158
Fig. 4.1-7	Computational details for shear	

	resistance	159
Fig. 4.1-8	Strain & stress distribution at failure (Reference 91)	160
Fig. 4.1-9	Failure model for punching failure in slabs (Reference 91)	161
Fig. 4.2-1	(a) Quadric solid three-dimensional element, (b) and (c) the corresponding degenerate shell element (Reference 97)	162
Fig. 4.2-2	Coordinate systems: (a) nodal and curvilinear systems, (b) local system of axes (Reference 97)	163
Fig. 4.2-3	Displacements of a point on the "normal" at node k (Reference 97)	164
Fig. 4.2-4	Nodal configuration of the three-quadric shell elements (Reference 97)	164
Fig. 4.2-5	One-dimensional representation of the concrete constitutive model (Reference 97)	165
Fig. 4.2-6	Two-dimensional stress space representation of the concrete constitutive model (Reference 97)	166
Fig. 4.2-7	Loading and unloading behaviour of cracked concrete illustrating tension stiffening behaviour (Reference 97)	166
Fig. 4.2-8	Overall structure of program CONSHELL	167-168
Fig. 5.1-1	Test set up	174
Fig. 5.1-2	(a) & (b) Test set up	175
Fig. 5.2-1	Plate instrumentation: concrete strain gage locations in plates P4, P5, FP4 and FP5	176
Fig. 5.2-2	Plate instrumentation: concrete strain gage locations in plates P6, P7, FP6 and FP7	177
Fig. 5.2-3	Steel strain gage locations	178
Fig. 5.3-1	Stress-strain curve for steel reinforcing bar #10	179

Fig. 5.3-2	Stress-strain curve for steel reinforcing bar 6mm diameter	179
Fig. 6.2-1	Load-deflection curves	208
Fig. 6.2-2	Bottom plate concrete strains vs. load	209
Fig. 6.2-3	Bottom plate concrete strains vs. load	210
Fig. 6.2-4	Top plate concrete strains vs. load	211
Fig. 6.2-5	Top plate concrete strains vs. load	212
Fig. 6.2-6	Flexural steel strains vs. load	213
Fig. 6.2-7	Flexural steel strains vs. load	214
Fig. 6.2-8	Shear steel strains vs. load	215
Fig. 6.2-9	Load-central deflection curves	216
Fig. 6.2-10	Load-central deflection curves	217
Fig. 6.2-11	Load-central deflection curves	218
Fig. 6.2-12	Load-central deflection curves	219
Fig. 6.2-13	(a) Failure pattern P4: top surface (b) failure pattern P4: bottom surface	220
Fig. 6.2-14	(a) Failure pattern P5: top surface (b) failure pattern P5: bottom surface	221
Fig. 6.2-15	(a) Failure pattern P6: bottom surface (b) plate P6: bottom surface, failure detail	222
Fig. 6.2-16	(a) Failure pattern P6: top surface (b) failure pattern P6: bottom surface	223
Fig. 6.2-17	Failure pattern FP4: bottom surface	224
Fig. 6.2-18	Failure pattern FP6: bottom surface	224
Fig. 6.2-19	(a) Failure pattern FP5: top surface (b) failure pattern FP5: bottom surface	225
Fig. 6.2-20	(a) Failure pattern FP7: top surface (b) failure pattern FP7: bottom surface	226
Fig. 6.2-21	Plate P5; bottom surface, failure detail	227

Fig. 6.2-22	Plate P5: concrete surface exposed to coe	227
Fig. 6.2-23	Plate FP5: bottom surface, failure detail	228
Fig. 6.2-24	Plate FP6: bottom surface, failure detail	228
Fig. 6.2-25	Plate P7: bottom surface, failure detail	229
Fig. 6.2-26	Plate FP6: bottom surface, failure detail	229
Fig. 6.2-27	Plate without fibres: punching cone	230
Fig. 6.2-28	Plate with fibres: punching cone	230
Fig. 6.2-29	(1) Plate FP7: before cracking (2) plate FP7: loading step no. 8	231
Fig. 6.2-29	(3) Plate FP7: loading step no. 9 (4) Plate FP7: loading step no. 10	232
Fig. 6.2-29	(5) Plate FP7: loading step no. 11 (6) Plate FP7: loading step no. 12	233
Fig. 6.2-29	(7) Plate FP7: loading step no. 13 (8) Plate FP7: loading step no. 14	234
Fig. 6.2-29	(9) Plate FP7: loading step no. 15 (10) Plate FP7: loading step no. 16	235
Fig. 6.2-29	(11) Plate FP7: loading step no. 17 (12) Plate FP7: loading step no. 18	236
Fig. 6.2-29	(13) Plate FP7: loading step no. 19 (14) Plate FP7: loading step no. 20	237
Fig. 6.2-29	(15) Plate FP7: loading step no. 21 (16) Plate FP7: loading step no. 22	238
Fig. 6.2-29	(17) Plate FP7: loading step no. 23 (18) Plate FP7: loading step no. 24	239
Fig. 6.2-29	(19) Plate FP7: loading step no. 25 (20) Plate FP7: loading step no. 26	240
Fig. 6.2-29	(21) Plate FP7: loading step no. 28 (22) Plate FP7: loading step no. 29	241
Fig. 6.2-29	(23) Plate FP7: loading step no. 36 (24) Plate FP7: loading step no. 37	242
Fig. 6.2-29	(25) Plate FP7: loading step no. 38 (26) Plate FP7: loading step no. 39	243

Fig. 6.2-29	(27) Plate FP7: loading step no. 40	
	(28) Plate FP7: loading step no. 41	244
Fig. 6.2-29	(29) Plate FP7: loading step no. 42	
	(30) Plate FP7: loading step no. 43	245
Fig. 6.2-29	(31) Plate FP7: loading step no. 44	246
Fig. 6.2-30	Failure load variation with the compressive strength	247
Fig. 6.3-1	Finite element mesh (one-quarter of the plate)	248
Fig. 6.3-2	FEM predicted vs. Experimental load- deflection curves - P4	249
Fig. B-1	Graphic interpretation of Equation B-5	282

LIST OF TABLES

		Page
Table 2.2-1	Grading of course and fine aggregates	62
Table 2.2-2	Physical properties of course lightweight aggregates	63
Table 2.2-3	Physical properties of fine aggregates	64
Table 3.3-1	Compressive strengths of lightweight aggregate and steel fibre reinforced lightweight aggregate concretes	92
Table 3.3-2	Comparison of strengths of LAC and SFRLAC	92
Table 3.3-3	Comparison of strengths of LAC and SFRLAC	93
Table 3.3-4	Comparison of strengths of LAC and SFRLAC	93
Table 3.3-5	Influence of improper curing on the compressive strength of LAC	94
Table 3.4-1	Modulus of elasticity of LAC and SFRLAC	95
Table 3.4-2	Comparison of E values of LAC and SFRLAC	95
Table 3.4-3	Comparison of E values of LAC and SFRLAC	96
Table 3.4-4	Dependence of E on the compressive strength	96
Table 3.4-5	Computed E values	97
Table 3.4-6	Computed E values as a function of age	98
Table 3.5-1	Modulus of rupture of LAC and SFRLAC	99
Table 3.5-2	Flexural loads of SFRLAC beams	99
Table 3.5-3	Flexural loads of SFRLAC beams	100
Table 3.5-4	Modulus of rupture of LAC at higher rate of loading	100
Table 4.1-1	Predicted ultimate flexural and punching shear loads of LAC and SFRLAC plates	153

Table 4.1-2	Predicted ultimate punching shear strengths of LAC and SFRLAC plates	154
Table 6.1-1	Synopsis of experimental results	201
Table 6.1-2	Properties of concrete used for plates	202
Table 6.2-1	Measured displacements, loads and strains	203
Table 6.2-2	Details of measured loads and strains	204
Table 6.2-3	Measured loads, deflections and strains at failure	205
Table 6.2-4	Salient results obtained from experiments	206
Table 6.3-1	(a) Theoretical predictions using measured maximum steel strains (b) Theoretical predictions using measured average steel strains	207
Table 6.3-2	Computed punching strength using available methods	208
Table 6.3-3	Comparison of experimental and finite element analytical values	209

NOTATION

NOTE: The notations are listed in alphabetic order.

a, L	=	free span of the plates, mm
a_f	=	the fibre cross-sectional area
ACI	=	American Concrete Institute
AEA	=	Air-entraining agent
API	=	American Petroleum Institute
A_s	=	flexural tension reinforcement area per unit width of plate, mm ²
aspect ratio	=	individual fibre length to diameter ratio = L_f/d_f
ASTM	=	American Society for Testing and Materials
b	=	the unit width of the plate, mm
BB	=	main structural unit of a CIDS
B, c	=	diameter of the loaded area, mm
BOSS	=	Behaviour of Sea Structures
b_0	=	pseudo-critical perimeter situated at $d/2$ from the loaded area, mm
b_1	=	average width of the specimen, mm
BS	=	British Standard
b_2	=	the width of the patch load; in this case, the equivalent width of the patch load, $b_2=13.3$ cm
c_1^i, c_2^i	=	pseudo-critical perimeters, mm
CIDS	=	Concrete Island Drilling System
COE	=	Cold Ocean Environment

CRI	=	Caisson Retained Island
C ₃ A	=	tricalcium aluminate
d	=	effective depth to centroid of tensile reinforcement, mm
d ₁	=	average depth of the specimen, mm
DC	=	Dense Concrete (Normal Weight Concrete)
DnV	=	Det Norske Veritas
DOF	=	degree(s) of freedom
DSB	=	Deck Storage Barges
E	=	Static Modulus of Elasticity (Young's Modulus of Elasticity), MPa (psi)
E _C	=	Concrete Static Modulus of Elasticity (Young's Modulus of Elasticity), MPa (psi)
EEC	=	European Economic Community
E _t	=	modulus of elasticity at t days of age, MPa (psi)
E ₃₀	=	modulus of elasticity at 30 days, MPa (psi)
F _C	=	resultant of the compressive stresses in concrete, N or kN
f _{cts} , f' _t	=	splitting tensile strength of concrete, MPa (psi)
f _{cu}	=	cube strength of concrete, MPa (psi)
f' _C	=	concrete cylinder compressive strength at t days of age, MPa (psi)
FEM	=	Finite Element Method
FDM	=	Finite Difference Method
F _{ft}	=	resultant of the tensile force due to the fibres, N or kN
FIP	=	Federation International de la Precontrainte
FPI	=	SFRLAC plate # i

FRC	=	Fibre Reinforced Concrete
FRLAC	=	Fibre Reinforced Lightweight Aggregate Concrete
f_s	=	yield stress of the steel reinforcement, MPa (psi)
F_{st}	=	resultant of the tensile force in flexural tension reinforcement bars, N or kN
f_{30}	=	concrete cylinder compressive strength at 30 days, MPa (psi)
G	=	shear modulus of elasticity, MPa (psi)
g	=	9.807 m/s ² , gravity acceleration
GBS	=	Gravity Based Structure
GCS	=	Global Coordinate System
h	=	overall depth of the plate, mm
h_2	=	height of the dropped weight, m or mm
ISAT	=	Initial Surface Absorption Test
ISCT	=	Inverted Slump Cone Test
k_2	=	depth of centroid of compression block, mm
Kg/m^3	=	Kilograms/cubic metre
l	=	span of the beam, mm
LA	=	Lightweight Aggregate
LABE	=	Laboratory environment
LAC	=	Lightweight Aggregate Concrete
Lbs/ft^3	=	pounds/cubic feet
LC	=	Lightweight Concrete
l_c	=	critical length of fibre, mm
l_f, d_f	=	length, diameter of the fibre, mm
LNG	=	Liquefied Natural Gas

LPG	= Liquefied Petroleum Gas
LVDT	= linear voltage displacement transducer
M, m_o	= yield moment per unit width due to the applied loading, Nm
m	= yield moment per unit width due to self weight of the plate, Nm
m'	= negative bending moment per unit width, Nm
MAI	= Mobile Arctic Island
MB	= Mud Base
MEL-lite	= trade-name of an expanded shale light-weight aggregate
MOR, R, R_b	= modulus of rupture, MPa (psi)
M_T	= total yield moment per unit width, Nm
MUN	= Memorial University of Newfoundland
NSERC	= Natural Sciences and Engineering Research Council
OMAE	= Offshore Mechanics and Arctic Engineering
OTC	= Offshore Technology Conference
p	= the fibre perimeter
pcf	= pounds per cubic foot
pH	= hydrogen power
P_i	= LAC plate # i
psi	= pounds per square inch
P_u, P	= maximum (collapse) load, N or kN
P_u', V_f	= shear strength provided by fibres, N or kN
q	= uniformly distributed self weight (assumed density = 1765.8 Kg/m^3), N/m^2
SF	= Steel Fibres
SFRC	= Steel Fibre Reinforced Concrete

SFRLAC	= Steel Fibre Reinforced Lightweight Aggregate Concrete
SFRM	= Steel Fibre Reinforced Mortar
SHADS	= Sonat Hybrid Arctic Drilling Structure
SSD	= surface-saturated-dry
T, I	= cross-section shape of the structural elements
TLP	= Tension Leg Platform
UK	= United Kingdom
USA	= United States of America
V, V_r	= total shear resistance, N or kN
V_c	= concrete shear resistance or factored shear resistance, N or kN
V_{calc}^i, V_{calc}	= calculated ultimate shear capacities, N or kN
V_{cu1}	= concrete shear resistance, failure surface 1, Fig. 4.1-7, N or kN
V_{cu2}	= concrete shear resistance, failure surface 2, Fig. 4.1-7, N or kN
V_{f1}	= volume fraction of fibres
V_{flex}	= ultimate flexural capacity determined from yield line analysis, N or kN
V_s	= shear steel resistance or factored shear resistance, N or kN
V_u	= ultimate shear capacity, N or kN
W	= available weight in laboratory, Kg
w	= vertical deflection, mm
W-C	= Water/Cement Ratio
W_e	= equivalent static loading, N
x	= depth of the compressive block, mm

γ_c	=	air-dry mass density, Kg/m ³
η_o	=	orientation factor
η_l	=	length correction factor
η_b	=	bond efficiency factor
τ	=	bond strength between concrete and fibre or interfacial bond strength, MPa (psi)
σ_{cu}	=	ultimate strength in tension of SFRLAC or post-cracking tensile strength of SFRLAC, MPa (psi)
σ_f	=	the strength of the fibres
σ_m	=	flexural strength of LAC
ϵ_{cu}	=	strain in concrete at failure
ϵ_o	=	strain in extreme fiber of elastic uncracked tension zone
$\frac{\sigma}{f_c}$	=	ratio of flexural tension reinforcement
μ_s	=	coefficient, see page 121
f_c	=	concrete tensile strength, MPa (psi)
β_c	=	ratio of the long side to short side of the concentrated load or reaction area, mm
λ	=	factor to account for low density concrete
ϕ_c	=	resistance factor for concrete
ϕ_s	=	resistance factor for reinforcing bars
θ	=	angle made by the failure surface with the horizontal plane
u	=	element field displacement matrix
N	=	element shape function matrix
d	=	element vector variables
e	=	strain vector
B	=	strain matrix

\underline{S}	= stress matrix
\underline{D}	= general elasticity matrix
\underline{e}_0	= the initial strain vector, e. g. generated by temperature variations
\underline{K}_e	= element stiffness matrix
\underline{f}_e	= internal force vector

CHAPTER 1: LITERATURE REVIEW AND INTRODUCTION

1.1. Concrete for Marine and Offshore Applications

Pozzolanic cement mortars and concretes have been used in marine civil engineering works since Roman times for harbour works and breakwaters. The rowing boat, built in 1848 by Lambot, is considered the first reinforced concrete structure - the prototype of ferroceement which is widely used nowadays for yachts and small boats [1]. During the First World War, large seagoing reinforced concrete vessels were built in USA, some of which remain in use as breakwaters up to this day, and accentuate the fact that well made concrete structures are lasting. Cast in situ concrete was largely used for coastal and harbour engineering applications, such as quays, sea-walls, and groins, as well as large precast units, e.g. dolos and hammer-heads used for breakwater systems [1, 2, 3].

Beginning with 1920's, platforms made of cast in situ concrete on driven concrete piles were used for oil production from Lake Maracaibo, Venezuela, in up to 40 m of water depth.

Prestressed concrete barges were constructed in Germany, during 1943, in the Phillipines during 1950's and in Hawaii during 1960. Later on, large rectangular prestressed concrete boxes have been

constructed to form seagoing barges for small factories or refineries, or to sustain LNG steel containers [4]. Kronen et al. [5] gave possible applications of concrete in the offshore industry such as offshore floating or submerged containers for storage of LPG and LNG.

In 1960-70's, the concrete gravity based structures (GBS) for oil and gas exploitation, in the North Sea, marked an important development regarding the offshore structures. They were selected in preference to the tubular steel "jacket" structures based on a few decisive considerations, viz., i) concrete was cheap and if properly constructed, was durable; ii) the required large, spread foundations were used as storage tanks for oil; iii) new concrete technologies such as slipforming were available; and iv) only a short time of calm weather was required to install the structures in position.

Up to the present moment, the offshore concrete structures could be classified into two generations. The first generation is made up by the gravity based structures (GBS), as those in the North Sea. The second generation, not so well exemplified, most of them being just in the project condition, includes: i) articulated compliant structures, which deflect under wave loading ; ii) sub-sea structures -fully submerged, thereby averting the effects of wave forces and ocean currents [6]; iii) floating structures - with improved hydrodynamic behaviour and

reduced risk of corrosion and fatigue [4, 7] - as those considered for the Grand Banks of Newfoundland [4] and iv) hybrid steel-concrete structures, such as the steel framed tower hinged to a concrete oil storage caisson [8, 9] or concrete TLP in water depth up to 1000 meters [10].

It is possible that theoretical developments, accumulated real life experiences, future improvements and development of concrete having new properties, such as microsilica concrete [11], would open up a new era in concrete offshore structures.

1.2. Lightweight Aggregate Concrete for Marine and Offshore Applications

The availability of lightweight aggregates (LA), natural and artificial, and the properties of the resulting concretes (LAC) have attracted the designers' attention for quite a long time. Some of them, of interest to the present work, are presented in section 1.2.1. Based on well-grounded experimental studies as well as on theoretical principles of computation, LAC has been employed in offshore applications, proving that it is a reliable and trustworthy structural material: relevant applications are shown in section 1.2.2.

1.2.1. Properties of Interest to the Designer

The main reason for the use of lightweight aggregate concrete (LAC), from the designer's point of view, is the reduction in the self weight of the structure, its use being governed first by economic considerations.

As its name implies, lightweight concrete is a concrete with a density - usually between 800.0 and 2000.0 Kg/m^3 - lower than the normal weight concrete [dense concrete (DC)] which ranges from 2200.0 to 2600.0 Kg/m^3 (140.0-160.0 lb/ft^3), and having a thermal insulation and fire resistance better than DC [12]. It can be further subdivided into structural, structural insulating, and insulating types as its density lies between 1600.0 and 2000.0 Kg/m^3 , between 800.0 and 1600.0 Kg/m^3 , and less than 800.0 Kg/m^3 , respectively.

The low density of lightweight aggregate concrete (LAC) - LAC unit weight is about 75 percent of the unit weight of the DC in air and 55 percent in water - is advantageous for float-out operations of a floating or immersed structure or for the buoyancy of the structures in shallow waters.

Three main methods of producing LC are known, the density of the resulting concretes being decreased by the presence of voids, which also reduce the concrete strength. However, high strength

durable concrete, as required by marine and ocean environments, was obtained with a careful mix design using high cement contents, over 400.0 Kg/m^3 [13] or 440.0 Kg/m^3 [3], added to the mechanically weak LA. The concrete strength is likely to increase with time due to the presence of "water release" phenomenon. This phenomenon, also termed as "internal curing" [14], is significant when using lightweight fine aggregates because of their pozzolanic property [3]. The minimum 28-days compressive strength is recommended to be between 30.0 to 45.0 MPa, depending on the exposure zone [3]; ACI [13] recommends 35.0 MPa for compressive strength and around 0.4 for the maximum W-C ratio.

The behaviour of the concrete varies when subjected to different load types: long-term and fluctuating, fatigue inducing and sustained, of infinite duration. When LAC is subjected to long-term and fluctuating loads, there are no significant differences between LAC and DC, if the loads are of low-frequency type. When LAC is subjected to sustained loading of indefinite duration, LAC strength decreases to about 70 percent of the strength reached for short-term loads, whereas for DC it is over 80 percent [3]. The same figures are also reported by FIP, based on a reduced number of tests [15].

The possible collision with ships, flotsam, ice, and icebergs requires additional tension and shear reinforcement and in-plane

prestressing [1]. Due to its low value of Young's modulus, high shrinkage and creep, losses in prestressing forces are larger in LAC than in DC at the same stress level. Therefore, ACI suggests the additional use of unstressed tendons and unbounded tendons to increase the energy absorption in the post-elastic range [3]. The impact resistance can be further improved using protective coverings - as steel or concrete grids - and energy absorbing materials such as LAC [13], steel fiber reinforced lightweight aggregate concrete (SFRLAC), timber rubbing stakes, flexible dolphins or resilient fenders [1, 16].

The mechanical performance of LAC subjected to temperature changes is better than that of DC; LAC has better and higher insulation capacity compared with that of the DC. This property makes LAC suitable for LNG carriers and for cold weather concreting [3]. The LAC freeze-thaw resistance is usually good if air entrainment is provided - according to Fagerlund [18]. Tachibana et al. [17] recommended 45 percent or less concrete saturation for LAC (reached when the initial aggregate moisture content is less than 5 percent) or non-air-entrained concrete using oven-dry aggregates for freeze-thaw resistance.

Different opinions exist among designers and researchers regarding the use of LAC instead of DC, both for on- and offshore applications, mainly because of the LAC low tensile strength, low modulus of elasticity and low bond strength. To

overcome these deficiencies steel reinforcement, prestressing, polymer additions and fibres are used together with good detailing and good construction practice. In spite of these differing opinions, published data show that LAC is suitable for many structural applications, including prestressed concrete, offshore [19, 20] and in particular, Arctic offshore structures [7, 21].

1.2.2. Previous Projects

Reinforced expanded shale aggregate concrete was used for ship and barge construction during the First World War [22]. In 1919 a 7500.0 tonnes tanker was built; two completed studies, first one after thirty-four years [3], and the second one after sixty-one years [14], proved the assumed durable concrete behaviour in sea-water. During the Second World War, vessels manufactured with lightweight aggregate concrete (LAC) and normal weight aggregate concrete (DC) were built in USA and UK. Three types of lightweight aggregates - Haydite, Rocklite, Nodulite - with a high cement content (about 530 Kg/m^3) were used (plus a retarding admixture) for the vessels. The principal characteristics of LA, typical mix designs and concrete engineering properties are described in Reference 3. The US Marine Commission outlined that the hulls of these ships seemed to be completely watertight with good riding qualities and little vibrations, with cool and acceptable interiors even after long service [3].

To increase the buoyancy of DC structures, LAC pontoons were built at most marinas. The used aggregates ranged from polystyrene expanded beads [23, 24] and perlite aggregate to expanded-shale aggregate. At Port Credit, Ontario, the floating-deck system was assembled using LAC post-tensioned cruciform units. This Haydite lightweight aggregate air-entrained concrete had a compressive strength of 28.0 MPa and a density of 1850.0 to 1950.0 Kg/m³ [3]. An economical structural solution was adopted for a prestressed concrete floating dry dock at Genoa, Italy [25], using a caisson structure of prestressed lightweight concrete, that encased a steel space frame.

Because of the low modulus of elasticity of LAC, which provides increased deformation capacity and eventually better absorption energy, it was decided to use LAC to fend away the impacts resulting from ships, ice, or flotsam colliding with piers, wharves, or other marine structures, e.g. the prestressed LAC fender piles for Sacramento River Bridge, California [3]. Jensen [26] recommended lightweight concrete covers for the spherical domes of the submerged offshore structures for impact resistance.

The various studies mentioned above concluded that LAC is economically preferable as a structural material instead of DC because of the reduced weight of the structure and possible savings in reinforcement costs, especially when the live load is small in comparison with the total weight of the structure; for

the particular project design at hand, an overall economic review would decide what kind of concrete should be used. On a volume for volume basis, the LAC can be more expensive than DC; Reference 24 points out that the mass savings, the improved thermal and fire resistance would be the primary factors that would influence LAC use instead of DC.

1.3. Arctic Concrete Offshore Structures

Although the concrete platforms in the North Sea are milestones in offshore oil exploitation and good offshore engineering practice for temperate and sub-Arctic offshore conditions, the Arctic environment requires structures with distinct engineering properties and characteristics [27].

The first Arctic concrete structures are considered to be the river bridge piers in the northern parts of Europe, Asia, North America, and the piers and breakwaters of harbors located within the Arctic Circle. Up to forty lighthouses were built in the Baltic Sea during the last forty years, and many Canadian lighthouses were constructed in the St. Lawrence Waterway since the turn of this century [28].

The Caisson-Retained Island (CRI), was developed as a suitable concept for the Arctic continental shelf; CRI is composed of a steel or concrete caisson made up of prefabricated units linked

together to form the receiving container for the infill. Tarsiut Caisson Retained Island, placed in 70.0 feet of water and completed in one construction season, is considered the first Arctic concrete offshore structure [29, 30]. Tarsiut CRI was constructed by Dillingham Corporation of Canada using semi-lightweight concrete (fly ash, herculite, pozzolith, air entrainment and super-plasticizer) and it required a concrete mix with a density of 1950.0 Kg/m³. The final reinforced concrete density was 2260.0 Kg/m³ with a 28-day compressive strength of about 40.0 MPa.

The gravity-base caisson concept was used for the completion of a few structures such as SSDC-1 [30], the Mobile Arctic Island (MAI), Gulf Canada's Molikpaq (MAC) and Texaco's Concrete Gravity Structures for its Schwedeneck-Ost-See in the Baltic Sea [30, 31]. For offshore drilling, Global Marine Development Inc. adopted a hybrid concrete steel structure, the Concrete Island Drilling System (CIDS) - named the Glomar Beaufort Sea 1 (GBS-1) [32]. The CIDS features a modular design: the Brick (BB44), two Deck Storage Barges (DSB) and the Mud Base (MB). These units are independently constructed and finally assembled to form the CIDS. The CIDS system may have one or more BRICKS as required by the design. A special combination of DC and LAC was selected over steel as structural material because of its advantages: great self weight, durability, less prone to progressive damage, more rigid than steel and cheap when compared with reinforced

steel structures. The external wall and the "Honeycomb" structure were made of LAC with a design compressive strength of 45.0 MPa. Additives were used to enhance the concrete fluidity, corrosion resistance, freeze-thaw resistance and concrete strength. The shear walls and the internal wall were cast using DC with a compressive strength of 55.2 MPa.

Knudsen et al. [33] proposed a possible concrete GBS for the Southern Bering Sea, particularly for the Navarin Basin, known for its poor soil conditions similar in many aspects to the soil in the Norwegian Trench area of the North Sea. The conceptual design was similar to a CONDEEP 3/19 platform; the 120 m high shafts were made of vertically prestressed LAC, featuring 50 degrees angle ice breaking cones on each shaft. LAC was chosen as structural material because the required structural sizes were reduced, increasing the payload capacity during tow to the field by approximately 10,000 tonnes and because of strength, construction method and cost analysis.

A second generation mobile Arctic drilling platform for exploration or production, the Sonat Hybrid Arctic Drilling Structure (SHADS), was proposed by Sonat Offshore Drilling [34]. The design used the optimum properties of steel and concrete: the ice wall midsection and the internal bulkheads were made of concrete, considered as the best material to resist and safely distribute high local ice loads; the ice wall was coated with

steel skin plates while the decks, central core and the base were made of steel.

General guidances for the design and construction of the Arctic and sub-Arctic structures is presented in API Bulletin 2N [35], while detailed analysis and design of concrete gravity structures in ice environments are provided by the ACI Report 357.R-84 [13] and ACI 318-83 Standard [36].

1.4. Materials and Durability

Cement type I, II, III corresponding to ASTM C 150 are considered satisfactory by most authorities for use in marine environment, while ACI 318 [36] recommends the use of Types IP (MS) or IS (MS); the C_3A minimum and maximum allowable content are debatable grounds and it is expected that future tests will establish these limits. It has been found that the use of blended blast-furnace slag or of pozzolan portland cement corresponding to ASTM C 150 improves concrete durability, decreasing its permeability; the use of pozzolans and slag cement reduces the heat of hydration and eventually the thermal curing strains. Silica fume concretes (with high strength and low permeability [11, 28]) obtained by combining silica fume with normal portland cement, are considered well suited for the Arctic environment.

The aggregates should conform to ASTM C 33 or ASTM C 330. They should be clean, durable, and have low water absorption capacity. Some authorities allow for the use of marine aggregates too, if they conform to the requirements of ASTM C 33. The moisture content of the aggregates is important for the slump and workability and, later on, for the physical properties of the hardened concrete. Therefore, it is recommended, when preparing concrete, to keep the moisture content as stable as possible or to change the batch constituents weights accordingly, and to use the LA only if its absorption characteristics are known. Some countries produce sealed surface lightweight aggregates, thus eliminating the risk of moisture absorption by the aggregates [27, 37].

All admixtures employed to obtain concrete should conform the appropriate ASTM standards. The chemical admixtures should be checked against: ASTM C 260 for air-entraining; ASTM C 494 for water-reducing, retarding, acceleration, water-reducing and retarding, water reducing and accelerating admixtures. The mineral admixtures are covered by: ASTM C 618 for fly ash and ASTM C 989 for slag; for silica fume no ASTM specifications are available yet.

Most authorities limit drastically the chloride content in both admixtures and concrete. ACI Committee 212 provides a total limit chloride content in concrete [38], while FIP [16] and DnV

[39] avoid the use of calcium chloride as accelerator for marine concretes.

Special attention should be paid to the quality of Arctic concretes, i.e. low permeability, good durability and high strength. Consequently ACI 357.1R [28] specifies - according to ACI Committee 357 [13], DnV [39] and FIP [16, 40] - limitations with respect to maximum W-C ratio, minimum compressive strength, minimum cement content, minimum air content and maximum chloride content. The W-C ratio cannot be lowered too much because the concrete has to be workable; values as low as 0.32 were used in conjunction with a super-plasticizer.

A satisfactory freeze-thaw concrete resistance means a durable concrete, and is obtained not only by using air entraining or admixtures but also by controlling the pore size distribution and spacing within the concrete mass. More specifications are to be found in ASTM C 457 and ACI Committee 345 on Concrete Bridge Decks.

Offshore structures require large concrete volumes; consequently, to avoid the internal thermal strains which may lead to cracking, cement with low heat of hydration, precooled aggregates, pozzolans, retarding admixtures and reduced rates of placing should be employed [16, 28].

The construction, transportation, and deployment of concrete structures for shallow Arctic waters raises the question of the weight of the structure; hence the dead weight becomes an important parameter for design. Two existing concrete structures, one made of semi-lightweight concrete [28, 30], the other one made of prestressed LAC in combination with dense concrete [30, 32], prove the feasibility and economic efficiency of LAC structures in the Arctic [17].

There are a few standards covering the use of reinforcing bars: ASTM A 615, A 616, A 617, A 706 and ACI 318. When using epoxy-coated bars or zinc-coated bars (galvanized), it is advisable to consult ASTM A 775 and A 767, respectively. As a result of the low temperatures the yield strength of steel increases while its maximum elongation and impact capacity decreases; the magnitude of these variations are related to the temperature values and steel chemical composition. The conventional low carbon and high ductility reinforcements are considered satisfactory for the Arctic environment [35, 39].

Generally, the chemical attack and disintegration of concrete in a marine environment occurs due to the presence of seawater salts, or, in colder regions, due to freeze-thaw cycles; eventually the corrosion of the embedded steel governs the concrete durability. The concrete deterioration processes likely to occur are related to the exposure zones, seawater temperature,

history of concrete before exposure, mechanical action of the waves, concrete composition, freeze-thaw damage, corrosion of the reinforcement, abrasion and biological attack [30, 41]. These processes are controlled by the quality control of concrete (high strength, low permeability) plus careful construction work. The water temperature influences the type and intensity of the chemical attack on concrete (the sulphate attack is increased at lower temperatures) [41]. Mehta claims, however, that there is no evidence that the rate of chemical attack is a function of the environmental temperatures [42].

Adequate curing periods before immersion, cement content (particularly important for cement paste quality), concrete additives and admixtures should be considered as prime factors for durability [16, 41]. The low in-place permeability is obtained by using sound, properly graded aggregates, rich mixes with a minimum cement content of 320.0 to 400.0 Kg/m³ in the splash zones [39], a water-cement ratio of less than 0.5, preferably less than 0.40 [16, 41], good handling practices and workmanship (to avoid segregation and cracking due to slip forming and plastic shrinkage). Water reducing admixtures, e.g. super-plasticizers, are required to obtain adequate workability with low values of water-cement ratio.

Electrochemical corrosion of embedded steel occurs due to the flow of stray electrical currents, contact between different

metals in concrete, and corrosion cells within concrete; all are accompanied by chemical reactions. The main type of electrochemical corrosion which occurs is due to the corrosion cells [2, 28]. Normally, the concrete surrounding the reinforcement is an alkaline environment of high pH that countermands the corrosion reactions, creating a passive iron oxide film around the reinforcement bar. While sea-water pH value is about 8.0, even for a cement paste with a pH value greater than 12.0 corrosion may occur, if the concrete cover does not protect the reinforcing bars against chloride and oxygen penetration [41]. If the pH value drops, the passive film is destroyed or at least broken and the bar corrosion starts, proceeding at a rate which depends on the electrical resistivity of the concrete and on the rate at which oxygen is supplied. The availability of a certain threshold value of chloride ions (depending on the concrete pH) contributes to the depassivation too.

Special corrosion protection include concrete bituminous or epoxy-coatings, epoxy coated reinforcement [28], corrosion inhibiting admixtures and cathodic protection using sacrificial anodes.

It seems that with or without protective coatings the fundamental requirement of a durable concrete for cold marine environment, Arctic in particular, is known: high quality

concrete with low permeability.

1.5. Steel Fibre Reinforced Concrete in Marine and Offshore Applications

1.5.1. Introduction

Steel reinforcement, prestressing, steel fibres (SF) or other fibre types and polymer addition to plain concrete are all used for the same purpose: to mitigate its relative low tensile capacity and increase its strain capacity. As a secondary effect, the steel fibres impart toughness, i.e., the structural elements can absorb high energy without total failure [43, 44]. Risk concerns associated with the use of asbestos fibres generated research efforts to find out and replace them with new, safer fibre types, including steel fibres. In Scandinavia, USA and EEC, the replacement of asbestos is well carried out, triggered by the banning of the asbestos-cement products by Scandinavian Government regulations [45]. The steel fibre reinforced concrete (SFRC) use should be based on careful considerations with regard to the steel fibres price, the skills required to mix, place, and finish SFRC, and last but not the least the SFRC performance as compared with the conventionally reinforced concrete [46, 47, 48].

SFRC is specified by strength and fibre content: a flexural

strength at 28-days of 4.8 to 6.9 MPa and a compressive strength of 34.5 to 48.3 MPa are considered typical values. The maximum percentage of steel fibres addition, by volume, for normal weight concrete, is indicated as 2.5 percent but no figure is provided for lightweight concrete [49]. Jamrozky studied the properties of SFRLAC [50], using expanded shale aggregates, and concluded that the effect of steel fiber addition to concrete yielded similar effects on concrete properties regardless of the aggregate type, i. e, dense or lightweight aggregate. Ritchie et al. [51] emphasized the effect of LA and fibres types on the structural strength of SFRLAC; some of their tests indicated no advantage when adding fibres to a certain type of LA.

The fibres with high modulus of elasticity, such as asbestos, glass, carbon, and chopped wire fibres improve the strength of the matrix before cracking, changing the brittle failure pattern into a ductile one, sometimes improving the FRC dynamic strength. The fibres with low E modulus, such as polypropylene, polyethylene, and nylon are used to increase the energy absorption capacity of structural concrete subjected to shock or impact loading [52]. The polyethylene fibre concretes behave better than SFRC when the speed of loading is increased [53], mainly because of the viscoelastic properties of polyethylene. The above mentioned classification becomes significant and easier to understand when one considers the fact that the fibres could have higher or lower modulus of elasticity than the matrix.

Kobayashi et al. used both fibre types, obtaining a hybrid fibre reinforced concrete which had the maximum hybrid effect when 1 percent steel and 1-3 percent polyethylene fibres were mixed [53].

It was reported that concretes containing fibres with end anchorages and high aspect ratio achieve the same performances as concretes with straight fibres, but with a reduction of 40 percent of the fibre volume [54], emphasizing the effect of the fibre geometry on concrete performance. A word of caution is necessary when comparing different types of fibres: the fibres should have the same aspect ratio in order to assess their performance correctly [55].

It is not intended to present here all the completed work, theoretical and experimental, on fibre concrete; good references are available [49, 56-62]. The results of the theoretical and experimental studies on steel fibre reinforced concrete (SFRC) have been applied mainly for onshore structures and applications. However, the available results are highly variable, depending on testing conditions (lack of widely accepted testing procedures), measurement techniques and intrinsic properties of the materials; some workers found that a certain property is influenced in a certain manner while others described the same property totally differently. As observed by Knoblauch [63] it is difficult to compare all the measured data with one another, and to find

theoretical principles to formulate the phenomena since there is such a large variety in the fibre/aggregate skeleton, on which the rheological and hardened state properties are based. A few relevant characteristics, properties and applications of SFRC and SFRLAC follow as they relate to the present study.

1.5.2. General Properties

Flexural Behaviour: Pre-cracking and Post-Cracking

The behaviour of SFRC in flexure is an important indicator of the material performance and points out the differences between SFRC and plain concrete. The load-deflection curve for a SFRC element in flexure has two main regions: up to the first crack load or the proportionality limit the material is considered to behave elastically and between the first crack up to collapse the specimen behaves inelastically. Patton et al. explained the "extensive slow stable crack growth" process of plain concrete, which is further improved by the fibres within concrete [64]. The first crack stress or the proportionality limit for a composite material, such as SFRC, can be predicted using the spacing concept and composite materials concept [56]. Hannant [60] observed that, for a usual fibre volume, the fibre presence influence on the first crack load is not quite significant, its influence being substantial on the ultimate flexural strength.

The fibre orientation, characterized by an efficiency factor, η_0 , contributes between 17 and 80 percent to the material performance; more experimental data is required to bring out the corresponding theoretical principles [56, 61, 64]. A similar orientation factor, η_0 , is defined in Reference 37, for the same purpose. Different values were used by researchers: 1/3 for two-dimensional and 1/6 for three-dimensional random distribution or 3/8 and 1/5, respectively. Generally, the maximum load occurs at a higher load level than the first crack load, depending primarily on the type, volume, aspect ratio, orientation, nature, angle of inclination of the fibres with respect to the fracture plane and bond strength [52, 56, 60, 61]. After the initial cracking has been developed, the behaviour of the material is nonlinear due to fibre pulling out, debonding, stretching and cracked concrete contribution [55]. Eventually, the flexural failure is due to the bond failure between the fibres and matrix [52].

The area under the load-deflection curve in a slow flexural test of an element, prior to complete separation or up to a required displacement level, is a measure of the absorbed energy - and/or ductility -, and is greater by at least one order of magnitude compared to plain concrete [56, 65]. Toughness or impact resistance can be also quantified by the area under the load-deflection curve in an impact test. The toughness, in the latter situation is a function of the type and rate of loading.

Toughness and ultimate strength are influenced by the fibres type, volume, percentage, aspect ratio, nature of deformation, orientation, and stress-strain curve of the fibre itself [61].

Strength

Quotable published results regarding the SFRC behaviour and properties were largely dependent on the test specimen size, shape, and preparation procedures. Thus, it is advisable, when testing SFRC, to conform to the requirements of ACI Committee 544 Report - "Measurement of Properties of Fiber Reinforced Concrete" [66]; typical mechanical properties are given in Reference 56. Edgington et al. [57], Hannant [60] and Hibbert [61] present comprehensive studies of SFRC under tensile, flexural, and impact loads; they also carried out pertinent post-crack behaviour analyses. Early concrete strength, at the beginning of hardening and shear gaining strength time, was measured by Raouf et al. [67].

The uniaxial tensile strength is improved by the fibres to a maximum of 30 percent for up to 3 percent fibre volumes. However the use of SFRC is not recommended for applications where direct tensile stresses occur [60].

Contradictory results were presented regarding the relationship between compressive strength and fibre addition. Some authors

found a lowered or slightly increased compressive strength by fibre addition [55, 60]; Raju et al. [68] observed an increase of 40 percent in compressive strength for a 3 percent fibre addition. Hannant describes the fiber addition as useful when considering the resulting ductile compressive failure [60], with wider plastic zones for SFRC than for DC. Gopalaratnam et al. [55] obtained, in compressive tests on FRC, satisfactory agreement between their test results and the modulus of rigidity as predicted by theoretical studies. The fibre addition to concrete seems to have the same effect on the compressive strength as the confinement for unreinforced concrete. Other researchers [56] observed that the effect of an increased volume of fibres on the compressive, flexural, and tensile strengths is small and linear.

The dynamic strength of FRC, measured by various methods of testing - explosive charges, dropped weights, dynamic tensile and compressive loadings - and sometimes special equipments, is characterized by higher values, up to ten times, than those for the concrete without fibres because of the greater energy requirements during fracture and collapse of tested specimens, i.e., to spall, fragment, de-bond, pull-out or yield, and/or fracture of the fibres [55, 56, 69]. Up to the present time, the results reported in literature could be divided into two classes : quantitative/qualitative tests and fundamental theories with regard to the material behaviour, and they are different as they

are obtained in different tests by different workers, sometimes being variable in the same report [69]. Reference 66 provides for a standard method of quantifying the impact strength, proposed initially in Reference 70; more work should be carried out with this proposed method in order to make it largely acceptable. Actually, in the 1983 revision of the ACI Committee 544 Report [66], it is mentioned that some of the test methods are to be changed. Significant work on new methods of testing are reported from Japan [37].

The fatigue life of SFRC beams, an important indicator for offshore structures, seemed improved when compared with conventional reinforced beams [37], though Hannant [60] calls for serious judgement when assessing the fatigue strength of SFRC, because of the limited available test results.

It is known that the freeze-thaw resistance of DC is controlled by the content of the entrained air and its distribution within concrete [16, 28, 39]. Observations on the freeze-thaw resistance of SFRC with dense aggregates showed better or equal resistance compared with plain concrete [37, 66], only if air entrainment was provided. Jamrozy [50] found out that despite a porous and absorbent LA, the frost resistance of SFRLAC was good. Laboratory tests conducted by Balaguru et al. [71] showed that for a W-C ratio less than 0.4, cement content greater than 415.0 Kg/m³, and air entrainment of 6 to 8 percent (preferably), fibre

reinforced concrete was sound, durable, with the air content being the most significant parameter in controlling the freeze-thaw behaviour.

Abrasion Resistance

Tests performed on 2.5 percent SFRC with pea gravel aggregates and plain concrete with gravel aggregates, showed that the SFRC abraded 27 percent less than the plain concrete [56]. Using a new testing method for abrasion-erosion generated by debris contained in water flowing over hydraulic structures, the effects of W-C ratio, compressive strength, concrete type, fibre length and type on abrasion-erosion resistance of FRC were investigated [72]; the laboratory results were complemented by field investigations. This study concluded that the FRC was less resistant than the plain concrete of the same aggregate type and W-C ratio, subjected to small particles of debris rolling over the surface at low velocity; it recommended the use of conventional concrete of the lowest practical W-C ratio and the hardest possible aggregate. Based on 72-hours abrasion-resistance of FRC, the study reported an enhanced behaviour of polymer-impregnated FRC compared with conventional concrete. Where cavitation and/or abrasion from high velocity flow together with impact of large debris are expected, the use of fibre concrete is suggested [60, 73]. Where improved wear resistance is required, SFRC use was considered a good alternative [37].

Corrosion of steel fibres

Steel fibre mortars and concretes elements, exposed for short and long periods of times (up to ten years) to aggressive environments generating steel fiber corrosion - salt water, sea-water with or without freeze-thaw cycles, deicing agents - showed corroded fibres near the exposed surface of the elements [44, 73-76]. If the mortar and concrete surrounding the fibres were sound, uncracked and of good quality when the elements were cast, different types and sizes of uncoated steel fibres seem to be equally susceptible to corrosion, which ranged from 1.0 mm to a maximum of 5.0 mm for DC or 6.0 mm for LC.

Similar results have been obtained on fibre concrete beams subjected to long term corrosion in Australia [75]: after ten years of sea-water tidal exposure, there was a thin layer - up to 3 mm - of carbonated concrete in which corrosion of the fibres occurred. It is assumed that the extent of steel fibre corrosion is based on the lack of fibres continuity, thus a corrosion cell is not likely to occur [74]. Schupack [73] studied the flexural strength and toughness of thin LC sections exposed to freeze-thaw cycles in sea-water tidal zone for up to ten years. He observed that for the uncracked concrete, the corrosion is limited to those fibres close to the surface of the specimen, even if the thickness of the element is small, i.e., 20 mm. He also mentioned that the entrained air lightweight concrete (LC)

showed no damage when exposed to freeze-thaw cycles (30-50 cycles/year) in sea-water. Even when the chloride ion content was higher than the allowable threshold for concrete, no corrosion of the fibres occurred [77]. The corrosion of steel fibres in cracked sections is not so well known; however, the fibre corrosion takes place, as a function of the fibre diameter and environmental conditions [60].

1.5.3. Mechanical Properties of SFRC and SFRM Exposed to Marine Environment

Lankard [74], based on observations collected during 9-10 years, evaluated the durability of Wirand mortars exposed in sea-water. He concluded that carbon steel fibre reinforced mortar, after 10 years of submergence in sea-water had 21 percent loss in compressive strength while Monel fibre reinforced mortar, after 9 years of exposure, showed a 3 percent loss in compressive strength; the plain mortar lost 40 percent in compressive strength. Analyzing the flexural strength, the author showed that after six months and one year of exposure there was no loss in strength, but between the first and second year the strength decreased about 40 percent. After 10 years of exposure, he registered 31 percent strength loss for fibre concrete and 36 percent strength gain for the plain mortar. No explanation was given; however, the steel fibres employed in the research work were brass coated type and probably due to the coating corrosion

up to a depth of about 19 mm, the strengths were affected as shown.

Schupack [73] summarized the effects of three different aggressive environments on SFRC durability, including SFRLAC; the exposure duration was up to a maximum of ten years. His main conclusions and findings were: surface fibre corrosion does not affect the structural performance of concretes, except thin sections, smaller than 20 mm; the SFRC has the same freeze-thaw resistance as the concrete without fibres provided that they are of good quality; further investigations are required to determine the effect of air entrainment in SFRC exposed to freeze-thaw cycles and to determine the optimal structural material and structural behaviour of the material; the corrosion of fibres in cracks should be properly investigated in future research studies; because concrete cracking is likely to occur in almost all the applications, the designer should make allowance for this aspect. Mangat et al. [77] completed an experiment on SFRC prisms exposed in the splash zone to 300 freeze-thaw cycles, finding that a proper mix could withstand the effect of this type of loading.

1.5.4. Mix Design of SFRC

It is known that the traditional mix design methods for DC or LAC are not applicable for SFRC [56]. The composition of fibre

concrete bears a resemblance to the conventional concrete, having much more cement, higher fines content, smaller coarse aggregate size and the fibres themselves. Therefore, the conventional mix procedures are replaced by new ones developed for solving specific jobs [73, 78, 79]. The factors influencing the uniform distribution of the fibres and the workability of the mix are the fibre volume percentage, aspect ratio, fibre geometry, coarse aggregate size, volume and gradation of aggregates, W-C ratio, and mixing method. Swamy [43] considered the relative volume of coarse aggregate to be the most important parameter along with the critical parameters mentioned above. When mixing small batches, the fibres should be added either mechanically or manually as recommended in Reference 56. Other researchers [71] mixed FRLAC following ASTM C 192 method, except that the fibre addition took place at the same time with cement and after $\frac{2}{3}$ of the mixing water was charged to the mix.

Knoblauch [63] suggested that a dry pre-mixing with 4-8 mm gravel aggregates and steel fibres produced a somewhat random uniform fibres distribution. Satisfactory results were obtained when the aggregates and fibres or just fibres were placed in the mould and a cement paste was poured afterward, filling the voids in the mix with it. The maximum fibres percent, by volume, that could be added to realize a uniform fibres distribution was 1.69 as observed on X-ray pictures. With higher percentages, the fibres distribution varies greatly in the specimen volume.

Edgington [57] investigated the mix workability as it related to coarse aggregate volume and fibre aspect ratio. His equation, later on simplified by Hannant [60], can be used to proportion the mixes and to establish the critical fibre percentage. Other authors recommended a different relationship between DC workability and volume fraction, length, aspect ratio and fiber diameter [37].

The plastic fibre concrete requires low W-C ratios, between 0.4 and 0.6, and relatively high cement contents, from 249.0 to 430.0 Kg/m³ [56]; hence the use of admixtures for water reduction, air entrainment, workability and shrinkage control becomes important. Fly ash in combination with cement positively affected the long term hardened material properties of reinforced concrete [56, 80]; when used with FRC [81], it reduced the internal mix friction, providing for good workability and compaction.

Slump, as a measure for concrete workability, may be measured using three methods: slump test - still extensively used in practice - conforming to ASTM C 143, inverted slump cone test (ASTM C 995) and V-B test [57, 60, 66].

Swamy [82] suggested sand-lightweight aggregate ratios of 1:1 to 3:1 with a ratio of 1.5:1 as a good starting point for a trial mix. Barab et al. [46] reported their experience as it related to SFRC mixing. Although they tried many procedures to avoid

balling during mixing, such as different methods of charging and distributing the fibres, aggregate proportion adjustments, water and/or cement adjustments, the trial results were not predictable; eventually they obtained a suitable mix for their application. Pomeroy [83] related fibre balling to a high aspect ratio of the fibres, greater than 100; however, he observed that in certain applications, such as guniting of sea walls and tunnel lining, the low workability of SFRC was advantageous.

Nevertheless, the selection of the basic mix quantities should be checked by trial batches. Appropriate quality control is compulsory, i.e., slump, air, density and strength tests.

1.5.5. Applications

Improved mechanical properties of SFRC and SFRLAC offered the designers a chance to use selectively these materials [56], with and without conventional reinforcement, in the areas of road pavements, refractories [43, 45], bridge and deck overlays [84], patching, new constructions and repairs on major hydraulic structures, industrial floors [85], thin shells, armour for jetties, rock slope stabilization (shotcrete), mine tunnel linings, mine roof support, highways, runway slabs [45], foundations for machinery [86], underground powerhouse [37], domes, and precast strong, stiff and tough products - such as

partition walls or exterior walls of small-scale residences, soundproof walls, gutter covers [37], and thin-walled units in rare cases [44].

Laboratory investigations proved that SFRC may be successfully used to replace stirrups for shear reinforcement in frames [87], beams [37, 88], in selected zones of precast, prestressed and cast-in-place concrete [89]. Swamy et al. [90] showed the influence of steel fibre addition - spread in the whole beam volume or just in the tension zone - on the behaviour and ultimate flexural strength of beams reinforced with conventional reinforcement; their proposed theoretical model seems to be in close agreement with the tests results. Swamy observed that the behaviour of fibre reinforced T, I, and rectangular beams was, generally, similar to that of equivalent members with stirrups [43]. Tested slabs and beams with or without fibres, when the fibre content was varied from 0.0 to 1.2 percent, proved that the fibre presence reduced the deflections and improved the control of cracking [90, 91].

The isotropic reinforcing action of the fibres and the ductility of FRC after initial cracking accentuated its usage in blast resistant structures, impact load resistant structures and other structures designed to resist dynamic loads [49, 56]. Kormeling et al. [47] carried out fatigue experiments on steel fibre reinforced beams with conventional reinforcement. These tests, of particular significance for offshore structures, showed the

increased fatigue life of the elements. This property together with the impact strength imparted by fibres (waterfront warehouse floors, wharf decking and underwater storage structures [56]) are to be seriously considered for marine and offshore applications. Ghalib [92] investigated experimentally eight SFRC composites and he proposed a design method for small plates with different support conditions and loadings.

Barab et al. [46] showed the improved dynamic impact resistance of SFRC dolos and observed that the use of steel fibres with conventional reinforcement had a noteworthy effect for lightly reinforced dolosse. One of the conclusions of their study pointed out the feasible limit up to which the fibres have their maximum positive effect on concrete properties.

Swamy et al. [93] employed SFRC to build a car park precast slab deck on a structural steel space frame at Heathrow Airport, London. They designed and experimentally checked the component units of the decking slab having different fibre contents, from 1 to 4 percent, and showed that these panels had better performances than plain concrete plates: reduced crack widths, increased ductility at failure proportional to the fibre content and a well defined failure pattern. Hannant [94] proved that the deflections of SFRLAC beams in bending are similar to those of DC. Since conventional reinforcements can be arranged within concrete in such a manner as to withstand almost any type of

loading and make it fail in a ductile manner, SFRC must be used where complex stress combination occur and/or where the conventional reinforcement cannot be used [83].

1.6. The Need of the Present Research and Rationale of Investigations

The discovery of oil in the North Sea and offshore North America and in other parts of the world including the Arctic, started the successful development of concrete structures for its exploitation. Based on the present experience and the knowledge of recent researches, it is expected that large new fixed and floating concrete structures will be utilized in the near future.

The design of offshore structures is more difficult than onshore structures and requires creativity and the use of recent results from research in interdisciplinary areas. Obviously, the final aim of all these efforts is to obtain safe, long lasting and economical offshore structures. Materials to be used in the construction are those with a proven record of good performance: steel and concrete. One important aspect that should be kept in mind is that the suitability of a structural material is based eventually on its ability to absorb energy before it fails. A high or very high strength is usually accompanied by a less favorable effect: brittleness. Steel fibres are provided essentially to obtain a high strength and ductile structural

material; the actual technologies of construction and deployment of Arctic concrete offshore structures point out the importance of the self weight of the structure. Hence, steel fibres added to a lightweight aggregate concrete could yield a concrete, SFRLAC, which corresponds to the required specifications. Recent tests have shown that steel fibre reinforcement could be successfully used with conventional bar and prestressed reinforcement, to give a material with high static and impact strength. However, few research investigations have been carried out on SFRLAC as a material for its structural behaviour: Swamy [91], Jaromzy [50], Ritchie et al. [51], Hannant [94], Paillère et al. [95] and Nemegeer [96]. The present study tries to supply data regarding SFRLAC properties, especially those related to offshore applications.

The main tests of the present research work, were directed towards the following objectives:

1. To establish the feasibility of using an available expanded shale lightweight aggregate, MEL-lite, as the coarse aggregate for the cold ocean environment offshore applications;
2. To determine the quantities of steel fibres that could be satisfactorily mixed with the expanded shale lightweight aggregate and the other constituents of the mix, without

fibre balling, clumping and matting in order to obtain SFRLAC;

3. To establish the plastic properties (rheological properties) of the LAC and SFRLAC;
4. To determine experimentally LAC and SFRLAC structural properties such as unit weight, compressive strength, modulus of elasticity and flexural strength;
5. To establish the effect of the simulated cold ocean environment (COE) upon the LAC and SFRLAC properties determined in point 4;
6. To obtain the influence of steel fibres on flexural and shear behaviour of the LAC plates;
7. To obtain the effect of the cold ocean environment (COE) on the plates capacity and behaviour, after over 100 days of immersion in cold ocean environment; and
8. To compare the theoretical predictions given by a finite element computer code [97] and other analytical methods with the experimental results of the LAC and SFRLAC plates.

CHAPTER 2. PRODUCTION OF LAC AND SFRLAC

2.1. Mix Proportioning Criteria

The specific values for the compressive strength, unit weight, slump, and air entrainment have been selected for the Arctic structural LAC and SFRLAC, respectively, and they are given below. The workability and W-C ratio are important too, from a construction standpoint. Some of the rheological properties—density, slump, entrained air, vibration, placing, finishing—were also investigated as shown in sections 2.3 and 2.4; the hardened state properties that were obtained are given in Chapter 3. The LAC recipe has been used to obtain SFRLAC, this providing a better indication of the fibre addition.

1. Compressive strength - Structural LAC, either all-lightweight or sand-lightweight, for onshore structures is defined as having a 28-days dry unit weight between 1400.0 and 1850.0 Kg/m^3 (90.0 to 115.0 Lbs/ft^3) and a 28-days compressive strength greater than 17.24 MPa (2500.0 psi), whereas the design considerations for structural concrete for marine and offshore applications require an average 28-days compressive strength over 27.58 MPa (4000.0 psi) [22] or over 41.37 MPa (6000.0 psi) [28]. Reference 3 indicates the cube compressive strength for marine and offshore

applications at 28-days as:

- 40.0 MPa - for exposure to salt water or salt spray;
- 30.0 MPa - where protected from salt water or salt spray;
- 45.0 MPa - where severe scouring is to be expected.

FIP [16] requires in the splash zone more than 400.0 Kg/m³ cement, W-C ratio less than 0.4, and a minimum 40.0 MPa compressive strength at 28-days. API Code [35] and Petroleum Directorate of Newfoundland [98] require respectively 42.0 MPa and 50.0 MPa for the compressive strength at 28-days. The structural LAC that was used in the present work had been designed to reach 41.37 MPa (6000.0 psi) as minimum compressive strength. The chosen strength was in accordance with the provisions of the mix design supplied by the manufacturer [99] for the delivered 1/2 in. to No. 4 expanded lightweight shale aggregate (MEL-lite). In accordance with the suggested mix design and in order i) to increase the compressive and bond strengths of concrete, ii) to improve the durability, corrosion protection (of the reinforcement) and workability and iii) to reduce the cement requirements and the shrinkage of concrete, the replacement of lightweight fines with ordinary, dense, fines aggregates (sand) was used. The compressive strength of SFRLAC was specified as for LAC,

- i. e., 41.37 MPa at a density not exceeding 2000.0 Kg/m³.
2. The unit weight depends on the density of the LA, cement, water, air content, normal weight aggregate, steel fibres and all the other constituent weights used. The complete replacement of the lightweight fines with ordinary (dense) fines, i.e. natural sand, increases the unit weight by 160.0 Kg/m³ (10.0 pcf) at the same strength level; despite an increased density, other properties are enhanced as mentioned before. Additional compressive strength is obtained by increasing the cement content while the unit weight increases only by about 48.0 Kg/m³ [22]. The latter solution is not feasible from an economical standpoint; consequently, a maximum value of the dry unit weight of 1900.0 Kg/m³ was fixed as one of the main objective of lightweight aggregate concrete proportioning. The fibre presence increased the unit weight of concrete, but trial batches were carried out to control this parameter, such that it would be around 2000.0 Kg/m³.
 3. Since the manufacturer of the LA suggested 75 mm (3 in.) slump [99], this value being recommended for a medium workability [12, 22], it was selected as the design slump value with an allowance up to 100 mm (4 in.). Higher values than 100 mm may cause segregation with the lightweight particles (LA) floating through the mortar to

the top - "surface" segregation. Likewise, prolonged vibration may lead to segregation much more readily than with dense aggregate. Thus it was considered worthwhile to obtain the lowest slump without affecting placing, consolidation and finishing properties of concrete.

4. The entrained air content improves the durability to freeze-thaw cycles, hence to cold ocean environment (COE) too, having a positive effect on workability: water requirement is reduced, maintaining the same slump, and the tendencies to bleeding and segregation are also reduced. The recommended values of total air content by volume are given, for LAC, in Reference 22. Air content in excess of these values lowers the compressive strength of sand lightweight aggregate concrete by about 1.03 MPa (150 psi) for each additional percentage of air [22]. For SFRLAC, the air entrainment is considered necessary for proper workability and freeze-thaw resistance regardless of the steel fibre addition. The design value of the air content was selected as 7 percent [99].

5. Workability is an important property of the freshly mixed LAC. Many LA are angular and have a rough surface producing harsh mixes, difficult to cast. The workability may be improved by using fine aggregates of ordinary weight; thus a total replacement of lightweight fines

yields: a reduction in water content of 12-24 percent, higher modulus of elasticity by 10-30 percent and reduced shrinkage by 15-35 percent compared with all lightweight aggregate mixes [32]. Pfeifer [100] showed the improved freeze-thaw behaviour of 3000.0 psi compressive strength concretes when sand replacement, partially or totally, was used, because of its positive effect on mortar properties. The entrained air also has a beneficial effect on workability as mentioned earlier. The high strength LAC has a low W-C ratio; this requires the use of a high range reducing agent and/or a chemical admixture to improve the workability.

6. Generally, the water-cement (W-C) ratio is not used to proportion LAC because the porous LA tends to absorb an unknown quantity of the total water required for mixing the materials. It is assumed, however, that the absorbed water is available for continuous hydration of the cement after the normal curing has ceased and it is recommended to proportion the mix on the basis of the cement content at a given or chosen slump of concrete [3]. When LAC is proportioned using the Weight Method, W-C ratio may be used, if the absorption of the aggregates is known. To avoid the variations in workability due to water absorption by the LA, it is recommended to wet uniformly the aggregates before mixing. Kobayashi mentioned that for SFRC, with dense

aggregate, the W-C ratio is to be limited to a certain upper value by compressive strength requirements [37].

2.2. Materials

Cement

Ordinary hydraulic Type 10 Normal Cement was used in production of LAC. The cement content should be between two limits, inferior and superior, as is usually given in standards or guidelines, e.g. Reference 22 requires for a 28-day compressive strength of 34.47 MPa (5000 psi) with a 3-4 in. (75-100 mm) slump and a 7 percent air content, a cement content of 356.0 to 445.0 Kg/m³; Reference 39 requires more than 300.0 Kg/m³ and not less than 400.0 Kg/m³ in the splash zones; Reference 3 recommends cement contents greater than 400.0 Kg/m³. The tricalcium aluminate content, C₃A, in cement, should be between 8 to 10 percent; it is related to the quality of the cement paste, which in its turn could avoid the risk of sulphate attack and corrosion of reinforcement [39, 41]. Besides, the 28-days cement compressive strength should be more than 35.0 MPa. Therefore, it seems that the quality of the cement paste is important for the concrete composition and its durability. The superior limitation is imposed knowing that the strength of the concrete made with the chosen aggregate, viz., expanded lightweight shale aggregate (MEL-lite) or any other LA, could

have a strength ceiling above which an increase in cement content does little to increase the strength of concrete.

Coarse Lightweight Aggregate

The main characteristic of LA is its porosity, which eventually yields the low concrete density. There are two principal categories:

- natural aggregates, such as diatomite, pumice, scoria, volcanic cinders, and tuff;
- artificial aggregates, according to the raw material used and method of manufacture:
 - expanded shale, clay, and slate, such as vermiculite, perlite, expanded lightweight shale aggregate (MEL-lite);
 - expanded blast-furnace slag, such as foamed slag;
 - clinker, known in USA as cinders.

The rotary kiln shale aggregates, such as expanded lightweight shale aggregate (MEL-lite), yield concretes having a density of 1400.0 to 1900.0 Kg/m³ and corresponding compressive strength; hence the concrete is classed as structural concrete [22].

The available structural lightweight aggregate that was used in this study is expanded lightweight shale aggregate (MEL-lite)

with a gradation conforming to the requirements of ASTM C 330 for lightweight aggregates for structural concrete. The results of the sieve analysis are shown in Table 2.2-1 and Fig. 2.2-1. A description of the particle shape and surface texture is given by the fabricator [99]:

MEL-lite is the trade name of an expanded shale light weight aggregate produced in Avon Aggregates Limited's rotary kiln plant located at Minto, New Brunswick. MEL-lite is manufactured to rigid control standards to produce a rounded, coated particle which is uniform in properties. This uniformity results in a concrete of better workability, lower water requirements and high strength than crushed, angular, porous aggregates.

The characteristic physical properties are listed in Table 2.2-2.

Grübl [102] determined a "limit compressive strength" after which the strength of LA employed dictates the compressive strength of concrete. ACI states that the reliable correlation between aggregate strength and concrete strength is to be given by the producer of LA [22], whereas in Rumania [103] and Germany [104] there are standard methods to determine the strength of LA which in its turn is related to the strength of LAC. Since MUN laboratory did not have the necessary equipment to determine this strength, the investigator could not find the relationship between the strength of LA and LAC.

The largest particle size was considered acceptable for

obtaining high compressive strength using reasonable cement content [22, 49]. A criterion for selecting the largest particle size for SFRC is provided in Reference 37 as about one half the steel fibre length, for proper mixing and workability.

Because the freeze-thaw resistance depends on the moisture content of the LA, its moisture content was determined prior to mixing; LA was wetted because of the mixing procedures, but hardly it could have been considered more than wet, nevertheless it was not even partially saturated. A good freeze-thaw resistance may be obtained if the LAC is allowed to dry in air for a well determined period of time prior to use in marine and offshore applications. Preliminary tests showed the 24 hours absorption of expanded lightweight shale aggregate (MEL-lite) to be 10.86 % ; the water added to the mixer together with the actual weight of the mix constituents were adjusted accordingly.

Fine Aggregate

Normal weight fine aggregate (sand) was used, conforming to the provisions of ASTM C 33. The grading of fine aggregate is presented in Table 2.2-1 and Fig 2.2-1.

The characteristic physical properties are listed in Table 2.2-3.

Admixtures

Two types of admixtures were used:

- air-entraining, and
- water-reducing (super-plasticizer).

Air-entraining agent (AEA) was used as indicated by the fabricator, at a rate of 62.5 ml for 100.0 Kg cement; the actual percent of AEA which was used had been determined by tests on freshly mixed concrete.

The super-plasticizer, a modified polycondensation product of melamine and formaldehyde (MELMENT L 10), a synthetic water-soluble plasticizer and at the same time a hardening accelerator, is to be used from 1.5 to 4.0 percent by weight of cement or 1.5 to 4.0 litres per 100.0 Kg of cement. For a watertight concrete with a W-C ratio of 0.4, the added amount of super-plasticizer is recommended as 1.5 percent by weight of cement and it was adjusted accordingly in relation to the concrete workability, at the mixer.

Steel Fibres

Usually, steel fibre reinforced concrete contains from 0.5 to 2.5 percent steel fibres by volume. The typical length of the fibre is between 15 and 50 mm, and its diameter between 0.2 and 0.5 mm. Typical properties of steel fibres are listed in Table

1.1 of Reference 56 as: from 276.0 to 2760.0 MPa for tensile strength, 119,955.0 MPa for modulus of elasticity, 5 to 35 percent ultimate elongation, and 7.8 specific gravity. The ASTM A 820-85 covers the specifications for steel fibres (SF); the fibres might also be specified by their brand name or by a short description including their mechanical properties. The bond of smooth steel fibres in concrete is about 0.5 MPa (72 psi), which means that the fibre will pull out before its ultimate strength is reached. To avoid this situation, the lateral surface of the fibre is deformed or end hooks are provided.

The influence of fibre aspect ratio, volume fraction, and chemical treatment on the concrete properties have been reported in literature [56]. The chemical treatment with epoxy resin had a positive effect on the compressive and tensile properties of SFRC in the hardened state [105]. Several types of steel fibres had been used in tests [54, 105, 106], e.g., Hughes et al. [106] mentioned the good behaviour in pull-out tests of straight fibres provided with mechanical anchorages at their ends or along their lengths. Among the fibre types, the fibres with hooked ends provide a good mechanical anchorage and increase the resistance to fibre pull-out during the post-cracking phase. The aspect ratio influences the strength of hardened concrete but it influences the workability of the mix, too: the longer the fibre, at the same diameter and volume content in the mix, the higher the strength of the concrete, but lesser workability. To

overcome both the problems, the use of glued bundles of fibres represents a good solution: it provides a short artificial low aspect ratio necessary for proper workability; during mixing, the glue is dissolved by water, providing the individual fibres with a high aspect ratio as required for a high ultimate strength of SFRC. The glued fibres are also effective in preventing the matted fibre balls getting accumulated during mixing.

Following the conclusions and recommendations of the investigators, DRAMIX ZP 50/.50 glued bundles steel fibres with deformed ends (hooked ends) were used to obtain the SFRLAC. The initial aspect ratio of SF was 30 (before introducing them into the mix); after their dispersion in the mix, it became 100.

Water

Fresh water was used as mixing water.

2.3. Method of Proportioning; Mixing

2.3.1. LAC

The producer of the expanded lightweight shale aggregate (MEL-lite) suggested [99]:

- the initial mix design be based on trial batch

method using loose dry volumes;

- the entrained air percent be from 5 to 7;
- pre-wetting of the lightweight aggregate; the weight of the moisture in the aggregate be determined and added to the converted dry weight used to represent the initial mix volumes. This weight of aggregate water is to be deducted from the water weight added to the mixer as determined in the initial trial mix;
- the maximum slump be not greater than 75 mm (3 in.);
- the uniformity of the mix be assured by frequent determination of the wet weight of concrete.

The factors which were taken into considerations by the designers, for proportioning LAC, were:

- absorption and moisture content of aggregates;
- gradation of the aggregates;
- water-cement (W-C) ratio;
- air-entrainment.

The aggregate supplier provided the following LAC recipe for a 41.37 MPa (6000.0 psi) specified compressive strength, 1/2 in. (12 mm) top size coarse lightweight aggregate particle and 1/2 to 2 in. (12 to 25 mm) slump [99]:

	m ³
Cement	363.0 Kg
Water	113.6-132.5 Kg
Air content	4-6 %
¼ - ¼ in. MEL-lite	431.0 Kg
¼ - 0 in. MEL-lite	181.0 Kg
Sand	245.0 Kg

It was thought that the provided recipe could be used as the basis for the first trial mix; however, a few considerations ought to be taken into account due to the actual conditions:

1. as presented in the above recipe, the 1/4 to 0 in. expanded lightweight shale aggregate (MEL-lite) size should be part of the mix. Because this size was not available, graded sand was used as fine aggregate; hence the provided recipe had to be suitably modified;
2. the minimum cement quantity was chosen using Fig. 3.3 of Reference 101 and taking into account the minimum cement provisions required by standards;
3. the water content was kept at a low value, around 0.4.

ACI Committee 211 suggests for the first trial mix, two methods, namely [101]:

- The Cement Content-Strength Method; and
- The Weight Method.

The Cement Content-Strength Method is applicable to all lightweight or semi-lightweight concretes and requires a cement content estimation, the total aggregate volume, fine to coarse lightweight aggregate proportion, mixing water content for a required slump and the specific gravity factor of LA.

The second method is used in determining the mix proportions just for semi-lightweight concretes (sand-lightweight concretes). To determine the weights of the constituents, as in the Cement Content-Strength Method, the method requires the specific gravity factor of lightweight coarse aggregate; based on this value, the weight of the plastic concrete is determined. When the effective mixing water is determined, the 24-hrs absorption of the lightweight aggregate must be known, too.

Taking into account the important factors, the first trial mix was designed using the Weight Method, considered suitable for this study. The mix design was adjusted in accordance with the constituents characteristics and properties following the same principles as for the trial mix design and the guidelines outlined in Chapter 4 of Reference 101.

Using Type I (Type 10) normal cement, expanded lightweight shale

aggregate (MEL-lite) with a specific gravity factor of 1.80 and an absorption (24 hours) of 10.86 percent, natural sand with the fineness modulus of 3.00 and absorption (24 hours) of 0.786 percent, air-entraining agent and a modified polycondensation product of melamine and formaldehyde (MELMENT L-10) as super-plasticizer, the mix has been determined as shown in Appendix A.

The obtained mix recipe was:

	m ³
Water (added)	183.0 Kg
Cement	500.0 Kg
Coarse agg. (dry)	460.0 Kg
Sand (dry)	646.0 Kg
AEA	0.3 Kg
Melment L 10	2.0 Kg

The combined aggregate gradation curve is shown in Fig.

2.3-1. For the subsequent batches, adjustments were needed for actual moisture content of the aggregates:

- the cement volume and weight were kept the same;
- the air content was kept the same;
- based on the dry weights of the aggregates, which were maintained the same, the new weights corresponding to the actual moisture content were

determined;

- the actual volumes displaced by the aggregates were computed;
- the water volume and weight of the added water were computed.

2.3.2. SFRLAC

SFRLAC was obtained using the requirements outlined in specifications. The optimum fibre volume addition was determined theoretically, from literature review [43, 78, 103], and, eventually experimentally. Using Schrader's formula for determining the critical fibre content, a value of 82.39 Kg or 1.0 percent by volume was obtained, with the sand-lightweight aggregate ratio 1.5 [78]. Although the method was initially used for DC, it was taken into account at least as a starting point in finding the proper fibres content; it yielded, in this case, dubious results, mainly as regards the cement content. The available data in Reference 37 suggests for a SFRC mix with a fibre content of 1.0 percent by volume, a W-C ratio of 0.5, maximum size of dense coarse aggregate 15 mm and a slump at about 80 mm, the optimum sand percentage content to be 50-60 percent. Schrader's [78] and Japanese [37] methods, would be probably reliable for DCs; as the prime interest, at this moment, was to find out the percent to be added to concrete in order to obtain SFRLAC, and the available methods yielded poor

results, it was decided that the proper fibre volume should be determined by trial laboratory tests.

The fibres were added to the already existing LAC mix recipe, dispensing them by hand, slowly, trying to avoid balling and clumping. A value of 0.815 percent by volume or 64.0 Kg/m^3 (steel fibre density 7850.0 Kg/m^3) added to the mixture yielded a plastic, workable mix:

	m^3
Water	183.0 Kg/m^3
Cement	500.0 Kg/m^3
MEL-lite (dry)	460.0 Kg/m^3
Sand (dry)	646.0 Kg/m^3
Steel fibres (0.815% by volume)	64.0 Kg/m^3
AEA	0.3 Kg/m^3
Melment L 10	4.4 Kg/m^3

Since the super-plasticizer has no influence upon the maximum amount of fibres that could be added to the mix [60], it was used just to obtain a workable mix.

When using steel fibres, the mixing procedure mentioned previously for LAC was changed because of the expected modified slump, workability and finishability of the mix. The ASTM C 192 Method was tried first, as follows:

- (1) The lightweight aggregate was dumped into the drum mixer, and the mixer was started;
- (2) The fine aggregate was added to the drum mixer;
- (3) The drum mixer was progressively charged with water, containing AEA, to about 1/3 out of the total amount;
- (4) The cement and fibres were progressively added (dispensing the fibres manually) and the rest of the water containing AEA was added;
- (5) The super-plasticizer was added;
- (6) The drum mixer was allowed to rotate 3 minutes;
- (7) The drum mixer was then stopped for 3 minutes;
- (8) The drum mixer was allowed to rotate for 2 more minutes;

This mixing procedure proved to be time consuming because of the time needed to batch the materials in the described sequence; balling occurred, too. Thus another trial method was used:

- (1) Part of the mixed aggregates and cement were dumped into the drum mixer;
- (2) 1/3 water containing air-entraining agent (AEA), was added to the mixture;
- (3) Steps 1 and 2 were repeated until all the quantities needed for the batch were exhausted, with the drum mixer rotating;
- (4) The steel fibres were dumped into the drum mixer;
- (5) Mixed for 15 minutes;
- (6) The super-plasticizer was added to the mix, gradually, as

it was needed;

- (7) Allowed to stand for maximum 3 minutes, usually 1-2 minutes, to check the fibre distribution and mix cohesion;
- (8) Mixed for another maximum 5 minutes, since it was necessary to move the mixer to the casting place and empty it.

The yielded mix was stiff, with poor workability. The most appropriate results to the specified values were obtained as follows:

- (1) Part of the mixed aggregates and cement were dumped into the mixer; the operation was repeated until all the aggregates and cement were exhausted;
- (2) The total amount of fibres and water, containing AEA, were divided into equal parts. One part of the fibres was added to the drum mixer, followed by one part of water with AEA, with the drum rotating, until all the water and fibres were exhausted too;
- (3) Steps 5, 6, 7, 8, were repeated as described on pages 56-57, the second trial procedure. The mixing time needed to obtain a corresponding mix seems to be in agreement with the results of other investigators [108].

The slump, air content, unit weight of concrete were 80 mm, 8.0 percent, and 2038.0 Kg/m³ respectively, as measured by the appropriate ASTM methods. The slump was determined, initially,

by the Inverted Slump Cone Test (ISCT) procedure as prescribed by ASTM C 995, and References 49 and 66. The test was supposed to give information regarding the workability and compactibility of SFRLAC; the main problem encountered was that the test time to empty the cone could not be measured as the cone never lost its whole concrete content, see Fig. 2.3-2. Problems in measuring the slump using ASTM C 995, for SFRC with hooked steel fibres were reported by Swamy too [81]. Therefore, the only test considered for workability was the slump test as prescribed by ASTM C 143.

As could be seen, the air content is higher than the specified value of 7.0 percent. It is believed that the entrapped air, in addition to that provided by the air-entraining agent had influenced this value. The unit weight was higher than the specified unit weight of LAC; it is normal to obtain a higher value for the unit weight since steel fibres were added and the constituents weights were adjusted at new values, resulting in this increased unit weight.

2.4. Placing and Curing

Without proper handling, LAC tends to segregate; because sand, super-plasticizer and AEA were employed, the concrete cohesion was good with no segregation and when the fibres were added, no special problems were encountered in handling of the SFRLAC.

The standard specimens were manually compacted, using a steel rod. At the moment of casting the first plate, it was observed that wherever the poker vibrator had been inserted, there were discontinuities, creating a disruption in the skeleton of the fresh concrete. Consequently, it was decided to use a vibrator with plate which gave proper compaction. The striking times and curing periods were about the same for LAC, SFRLAC as for DC.

Quality control tests (similar for LAC and DC) have been carried out to determine the moisture content of the aggregate, the density of the fresh concrete, the 28-days compressive strength and the absorption test for hardened concrete - e. g. some authorities recommend the initial surface absorption test (ISTA) [3, 103].

After the mold and formwork were removed at 24 to 72 hours from the moment of casting, the concrete standard specimens - cylinders and prisms - and/or the plates were subjected to two curing environments:

- (1) Laboratory environment (LABE) - The standard specimens were moist cured after the molds were removed until the scheduled moment of testing, i.e., they were kept immersed in fresh water tanks at laboratory temperatures - 21-22 °C. It is suggested to cover the concrete surface, with high-water-retention sheets, to avoid the water evaporation and

consequently the cracking of the surface, and to allow some of the absorbed water within the aggregate to be released. The internal moisture available, low thermal coefficients (expansion-contraction), similarities between the mechanical behaviour of the aggregate and the cement paste provided for less external and internal cracking during hydration for LAC than for DC [3]. Therefore, the plates were covered, immediately after casting, with polyethylene film for about 3-4 days in order to mitigate water evaporation; afterwards they were kept at the laboratory temperatures, splashing occasionally their surfaces with fresh water. Special attention was given to those cylinders which were used to determine the air-dry unit weight of concretes as required by ASTM C 567.

- (2) Simulated cold ocean environment (COE) - Seawater is not to be used for curing; only when the concrete has gained sufficient strength or is protected against seawater for the whole curing period, it should be immersed in seawater. It is considered that a watertight concrete with an adequate durability and minimum surface cracking would be obtained if the concrete is cured for not less than four days [109]. Immediately after removal from the forms, the standard specimens and the plates were cured for about 4-7 days in the same conditions as the specimens and plates cured in the laboratory environment (LABE); after that period, they were

immersed in sea-water at 0 °C. The temperature in the cold room, where the standard specimens were cured, was maintained until the scheduled moment of testing. The simulation of cold ocean environment on the concrete plates was carried out, during the winter time, using a tight water tank constructed outside the building: the plates were all the time immersed in sea-water below or at about 0 °C. The cylinders which were cast along with each plate, were cured under the same conditions as the plates.

Table 2.2-1 Grading of Course and Fine Aggregates

Sieve Size	Gradations	
	1/2" - #4	#4 - 0
	% Passing	
1"	100.00	100.00
3/4"	100.00	100.00
1/2"	99.00	100.00
3/8"	77.00	100.00
#4	10.00	88.00
#8	5.00	73.00
#16	3.00	52.00
#30	0.35	42.00
#50	0.00	26.00
#100	0.00	14.00
#200	0.00	6.30

Table 2.2-2: Physical Properties of Course
Lightweight Aggregates

Physical Property	Value	Method of Determination
Dry unit weight		
- loose	760.88 Kg/m ³	ASTM C 29
- rodded	864.38 Kg/m ³	ASTM C 29
Pycnometer specific gravity, S	1.5 - 1.93	ACI-211.2 Annex A
Absorption (24 h)	10.86%	ACI-2.11.2 Annex B
Maximum size particle Grading	12.7	ASTM C 330 ASTM C 330

Note: The S values were obtained using a 1.0 litre Mason jar, not a 1.9 litre as required in Annex A of ACI-211.2 [101].

Table 2.2-3: Physical Properties of Fine Aggregates

Physical Property	Value	Method of Determination
Dry unit weight		
- loose	1269.06 Kg/m ³	ASTM C 29
- rodded	1603.37 kg/m ³	ASTM C 29
Apparent specific gravity	2.64	ASTM C 128
Bulk specific gravity	2.58	ASTM C 128
Bulk specific gravity (SSD)	2.60	ASTM C 128
Absorption (24 h)	0.786%	ASTM C 128
Fineness modulus	3.00	ASTM C 33
Maximum size particle	4.22 mm	ASTM C 33

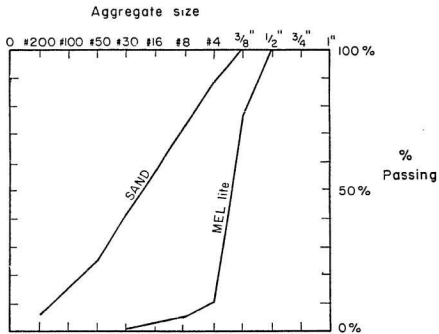


Fig.2.2-1. Granulometric curves of lightweight aggregates and sand.

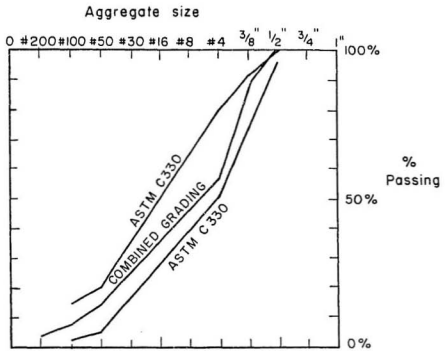


Fig. 2.3-1 Granulometric curves of concrete aggregates and domain of aggregates as per ASTM C 330.

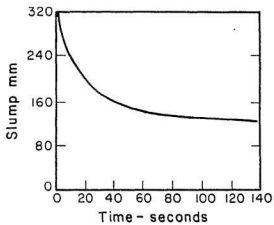


Fig. 2.3-2 Inverted slump cone results

CHAPTER 3. CHARACTERISTICS AND PROPERTIES OF LAC AND SFRLAC

3.1. Introduction

In order to meet the requirements to which concrete might be subjected, it must have a satisfactory mechanical strength and other strengths as required. The compulsory concrete properties which must be checked at any time are the unit weight and compressive strength. In this chapter, the following properties were determined:

- (1) Unit weight (density);
- (2) Compressive strength;
- (3) Time-dependent strength development;
- (4) Modulus of elasticity;
- (5) Tensile strength - Flexural strength;
- (6) Absorption.

All the tests have been carried out in the Concrete and Structures Laboratories at MUN.

3.2. Unit Weight (Density)

Usually, this test is required to obtain indications regarding the compressive strength of DC. A lower value of unit weight

than the specified one means a lower value of the compressive strength than that specified. As presented in section 3.3, for LAC the relationship between unit weight and compressive strength does not have the same intact significance as for DC although the unit weight is used to class the lightweight aggregate concrete as structural or otherwise. According to the job requirements, the unit weight was specified as 1900.0 Kg/m^3 for LAC and about 2000.0 Kg/m^3 for SFRLAC; the unit weight was determined, for the fresh concrete and 28-days air-dry concrete, in accordance with the procedures outlined in ASTM C 567. The fresh unit weights were determined at the time when the specimens or elements were cast, as was shown in section 2.3. At 28-days, the air-dry unit weight of LAC and SFRLAC were determined as 1856.0 Kg/m^3 and 1914.0 Kg/m^3 , respectively, based on three or more cylinder tests; the density for each concrete plate was determined by an approximate method, in order to obtain the actual unit weight (density) for the age and curing conditions to which it was subjected, weighing the cylinders related to each plate, and dividing those values by their volumes [they are listed later on in Table 6.1-2 (the unit weights of the reinforced plates are different, though not a great deal, due to the reinforcement)]. It seems that there is no significant difference between the fresh and hardened state density of concrete.

The relationship between unit weight of concrete, at different

ages, and its compressive strength is presented in Fig. 3.2-1 (a) and (b), based on the values presented in Table 6.1-2. It seems that LAC and SFRLAC have the unit weight around 1860.0 Kg/m^3 and 1960.0 Kg/m^3 , and that the unit weight increases with the compressive strength.

3.3. Compressive Strength

The strength of lightweight aggregate concrete is determined by the properties of the matrix, aggregates and their interaction [104]; hence their compressive and tensile strengths, modulus of elasticity, Poisson's ratio, along with creep and shrinkage characteristics of the matrix influence the compressive strength of concrete. Usually, the quality of LAC is judged on the basis of the compressive strength reached at 28 days.

Holm [14], FIP [15], and Gerritse [110] present comprehensive reviews of the phenomenological aspects of LAC subjected to compressive tests. A LAC with high mortar strength (the mortar strength depends on W-C ratio and in order to obtain a high compressive strength of mortar, and eventually of LAC, it is recommended to increase the cement content while the water is maintained at the same amount; if workability becomes critical, use admixtures) has a greater compressive strength but the compressive strength of LAC has a limiting value [14, 15], after which the influence of LA strength becomes important. The

"ceiling" value of the compressive strength is a function of quantity, size, shape, and distribution of the enveloped pores, but the decisive parameter is the strength of the largest individual particle (LA may have 30 to 60 percent voids volume). When using 10 mm maximum size lightweight coarse aggregate, strengths equal to or greater than dense concretes with the same amount of cement were obtained [14].

Compressive strength, in ceramics and metals, is related inversely proportional to porosity; however, this does not apply to LAC. The density of the aggregate and concrete cannot be a suitable indicator to characterize the LAC compressive strength; this relationship can be described by a range of values [15]. Using increased quantities of cement in the mix, and due to the compatible deformation of cement paste and aggregate, the cube compressive strength of LAC increases up to 60.0 MPa, even 70.0 MPa. Tests on differently cured specimens (different moisture contents) showed that water cured specimens behaved similar to high density concrete specimens, while the behaviour of partially dry specimens was not possible to be quantified due to the scattered results [3]. The replacement of the lightweight fines with sand is another method of increasing the LAC compressive strength because the sand mix requires less water, thus decreasing W-C ratio, and eventually increasing the compressive strength.

The compressive strength of LAC changes in time but there are no general accepted relationships between LAC compressive strength at different ages. The only way to find out these relationships, expressed as ratios, is by carrying out tests.

The compressive strength was determined as an average of three or more standard cylinders, 152.4·304.8 mm (6·12 in.), at different ages, i.e., about 30, 55, 95, 125, and 158 days, in accordance with the requirements of ASTM C 39; this method requires that the cylinders be moist cured until the moment of testing, while ASTM C 330 requires a different curing history for the cylinders - air-dried for the last 21 days at 50 percent humidity. It seems that the air-drying period improves the compressive strength of the cylinder; therefore ASTM C 39 yields lower strengths than ASTM C 330. The cylinders used for determining the compressive strength were moist-cured, and 3-4 days before testing they were removed from the curing environment and allowed to dry because of the necessity to cap them, i.e., to prepare them for the compressive test. Part of the cylinders were used to determine the modulus of elasticity following the procedures given in ASTM C 469. The specimens were cured as presented in section 2.4. The compressive strength of the specimen was obtained by dividing the maximum load attained during the test [using 600,000 pounds Soiltest Compression Testing Machine] by the average cross-sectional area of the specimen. It is known that the compressive strength increases with the rate of loading,

therefore the selected speed was 0.1 MPa/s - a value that comes close to the lowest speed loading provided by ASTM C 39.

Different failure types were noted for LAC and SFRLAC. Most of the LAC cylinders deteriorated in a cone and split type of failure, few of them exhibiting explosive failures with extended spalling. It is not possible to state exactly what type of fracture occurred in SFRLAC cylinders since only a few cracks were visible on the surface of the specimens; considering their position and distribution, it seemed as if most of the specimens failed in cone and shear type of failure.

The complete stress-strain curve obtained in a compressive test is an indicator of the concrete quality and fracture type; it was not recorded, although it was seriously considered:

- (a) using a LVDT between the compressometer rings in order to record the concrete compressive strains. Unfortunately, the laboratory had no LVDT of such dimension as needed; consequently, another attempt to measure the compressive strains was carried out, as described in point (b);

- (b) using electrical resistance strain gages glued on the cylinders surface in order to record the concrete compressive strains. This time, the complete curves were recorded in a few tests but the conversion and calibration

factors used, as indicated by the laboratory technicians, gave erroneous results; in other cases, the cracks on the cylinder surface passed under the strain gages, so that the results were wrong again.

Therefore the concrete strains were determined based on the compressometer readings.

The results of the tests are given in Fig. 3.3-1 and Table 3.3-1.

Analyzing the obtained results, it appears that:

- the specified value for the compressive strength, 41.37 MPa, was realized, except for SFRLAC in COE at 30 days of age;
- the compressive strength of concrete increases as it ages, regardless of the presence of fibres and curing environment;
- the increase in strength as a function of time is more dominant for SFRLAC than for LAC; the increase in strength, from 30 to 158 days, was 50.38 percent and 59.90 percent for SFRLAC in laboratory environment (LBE) and cold ocean environment (COE), respectively, while the increase in strength for LAC, for the same period of time, was 33.50 percent and 32.71 percent for LBE and COE, respectively;
- the strength increase at 120 to 130 days, for LAC in LBE

was slightly higher than for LAC in COE, i. e., 33.50 percent vs. 32.71 percent. The strength increase, during the same period of time, was higher for SFRLAC cured in COE than for SFRLAC cured in LABE, i.e., 59.90 percent vs. 50.38 percent;

- it seems that the fibre addition lowers slightly the strength for both environments, at almost all ages, see Table 3.3-2;
- the elastic properties of LAC vs. SFRLAC are given in Fig. 3.3-2. At values higher than the elastic limit of the material, SFRLAC exhibits larger deformation than LAC at the same value of loading. The curves were not completely recorded, the descending part missing due to the testing machine limitations; based on the failure mode and strain readings, it may be inferred that the SFRLAC toughness is greater than that of LAC. This is in agreement with the results obtained by Hughes et al. [111] regarding the energy absorption of SFRC in compression tests.

Conclusions

- the compressive strength values depend on the fibres orientation with respect to the loading direction: the fibre orientation is a critical parameter as it relates to the compressive strength. If the fibres could be dispersed within concrete mass as is needed for the expected loading

(perpendicular to the direction of loading in compressive states of loading and along the direction of loading in a tension state of loading), probably fibre reinforced concrete would be the ideal structural material. In fact, Edgington et al. [112] observed already the effect of table vibration, as a means of concrete compaction, on fibre orientation. Looking at the results, it seems that the fibres were not providing any improvement due to their random orientation, since the SFRLAC strength was slightly lower than for plain LAC. This absence of the stiffening effect might be accompanied by other factors, such as the pore size and distribution, leading to lesser strengths;

- the compressive strengths variation with the curing environment is given in Table 3.3-3. No definite relationship can be observed; since the cylinders were immersed in COE after seven days of curing in LABE, it seems, however, that COE lowers the compressive strength values;
- the strains sustained by concrete near 90-95 percent of the failure load increased with age and strength, except for SFRLAC in COE. For example, at 30 days, LAC in LABE having an average 47.94 MPa sustained strains of 0.0025 to 0.002946, while at 158 days, concrete having an average 64.0 MPa, sustained strains of 0.003195;
- the maximum measured strain on SFRLAC was 0.004297; the average measured strains on SFRLAC in LABE were:

-	at 30 days	0.002408
-	at 55 days	0.002913
-	at 95 days	0.002659
-	at 125 days	0.0029485
-	at 158 days	0.0028165

and the average measured strains on SFRLAC in COE were:

-	at 30 days	0.003402
-	at 55 days	0.003086
-	at 95 days	0.002723
-	at 125 days	0.002735
-	at 158 days	0.002778

- the maximum measured strain on LAC was 0.003514; the average measured strains on LAC in LABE were:

-	at 30 days	0.003293
-	at 55 days	0.002777
-	at 95 days	0.0029609
-	at 125 days	0.00247
-	at 158 days	0.003195

and the average measured strains on LAC in COE were:

-	at 30 days	0.002619
-	at 55 days	0.002852
-	at 95 days	0.0030865
-	at 125 days	0.002924
-	at 158 days	0.003167

- the change in compressive strength with age is related to 30-days value by ratios given in Table 3.3-4. It seems

- that the strength development, for both concrete types, proceeded at a higher rate in COE;
- a change in slope of the stress-strain curves occurred between 60-80 percent of the ultimate load, Fig. 3.3-2, indicating almost the same elastic limit for both materials;
 - the high strengths obtained in the cylinder tests were expected to a certain extent, since the mix had such a composition: rich in cement, cured, lightweight fines replacement with sand, careful aggregate selection and proportioning. It proved that the mix design was satisfactory;

Concrete which is exposed to COE, immediately after striking, for curing, had reduced compressive strength compared with the concrete cured as presented in section 2.4; a few cylinders, cured in different conditions were tested, to understand how much change occurs: the results showed a reduction of 50.40 percent or 52.50 percent in concrete compressive strength when seawater at 0 °C was used to cure the concrete compared with the concrete cured in fresh water at 23 °C, or with the concrete cured in laboratory air at 23 °C, respectively. The results are given in Table 3.3-5.

The frozen cylinders had, immediately after removal from COE, a glossy external surface. Following the testing, a closer look

within them revealed that only the outside layer of concrete was frozen while inside, closer to the middle of the cylinder, the concrete was weak and sandy. It might be mentioned that literature data points out to an opposite effect: the presence of some moisture in the hardened air-entrained concrete at low temperatures has a beneficial effect on strength due to the ice formed in the capillary pores system [30, 113]. The tests performed on the above mentioned concrete cylinders showed such a reduction in compressive strength probably because of the delayed hydration of the cement paste and the reduced resistance of the cement paste to the expansive forces developed by the water during freezing. Hence it is essential to protect fresh concrete from early freezing, even if a low W-C ratio of 0.4, high cement content, and all the prerequisites necessary for high strength, durable concrete were followed.

3.4. Modulus of Elasticity

The static chord (secant) modulus of elasticity in compression, E , was determined on standard specimens, around 30, 55, 95, 125, and 158 days, in accordance with ASTM C 469, between an upper test stress equal to 40 percent of the cylinder compressive strength and a lower test stress of small magnitude corresponding to 50 millionths strain level.

A few observations were made, as follows:

- the obtained E values, see Table 3.4-1 and Fig. 3.4-1, are in the expected range for LAC (20,000 and 24,000 MPa), with a few exceptions, and do not seem influenced too much by the fibres presence, higher variability of the E values being observed for COE than for LABE, see Table 3.4-2;
- the curing influence of the environment, see Table 3.4-3 is more present for SFRLAC, the actual values varying from-22.63 to 12.51 percent, while for LAC the actual values are varying between -10.88 and 4.67 percent. All the values are compared with respect to the LABE;
- no clear time-dependence of the E values could be established. Using Eqn. 1, applicable to lightweight concrete, the results are presented in Table 3.4-4:

$$E_t = E_{28} \cdot (0.4 + 0.6 f_c' / f_{28}) \quad (1)$$

in which a few terms were replaced:

$$E_t = E_{30} \cdot (0.4 + 0.6 f_c' / f_{30})$$

Eqn. 1 gives reliable results if the ratio between (f_c' / f_{30}) has not a significant greater value than 1, as it is the case in this work, specially up to one hundred days.

- the theoretical values for the modulus of elasticity are

given in Table 3.4-5. They are computed as follows:

(i) Canadian standard [114]:

$$E_c = 0.043(\delta_c^V)^{1.5} \sqrt{f_c'} \quad (2)$$

(ii) Ola Berge's formula [15]:

$$E = k \delta_c^V (f_c')^{1/3} \quad (3)$$

in which $k = 3.5$, a constant. k has been assigned different values, viz., 3.05, 3.3 and 3.5 FIP [15], or 3.5 by the Norwegian Code.

(iii) CEB-FIP Model Code formula [15]:

$$E = 9.5 (f_c')^{1/3} (\delta_c^V / 2400)^2 \quad (4)$$

(iv) Teychenné et al. formula [115]:

$$E = 9.5 (f_c' + 8)^{0.33} (\delta_c^V / 2400)^2 \quad (5)$$

The values of the unit weight and the compressive strength used to compute the modulus of elasticity are those determined as shown in sections 3.2 and 3.3.

- as observed in section 3.3, concrete strength increased

with age, due to matrix properties changes; therefore, a similar increase was expected for E values. In this study E of SFRLAC increased by 3.25 percent and 26.34 percent for LABE and COE, respectively, during 128 days. It is difficult to visualize the factors that cause the increase in modulus of elasticity when comparing LAC with SFRLAC. When SFRLAC shows higher E, that gives the idea that the fibres are forming stiff inclusions, working as points of stress concentrations within the material [64];

- the causes of the results variability may be due to imprecision of the compressometer readings at the testing moment, and in SFRLAC case, to the fibres distribution within concrete;
- the theoretical modulus of elasticity variation with respect to age is presented in Table 3.4-6. As it is shown, no clear relationship was established among E values due to their variability.

3.5. Tensile Strength - Flexural Strength

One of the important characteristics of SFRC is its tensile strength; the greater the tensile strength, the better is the concrete performance, especially as regards its shear resistance, anchorage and bond strength. There are three types of tests [15] which provide data regarding the tensile strength due to the different stress distributions in the cross section

when fracture occurs:

- flexural tensile test; it provides the tensile strength known as modulus of rupture (MOR) and is determined on small beams; it could be related to the cube compressive strength [15]. Actually, MOR is a characteristic of fibre concrete, briefly discussed in section 1.4.2. Paillère et al. [95] highlighted the improved cracking and bending strength of SFRLAC with hooked collated fibres as compared with straight fibres. Even the deflections are reduced under sustained flexural loading [43]. In a structure, however, the presence of well distributed reinforcement increases the experimentally obtained values up to 25 % [15];
- splitting tensile test; useful in providing an estimate for the diagonal tensile resistance of structures. FIP recommends the following relationship related to cube compressive strength [15]:

$$f_{cts} = 0.23(f_{cu})^{2/3} \quad (6)$$

- the European Concrete Committee recommended for the splitting tensile strength the following formula:

$$f'_t = 9.5 \sqrt{f'_c} \quad (7)$$

where $f'_t = f_{cts}$, f'_c are in psi

- pure tensile strength; quite difficult to realize a "pure" tensile test but there are formulae which quantify this value [15].

Gerwick [1] suggests the idea of implementing within the standards a limit value of the flexural tensile strength as it has already been done [116]: a tensile "characteristic" strength could be determined on prismatic pieces by:

$$R_b = 0.7 + 0.06f'_c \quad (8)$$

The values listed in Table 3.5-1 are just indicative, since the experimental compressive strength values were taken from section 3.3; however, the above relationship yields lower results than the actual experimental values.

In the present study, the flexural strength was obtained experimentally, carrying out tests on two sets of beams 100-100-800 mm manufactured with LAC and SFRLAC respectively, on a 300 mm span, tested under third-point loading; the beams were arranged with the trowelled face on one side. The tests conformed to the procedures outlined in ASTM C 78 and ASTM C 1018.

The beams were cast in oiled wooden formwork and within another 24 hours - while protected against humidity loss - were removed

from the formwork and stored in water at about 20 °C. Part of them were removed from water after 4-7 days and stored in seawater at 0 °C. It is assumed that this mode of curing is appropriate in simulating the cold ocean environment (COE).

Published research data emphasize the importance of the strain rate of loading on the test results: increased strain rate loading, increases the modulus of rupture (MOR) and the deflection at maximum load for unreinforced specimens due to the decreased process of internal cracking. The same trend was observed for fibre reinforced concrete; therefore the lower the strain rate, the worst possible results are obtained. A moderate strain loading case is one in which the strain rate is 10^{-2} to 10^{-5} /minute.

At about 30, 60 and 90 days, the flexural strength was determined in a three-point bend test at a loading rate of 0.0671 N/s or 15.1 KPa/s, at the extreme fibre, using a closed-loop MTS machine. The load and deflection signals from the MTS machine were recorded by the X-Y plotter automatically. The flexural strength (MOR) was determined based on ASTM C 78 calculations. Because the crack initiation occurred in the constant moment zone and the crack propagation took place through the same crack without the development of supplementary cracks, the formula used to compute the MOR values was:

$$R = Pl/b_1d_1^2 \quad (9)$$

and the results are given in Table 3.5-1. Representative load-deflection curves are presented in Figs. 3.5-1 and 3.5-2. The initially obtained curves exhibited upwards concave curves immediately after start due to the unevenness ("high spot points") and unparallelism of the specimen surfaces resting on the blocks of the testing machine. Since the rigidity of the tested specimen cannot increase during testing, these portions of the curves were excluded and the "real" load-deflection curves of the prisms were analysed - Figs. 3.5-1 and 3.5-2. The approximation has been used previously by Johnston [117]; a change in the slope of the load-deflection curve for SFRLAC, at about 60-85 percent of the maximum load occurred - value of the loading considered as the proportional limit. It is worth mentioning that tests were carried out to calibrate the testing machine, and to obtain the deflection within the three-point testing apparatus. This deflection (within the apparatus) has been subtracted from the total deflection given by the built-in testing machine transducer; thus the "real" deflection was found.

Conclusions:

- the large variation of results are to be attributed to the particular mix design used and the effect of random

- uncontrolled steel fibre distribution. Should bigger beam size be used, probably the results would make more sense; the size of the specimens was chosen in order to be significant for this study, and have a means of comparison with previous tests of this type [66];
- the shapes of the obtained load-deflection curves for SFRLAC are not similar with that provided in Reference 66; ACI graph for MOR seems to be for SFRC with straight, not deformed ends (hooked) fibres [53];
 - as expected, SFRLAC modulus of rupture, as defined in Reference 66, has higher values than the corresponding ones for LAC, and a distinct first crack as opposed to the ultimate tensile strength of LAC; the MOR test yields higher values than it should for SFRLAC, because the material is supposed to behave elastically up to failure [57, 65]. However, Hibbert et al. [65] justified the use of the method as long as the final application of SFRC is for flexural systems.
 - the modulus of rupture for SFRLAC (computed as required by Reference 66) increases with age, 58 percent for LABE and 40 percent for COE, respectively, during about 60 days, Table 3.5-1;
 - LAC modulus of rupture also increases with age, about 32 percent for LABE and about 167 percent for COE, respectively, Table 3.5-1;
 - the tests performed on SFRLAC to obtain the maximum load in

- flexure, with the speed recommended in ASTM C 78 (14-21 KPa/s at the extreme fibre of the section - actually 15.1 KPa was used), yield the results as given in Table 3.5-2;
- using ASTM C 1018 (speed of loading was 0.001 mm/s), the maximum load in flexure are listed in Table 3.5-3. It can be observed from this study, that the results obtained using ASTM C 1018 are not far away from those obtained using ASTM C 78; it seems that an increased strain rate of loading does not increase the MOR values, as expected, for SFRLAC;
 - for LAC, a higher rate of strain loading, at 34 and 52 days (results given in Table 3.5-1), gives, with one exception, higher values for MOR; at 84 days, this is not valid anymore, Table 3.5-4 vs. Table 3.5-1;
 - the average flexural strengths of plain concrete specimens represent 10.5 and 6.5 percent of the average strengths of 152.4*304.8 mm (6*12 in.) cylinders, at about 30 days of age, for LABE and COE, respectively;
 - the average flexural strengths of SFRLAC specimens represent 13.5 and 20.2 percent of the average compressive strength of 152.4*304.8 mm (6*12 in.) cylinders, at about 30 days of age, for LABE and COE respectively;
 - future investigations are needed to improve the uniform fibre distribution within concrete (isotropy) and better guidelines for measuring properties with a simple apparatus.

3.6. Absorption

Haynes [118] emphasizes the difference between concrete permeability to freshwater and seawater, respectively. In some of his monitored tests, the concrete exposed to seawater showed decreased permeability, explained as the effect of the precipitation of chemical reactions outputs into the porewater of the cement stone, thus impeding the seawater from entering the concrete. The increase in watertightness of concrete exposed to seawater is known [119], although there is no generally accepted theory with regard to the mechanism or mechanisms which causes it.

Permeability depends on the void system within concrete, i.e., size, distribution and continuity of the four types of voids: (1) air voids filled with entrapped air during mixing or intentionally entrained air, using AEA; (2) sub-microscopic capillary voids, replacing the space occupied by the mixing water; (3) sub-microscopic gel voids, created as the cement hydrates; (4) voids within aggregates, such as within LA. Since the air voids are not interconnected, the permeability is not increased by entrained air. It seems that the capillary voids control the permeability; they can be best controlled, keeping as low as possible the W-C ratio, and allowing for a complete hydration of the cement paste.

Bueufel et al. consider the porosity in the cement paste to be produced mainly by the capillary spaces, and secondarily by the gel pores within the cement gel [119]. The LA may have 30 to 60 percent voids volume; these voids are interconnected within the aggregates, and could be unfavourable for concrete permeability. However, it was shown that concrete permeability does not depend on LA permeability (porosity), but on the cement paste permeability surrounding each aggregate particle [118].

Since MEL-lite concrete was supposed to be made for a marine application, its absorption and wet density were looked at, both being dependent on permeability. LAC cylinders were air-dry cured in laboratory for about 90 days, and then were immersed in fresh water for about 3 days (since the absorption for fresh water is greater than for seawater), and then the surface-saturated-dry (SSD) weight was determined, weighing them; thereafter, they were oven-dried until they reached a constant weight. The theoretical wet density at 3 days, was determined as 2034.0 Kg/m³. It is worth mentioning that this could be considered just a relatively saturated concrete (since the investigator did not monitor the weight constancy of the wet cylinders after 3 days, it is difficult to say when the concrete reached its saturated condition). Probably an initially oven-dry specimen instead of a LAGE-dry specimen gives more than 5.4 percent absorption. The presented results are not a substitution for the initial surface absorption test (ISAT), but gives a

better idea about the material employed. It is thought that the absorption by concretes, higher for LC, and which influences its durability, is governed by the cement paste quality [22, 41, 118, 119], the amount of air-entrained and the quality of the aggregates. Consequently, the concrete permeability depends primarily on the quality of the cement paste.

Table 3.3-1: Compressive Strengths of Lightweight Aggregate and Steel Fibre Reinforced Lightweight Aggregate Concretes

Age (Days)	Compressive Strength [MPa]			
	LAC		SFR/LAC	
	LABE	COE	LABE	COE
30	47.94	44.23	41.60	37.76
55	48.15	49.04	41.87	42.67
95	49.82	46.00	49.73	45.13
125	53.25	53.24	57.31	50.31
158	64.00	58.70	62.56	60.38

Table 3.3-2: Comparison of Strengths of LAC and SFR/LAC

Age (Days)	Compressive Strength Variation with Steel Fibres Addition			
	LABE		COE	
	LAC	SFR/LAC	LAC	SFR/LAC
30	100%	-13.22%	100%	-14.63%
55	100%	-13.04%	100%	-12.99%
95	100%	- 0.18%	100%	- 1.89%
125	100%	+ 7.62%	100%	- 5.50%
158	100%	- 2.25%	100%	+ 2.86%

Table 3.3-3: Comparison of Strengths of LAC and SFRLAC

Age (Days)	Compressive Strength Variation with Curing Environment			
	LAC		SFRLAC	
	LABE	COE	LABE	COE
30	100%	- 7.73%	100%	- 9.23%
55	100%	+ 1.84%	100%	+ 1.91%
95	100%	- 7.67%	100%	- 9.25%
125	100%	+ 0.00%	100%	-12.21%
156	100%	- 8.28%	100%	- 3.48%

Table 3.3-4: Comparison of Strengths of LAC and SFRLAC

Concrete	Strength Ratios at Different Ages, LABE			
	30/55	30/95	30/125	30/158
LAC	0.996	0.962	0.900	0.749
SFRLAC	0.993	0.889	0.772	0.707
Strength Ratios at Different Ages, COE				
LAC	0.902	0.961	0.830	0.753
SFRLAC	0.885	0.837	0.750	0.625

Table 3.3-5: Influence of Improper Curing on the Compressive Strength of LAC

Curing Period 28 days		Compressive Strength MPa
24 hours in mould, thereafter submerged in fresh water at 23°C	CYL-1	46.06
	CYL-2	51.85
24 hours in mould, thereafter cured in air at 23°C	CYL-1	48.26
	CYL-2	45.81
24 hours in mould, thereafter cured in sea-water 0°C	CYL-1	26.82
	CYL-2	22.56

Table 3.4-1: Modulus of Elasticity of LAC and SFRLAC

Age (Days)	Modulus of Elasticity (MPa)			
	LAC		SFRLAC	
	LABE	COE	LABE	COE
30	24,765.0	25,923.0	24,556.0	19,003.0
55	24,497.0	22,526.0	21,427.0	22,392.0
95	21,790.0	19,419.0	24,534.0	27,716.0
125	20,288.0	21,147.0	23,400.0	21,044.0
158	23,294.0	22,624.0	25,355.0	24,009.0

Table 3.4-2: Comparison of E Values of LAC and SFRLAC

Age (Days)	Modulus of Elasticity Variation due to Steel Fibre Presence			
	LABE		COE	
	LAC	SFRLAC	LAC	SFRLAC
30	100%	99.16%	100%	73.30%
55	100%	87.47%	100%	103.84%
95	100%	112.60%	100%	142.73%
125	100%	115.34%	100%	99.51%
158	100%	108.85%	100%	106.12%

Table 3.4-3: Comparison of E Values of LAC and SFRLAC

Age (Days)	Modulus of Elasticity Variation due to the Curing Environment			
	LAC		SFRLAC	
	LABE	CCE	LABE	COE
30	100%	104.67%	100%	77.37%
55	100%	92.00%	100%	104.50%
95	100%	89.12%	100%	112.51%
125	100%	104.23%	100%	89.93%
158	100%	97.12%	100%	94.70%

Table 3.4-4: Dependence of E on the Compressive Strength

Age (Days)	Modulus of Elasticity [MPa] and Compressive Strength [MPa]							
	LAC				SFRLAC			
	LABE		CCE		LABE		COE	
	f'_c	E	f'_c	E	f'_c	E	f'_c	E
30	47.94	24765.0	44.23	25923.0	41.60	24556.0	37.76	19003.0
55	48.15	24830.0	49.04	27614.0	41.87	24652.0	42.67	20485.0
95	49.52	25348.0	46.00	26545.0	49.73	27435.0	45.13	21228.0
125	53.25	26411.0	53.24	29091.0	57.31	30120.0	50.31	22792.0
158	64.00	29743.0	58.70	31011.0	62.56	31979.0	60.38	25833.0

Table 3.4-5: Computed E Values

Equation	Computed LAC Modulus of Elasticity [MPa]									
	30 Days		55 Days		95 Days		125 Days		158 Days	
	LABE	COE	LABE	COE	LABE	COE	LABE	COE	LABE	COE
Eqn. 2	23633	22700	23819	24039	24711	23745	25885	25882	27395	26236
Eqn. 3	23483	22861	23607	23751	24193	23558	24953	24951	25913	25177
Eqn. 4	20439	20049	20625	20751	21415	20853	22282	22281	22604	21961
Eqn. 5	21518	21031	21709	21823	22505	21998	23346	23345	23508	22917
Experimental	24765	25923	24497	22526	21790	19419	20288	21147	23294	22624
Computed SFRAC Modulus of Elasticity [MPa]										
Eqn. 2	24075	22937	23830	24057	27112	25828	31505	29519	29466	28949
Eqn. 3	23776	23020	23514	23764	25735	24916	28446	27237	27205	26885
Eqn. 4	21965	21267	21621	21758	24248	23476	28257	27056	25101	24806
Eqn. 5	23291	22674	22919	23041	25485	24789	29155	28420	26128	25856
Experimental	24556	19003	21427	22392	24534	27716	23400	21044	25355	24009

Table 3.4-6: Computed E Values as a Function of Age

Particulars		Theoretical LAC Modulus of Elasticity [MPa] vs. Age									
		30 Days		55 Days		95 Days		125 Days		158 Days	
		LABE	COE	LABE	COE	LABE	COE	LABE	COE	LABE	COE
Equation 1 Page 89	2	23633	22700	23695	24181	24189	23245	25204	25475	28383	27156
	3	23483	22861	23545	24353	24035	23410	25044	25656	28203	27348
	4	20439	20049	20493	21357	20920	20530	21797	22499	24548	23984
	5	21518	21031	21574	22403	22024	21536	22948	23602	25843	25159
Experimental		24765	25923	24497	22526	21790	19419	20288	21147	23294	22624
		Theoretical SFRLAC Modulus of Elasticity [MPa] vs. Age									
Equation 1 Page 89	2	24075	22937	24169	24726	26898	25623	29530	27511	31353	31181
	3	23776	23020	23869	24816	26564	25716	29163	27611	30964	31293
	4	21965	21267	22051	22927	24540	23759	26942	25508	28605	28911
	5	22291	22673	23382	24442	26022	25328	28568	27194	30332	30822
Experimental		24556	19003	21427	22392	24534	27716	23400	21044	25355	24009

Table 3.5-1: Modulus of Rupture of LAC and SFRLAC

Age (Days)	Modulus of Rupture (MOR) [MPa]							
	LAC				SFRLAC			
	LABE	*	COE	*	LABE	*	COE	*
30 to 40	5.03	3.58	2.86	3.35	5.60	3.20	7.63	2.96
50 to 60	6.36	3.59	4.84	3.64	5.80	3.21	7.50	3.26
80 to 90	6.62	3.69	7.65	3.46	8.88	3.68	10.75	3.41

Note: The values listed in * columns are calculated using Equation 7

Table 3.5-2: Flexural Loads of SFRLAC Beams

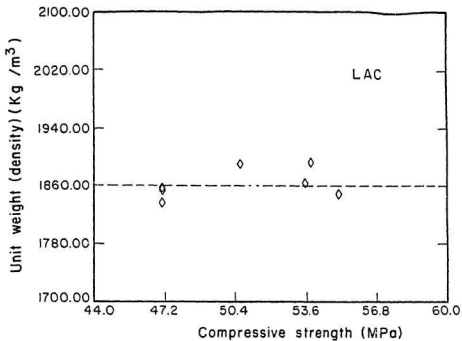
Environment	Age Days	Load Levels (kN)	
		At first crack	At maximum load
LABE	36	10.65	18.67
	60	8.34	19.33
	90	18.30	29.60
COE	38	25.50	25.43
	53	16.80	25.00
	90	26.33	35.83

Table 3.5-3: Flexural Loads of SFRLAC Beams

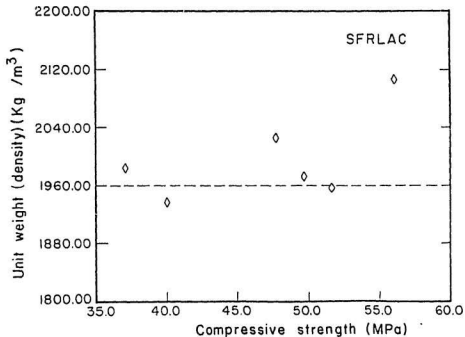
Environment	Age (Days)	Load Levels (kN)	
		At first crack	At maximum load
LABE	40	12.86	18.76
	52	23.54	43.25
	90	23.01	35.77
COE	34	16.56	20.08
	52	22.58	34.38
	90	23.96	31.82

Table 3.5-4: Modulus of Rupture of LAC at Higher Rate of Loading

Age (Days)	LAC - MOR (MPa)	
	LABE	COE
34	1.73	2.27
52	5.73	5.34
84	7.06	8.14



(a) LAC



(b) SFRLAC

Fig.3.2-1 The relationship between compressive strength and unit weight (density)

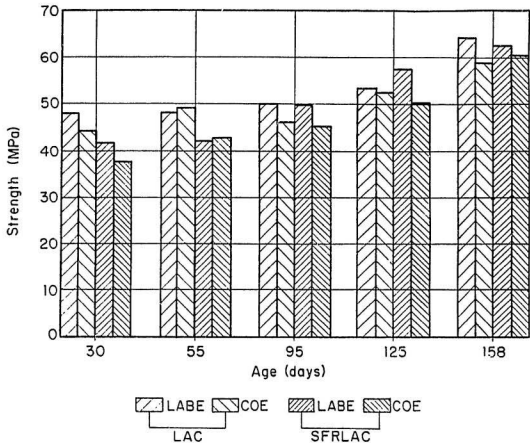


Fig. 3.3-1 Variation of compressive strength of concrete cylinders with age (each value is an average of three or more tests)

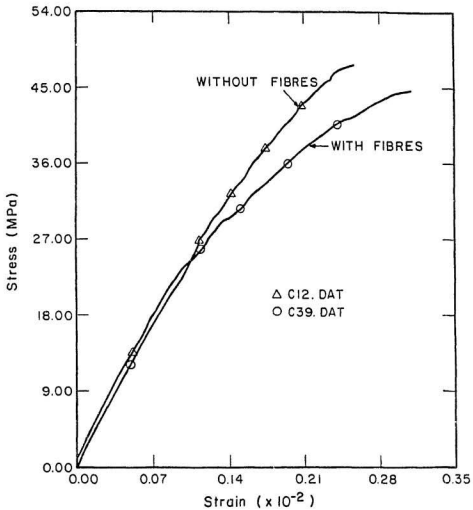


Fig. 3.3-2 Compressive strength vs. axial strain - Typical stress-strain curves for FRLAC and LAC cylinders

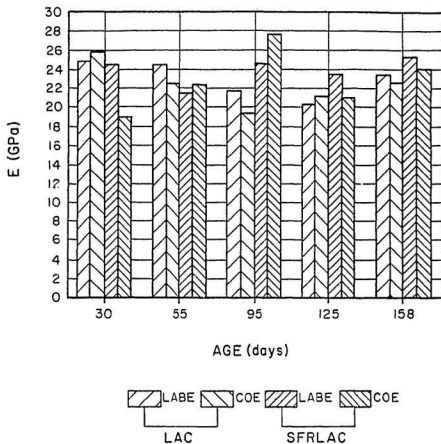


Fig.3.4-1 Dependence of modulus of elasticity on the age of the cylinder (average of three or more values)

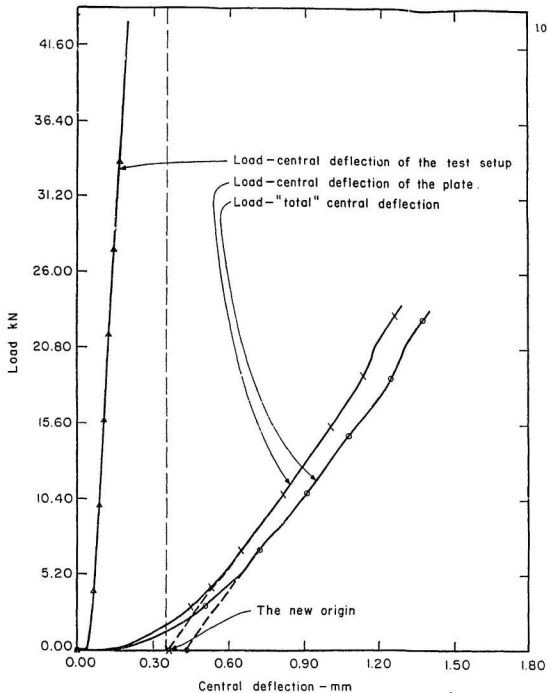


Fig.3.5-1 Representative LAC load-central deflection curves obtained in flexural test.

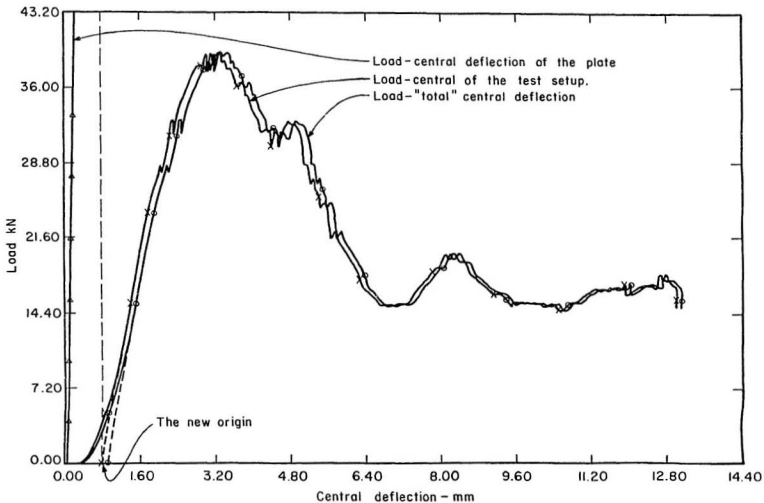


Fig. 3.5-2 Representative SFRLAC load-central deflection curves obtained in flexural test.

CHAPTER 4. THEORETICAL STUDY: LAC AND SFRLAC PLATES

As shown in Chapter 3, LAC and SFRLAC are satisfactory with regard to the specified quality. In this chapter, the structural properties are to be determined, and consequently the structural behaviour of the materials.

4.1. Plate design

In general, a concrete structure designed for Arctic or sub-Arctic environment, such as offshore Newfoundland, has a surrounding concrete wall interconnected with concrete stiffeners running in both vertical and horizontal directions [120]. Large dynamic loads are likely to occur on such an offshore plated structure due to extreme environmental forces: wave slamming, dropped objects, lateral collision with flotsam, ships or ice, due to explosion, or loss of pressure differential [13, 14]. A meaningful understanding of the dynamic behaviour of the structure or its components under this type of loadings is possible when carrying out dynamic tests or the results obtained in static tests are extrapolated to characterize their dynamic behaviour.

During the initial stage of the research programme, a plan was laid to carry out theoretical and experimental studies regarding

the behaviour of fixed LAC and SFRLAC plates subjected to static and dynamic (impact) loadings. Different plate dimensions were considered: 1.95·1.95·0.10 m, 1.70·1.70·0.10 m, 1.00·1.00·0.10 m, with a free span of 1.75 m in either direction for the first type of plates, 1.50 m and 0.75 m, respectively, for the smaller type of plates; the thickness was chosen as 100 mm (4 in.) - the minimum possible thickness for proper construction. Thus the effect of free span variation on the behaviour of the plates could be studied.

Eventually, the tested plates were 1.95·1.95·0.10 m and 1.70·1.70·0.10 m, on a free span of 1.50 m. Since it was assumed that the supports were not influencing the failure modes, the chosen geometry proved useful in designing the panels for punching shear failures or flexural failures. The flexural reinforcement used consisted of bars No. 10, Grade 400, and the shear steel was 6.35 mm diameter round bars, Grade 300. The experimental steel stress-strain curves are given later in Figs. 5.3-1 and 5.3-2. The concrete, either LAC or SFRLAC, had the same recipe as presented in Chapter 2. The concrete properties, at the time of testing, were determined and used in assessing the theoretical results; they are given in Chapter 6. Chapter 5 presents the loading procedure, instrumentation and monitoring of the plates.

An initial rough assumption regarding the loads was made

considering the elastic behaviour of the plates and assuming that under the equivalent static loading the plates could deflect as much as $L/360=4.17$ mm at the middle of the plates; the equivalent static loading was calculated based on the potential energy stored in the plate:

$$Wg(h_2+w) = 1/2 W_e w \quad (10)$$

where

$h_2 = 2.0$ m, dropped weight height

$w = 4.17$ mm, vertical deflection

$W_e =$ equivalent static loading

$W = 235.5$ Kg (2309.55 N), the biggest available weight in the laboratory

Replacing these values in equation (10), we obtain:

$$2309.55 \cdot (2000+4.17) = 1/2 W_e \cdot 4.17 \quad (11)$$

where from, $W_e = 2220.0$ kN.

This value is obviously pretty high, therefore changing the dropped weight height to 1.2 m and keeping $w = 4.17$ mm, Eqn. (11) yields:

$$2309.55 \cdot (1200+4.17) = 1/2 W_e \cdot 4.17 \quad (12)$$

where from, $W_e = 1333.86$ kN, which again is too high; besides the available equipment in the laboratory cannot provide this loading. Therefore, this approach proved to be too approximate and not precise; consequently the panels were not designed and tested for impact loads. Since it was decided to carry out only static tests, other precise theories were not employed [26, 121]. The testing arrangement planned for the static tests conducted in this study, is indicative of a heavy concentrated load acting on the centre of the plate allowing the use of the available laboratory in terms of test machine, recording equipment and other monitoring devices; the results obtained from this study would serve as a basis of comparison for the dynamic tests, planned for the future phase of investigation.

Computation of the Ultimate Flexural Strength

It is known that the yield-line methods give good prediction for plain and steel fibre reinforced concrete [26, 88, 92, 122]. The design approaches are based either on the static methods (lower bound solutions) or on kinematic methods (upper bound solutions). The kinematic methods fulfill the compatibility of the deformation at the ultimate limit state, but do not give an optimum design. The static methods lead to an optimum design, but, generally, the compatibility of the deformation is not fulfilled. Although the yield line method implies a pure mode of failure of the plate, the real case is likely to be a combined

punching shear and flexural failures of the plate. Hence the analysis must consider not just the moment alone, but also the punching shear or diagonal tension failure too, which is presented further on. It was expected that the calculated load by yield line methods would be less than the test results - the increase in load would appear due to the membrane action; consequently, the plate carrying capacities were computed using yield-line methods; thereby it was possible to predict the approximate maximum loads that could be carried by the plates.

The first set of plates, Series I, were designed to fail in punching shear, with the flexural bars arrangement shown in Fig. 4.1-1; the plates had 10 No. 10 bars/m width of plate; the ultimate resisting moment, M_r , was calculated conforming to the standard requirements, as 25945.0 Nm/m width of plate [114]. Two plates, P1 and FP1, were reinforced with 10 No. 10 bars/m width of plate as shown in Fig. 4.1-1 [also see Table 6.1-1].

Initially, the plates were supposed to be clamped along the edges in order to carry out the dynamic tests. Hence, in order to avoid cracking of the top surface of the slab, corner reinforcement was provided, as much as to allow one to consider that $m' = \frac{1}{4}$ of the middle field moment M_r could occur at these locations. The needed area of reinforcement was selected as wire mesh 102•102 - MW18.7•MW18.7 with equal uniform distributed area in either direction, as shown in Fig. 4.1-2.

The M_r value was computed assuming the concrete compressive strength as $f'_c = 41.37$ MPa and the steel yield stress as $f_s = 400.0$ MPa. M_r is written as:

$$M_r = m + M \quad (13)$$

The assumed collapse mechanism is shown in Fig. 4.1-3, and the yield moments per unit width of plate were determined as follows:

- (1) Due to the self weight [123]:

$$m = qL^2/23 = 169.41 \text{ Nm} \quad (14)$$

where

$$L = 1.5 \text{ m, free span;}$$

- (2) Due to the concentrated load in the middle of the plate [123]:

$$M = P_u/7.15 \quad (15)$$

Eqn. (13) yields $P_u = 184.29$ kN.

Ong et al. [124] give a formula for computing the ultimate flexural strength:

$$P_u = 8M[1/(1-b_2/2L)-3+2\sqrt{2}] \text{ in which} \quad (16)$$

Replacing the actual values in Eqn. 16, it yields $P_u = 180.43$ kN.

The Joint ACI-ASCE Committee provides for the following formula [125]:

$$V_{flex} = m_o[8/(1-c/a)-1.37] = 193.83 \text{ kN} \quad (17)$$

The results are listed in Table 4.1-1.

The second set of plates, Series II, with the flexural bars arrangement given in Fig. 4.1-4, had 6 No. 10 bars/m width of plate, and it was used for P2, FP2, P3, FP3, P4, FP4, P5, FP5, P6, FP6, P7 and FP7. The plates pertaining to this set, were designed to fail, first of all, in flexure; the ultimate flexural resisting moment, M_r , was calculated as for the first set of plates, $M_r = 16221.18$ Nm/m width of plate [114].

Using Eqns. (13) to (17), the maximum force that could be applied on the plates was determined similarly as for Series I, and the results are listed in Table 4.1-1.

The shear reinforcement arrangements are shown in Figs. 4.1-5, 4.1-6, and 4.1-7; the corner reinforcement was used for this

Series too, for the sake of comparison.

Fibres Contribution to Flexural Resistance

Swamy presents a comprehensive study of the ultimate flexural strength of SFR lightweight concrete slabs [91]. Basically, the proposed method assumes that after cracking, just the fibres alone carry the tensile stresses as it should be the case in pure tension, assuming perfect bond between the fibres and the matrix. The stress provided by fibres, σ_{cu} , was computed using the method recommended by Swamy [90]; due to the lack of data for obtaining the length correction factor, it was assumed that $\eta_1 = 0.7$. The other parameters were taken as $\eta_0 = 0.41$, $\eta_b = 1.0$, and the bond strength, $\tau = 2.5$ MPa [90]. Therefore the post-cracking stress after concrete has cracked:

$$\begin{aligned}\sigma_{cu} &= 2 \cdot \tau \cdot \eta_0 \eta_1 \eta_b (L_f/d_f) V_{f1} \\ &= 2 \cdot 2.5 \cdot 0.41 \cdot 0.7 \cdot 1.0 \cdot (50/0.5) \cdot 0.008 \\ &= 1.15 \text{ MPa}\end{aligned}\tag{18}$$

A more realistic approach has been used by the author to determine the σ_{cu} value as shown in Appendix B, i. e. $\sigma_{cu} = 1.01$ MPa.

The calculations of the flexural strength of the plates were completed as indicated in Reference 90 and based on the

theoretical concepts of Reference 91. The required assumptions are shown in Fig. 4.1-8. The calculations are shortly outlined below and in detail, in Appendix C - "Iterative Process to Determine x and f_s ".

Series I

- forces in the tension zone, Fig. 4.1-8 (a)

$$F_{ft} = \sigma_{cu}b(h-x) \quad (19)$$

$$F_{st} = A_s f_s \quad (20)$$

- forces in the compression zone, Fig. 4.1-8 (b)

$$F_c = (0.72f_{cu}/\epsilon_{cu})(\epsilon_{cu}-\epsilon_o/3)bx \quad (21)$$

$$k_2 = [[(2-\epsilon_o/\epsilon_{cu})^2+2]/[4(3-\epsilon_o/\epsilon_{cu})]]x \quad (22)$$

The SFRLAC strains in compression were limited to 0.002408 - an average ϵ_{cu} value - at 30 days for SFRLAC in LABE, obtained using the experimental stress-strain curves as shown in Chapter 3.

The forces equilibrium in the cross section is given by:

$$F_{ft} + F_{st} = F_c \quad (23)$$

wherefrom x was determined.

From the known values of ϵ_{cu} and x , the steel stress in the flexural bars was obtained. Thereafter, the f_s value was substituted in Eqns. 19 and 23, and a new value of x was obtained. This iterative process was repeated until the values of x and f_s converged, see computer program in Appendix C. The actual stress-strain curve shown in Fig. 5.3-1 was used to take in consideration the real stress (strain hardening effect). The resulting values were $x = 24.36$ mm and $f_s = 545.35$ MPa.

The resisting moment M_r , was calculated as:

$$\begin{aligned} M_r &= F_c(x-k_2) + F_{st}(d-x) + F_{ft}(h-x)/2 \\ &= 44650.34 \text{ Nm.} \end{aligned} \quad (24)$$

Applying Eqns. 15, 16, 17 and 24 the values of the ultimate loading are computed, and listed in Table 4.1-1.

Series II

The same calculations were used as they apply to the specific conditions of the plates pertaining to this Series; the results are to be found in Table 4.1-1.

The results given by Eqn. 16 are used to compute the shear resistance of the plates.

Computation of the Punching Shear Capacity

Generally, the methods employed in computing the shear capacity are based on simple mechanical models. In reinforced concrete, without shear reinforcement, considering the equilibrium forces along a diagonal crack, the external shear is resisted by the concrete in the compression zone at the tip of the diagonal crack, aggregate interlock action and dowel action of the longitudinal bars [91, 129]. If shear reinforcement is present, its effect in resisting the external shear is added to the above mentioned concrete resistance. The most difficult part is to assess the concrete resistance since it has so many contributions to it. Usually, all the contributions are lumped in one term, the concrete shear resistance, V_C , which is assumed be equal to the shear at the diagonal cracking.

When shear reinforcement is used, all the possible failure modes are to be considered. A wide beam mode of failure is not likely to occur in a plate. In order to avoid the failure surface to develop between the load perimeter and the innermost shear reinforcement, the distance to the first shear bars is recommended as $d/2$ [121, 129]. If the failure outside the shear reinforcement is considered, the punching resistance could be predicted by the formulae used for shear punching resistance in plates without shear reinforcement, if the appropriate perimeter is considered. If the failure is considered within the region of

the shear reinforcement, then a combination of components V_S , from steel, and V_C , from concrete, are to be considered. Regan [129] explains how the shear steel resistance component and concrete resistance component vary with the inclination and position of the potential failure surfaces passing through reinforcement. Tests showed that the shear cracking (diagonal cracking) occurs, in a slab without shear reinforcement, at about 70 percent of the punching strength and that the diagonally cracked structure is stable as the load reaches 100 percent of the punching strength. This suggests that, the shear resistance of a cracked slab with shear reinforcement could be considered as made up by the shear steel resistance component(s) and concrete resistance component, but V_C is not necessarily identical with the resistance of a slab without shear reinforcement. V_C could be less than 30 percent after the diagonal cracking had occurred, depending on the cracking width, and shear reinforcement arrangement.

Eventually, a 45° failure surface is a reasonable assumption for computations; therefore

$$V = V_S + V_C$$

In BS 8110, V_S is taken as the sum of the resistances of two layers of shear steel spaced $0.75 d$ apart, while the Code [114] requires to take into account all the potential failure surfaces

without being specific.

The shear resistance of a structural element is allowed to be computed using different methods, employing analytical models if there is reason to believe that the method and failure criterion represent a real state of stress and mode of failure. In this work, the shear resistance of the plates without conventional shear reinforcement was computed, using

- (a) Regan's method [130];
- (b) Sorensen's method [121];
- (c) Canadian Code [114];
- (d) The provisions of the Joint ACI-ASCE Committee [125];
- (e) Ferguson's method [131], and
- (f) A method proposed by the author, based on the concepts of Swamy's work [91].

For the plates with conventional shear reinforcement, the shear resistance was computed using:

- (a) The Canadian Code [114], slightly modified, especially for the shear reinforcement distribution;
- (b) The provisions of the Joint ACI-ASCE Committee [125].
- (c) The method proposed in point (f).

The punching shear resistance of lightweight concrete plates was

taken as 0.85 of the normal concrete (DC) plates.

Fibre Contribution to Shear Resistance

The fibres contribution in resisting the external shear, i.e., the cracked concrete contribution due to the fibres bridging the cracks, was considered at the ultimate loading stage, assuming that the fibres provide an ideal uniform tensile stress $\sigma_{cu} = 1.01$ MPa, see Appendix B, acting on the assumed or suggested formed body before failure by different theories.

The concrete resistance, V_c for SFRLAC, has been computed using the conventional reinforced concrete theory, replacing f'_c of LAC with f'_c of SFRLAC.

Plates Without Shear Reinforcement

(a) Regan [130] found out, for DC, two empirical expressions for computing the punching resistance: one takes into account the flexural reinforcement contribution, while the other one is a simplification of the plastic theory for punching shear. The first formula is:

$$P_u = 0.13 \mu_s \pi h (B + hc \cot \theta) \sqrt{[1 + (\cot \theta)^2]} \sqrt[3]{(100 \frac{p}{f_s} f_{cu})} \quad (25)$$

where

$$\begin{aligned} \cot\theta &= 2.5 \\ \mu_s &= \frac{\sqrt[4]{500/d}}{\sqrt[4]{500/84.35}} = 1.56 \end{aligned}$$

Applying the 0.85 coefficient for lightweight concrete and assuming $f_c' = 41.37$ MPa results that

For Series I,

$$P_u = 218.02 \text{ kN, see Appendix D}$$

For Series II,

$$P_u = 184.20 \text{ kN, see Appendix D}$$

The second formula relates the punching resistance to a nominal vertical shear stress on a failure surface, a truncated cone, as follows:

$$\begin{aligned} P_u &= 0.177(f_{cu})^{2/3} \pi h (B + h \cot\theta (\tan\theta)^{3/2} \cdot \sqrt{1 + (\cot\theta)^2}) \\ &= 194.19 \text{ kN} \end{aligned} \quad (26)$$

$$\text{for LAC, } P_u = 0.85 \cdot 194.19 = 165.06 \text{ kN}$$

The post-cracking tensile stress of SFRLAC was used in Eqns. 25 and 26 in order to assess just the fibres contribution to shear resistance. It was assumed that the fibres are effective on half of the depth of the assumed failure surface.

$$\begin{aligned} P_u &= \sigma_{cu} \cdot \pi \cdot h / 2 \cdot (B + h / 2 \cdot \cot\theta) \cdot \sqrt{1 + (\cot\theta)^2} \\ &= 117.41 \text{ kN} \end{aligned} \quad (27)$$

The effect of both concrete and fibres on shear resistance is obtained adding the corresponding values, Table 4.1-1.

(b) The punching strength, P_u , is computed assuming vertical uniformly distributed stresses equal to the tensile strength of concrete, f_t , taken as 0.1 of the compressive strength - acting on the lateral surface of the truncated cone ultimate fracture surface:

$$P_u = \pi \cdot (d/0.707) \cdot (B+d) f_t = 363.20 \text{ kN} \quad (28)$$

This is a very simple approach (an angle of 45° with the horizontal plane of the plate is considered for the failure surface) to the real stress distribution but the formula and hypothesis could describe the actual behaviour of the cone formed body just before punching failure.

The fibres contribution is:

$$P_u' = \pi \cdot (d/0.707) (B+d) \cdot \sigma_{cu} = 88.67 \text{ kN} \quad (29)$$

(c) The Canadian standard gives a method to analyse and design the elements for shear punching [114]. The shear capacity of concrete is computed as:

$$V_c = (1+2/\beta_c) \cdot 0.2 \cdot \lambda \cdot \phi_c \sqrt{f_c'} b_o d < 0.4 \cdot \lambda \cdot \phi_c \cdot \sqrt{f_c'} b_o d \quad (30)$$

and ϕ_C are given in Clause 11.2.3. and Clause 9.3.2. of the Canadian standard as 0.85 for structural semi-low density concrete and 0.6, respectively.

$$V_{C,max} = 0.4 \cdot \lambda \cdot \phi_C \cdot \sqrt{f'_C} b_o d = 81.44 \text{ kN}$$

The Canadian code formula for shear resistance, Clause 11.10.2.2, is based on a single strength calculation at $d/2$ from the face of the concentrated load, i.e. a pseudo-critical distance. There is nothing implied about the failure surface, thus the fibres contribution has not been determined. This observation is valid for points (d) and (e).

(d) Using Moe's formula for design [125]:

$$\begin{aligned} V_u &= 0.85[9.23 - 1.12(c/d)] \cdot \sqrt{f'_C} b_o d \\ &= 203.88 \text{ kN} \end{aligned} \quad (31)$$

(e) Using the method proposed by Ferguson, the maximum concrete shear capacity is given by [131]:

$$V_C = 1/3 \cdot \sqrt{f'_C} b_o d \quad (32)$$

Replacing these values with $b_o = 735.86 \text{ mm}$, $d = 84.35 \text{ mm}$, $f'_C = 41.37 \text{ MPa}$, Eqn. (47) yields $V_{C,max} = 133.08 \text{ kN}$.

(f) The ultimate punching shear strength of a plate with fibres is given by concrete, shear reinforcement - if any, and fibres - because they act as shear reinforcement [91], see Fig. 4.1-9. It is assumed that the failure surface is the lateral surface of a truncated cone which makes an angle θ with the horizontal plane; the fibres are acting on a fraction of the overall depth of the plate.

$$V_u = V_C + P_u' \quad (33)$$

$$V_C = f_c' \cdot \pi \cdot (B+x \cdot \cot\theta) \cdot x \cdot \sqrt{(1+(\cot\theta)^2)} \quad (34)$$

$$P_u' = \sigma_{cu} \cdot \pi \cdot (B+x \cdot \cot\theta) \cdot x \cdot \sqrt{(1+(\cot\theta)^2)}$$

The assumed values for θ and x were 30° and one third of the depth of the plate respectively. Therefore,

$$V_C = 220.20 \text{ kN}$$

$$P_u' = 43.07 \text{ kN}$$

$$V_u = V_C + P_u' = 264.07 \text{ kN}$$

Plates with Shear Reinforcement

Based on the computations carried out for the shear resistance following the Code [114], the Series I plates with or without fibres would fail in punching shear ($180.43 \text{ kN} > 81.44 \text{ kN}$, and

311.36 kN > 81.44 kN). For Series II, the situation is the same, i.e., 112.36 kN > 81.44 kN, and 228.92 kN > 81.44 kN. Since the initial assumption was to design the Series II plates to fail in flexure, shear reinforcement was sought to increase the shear capacity of the plates. The Canadian Code [114], requires shear reinforcement as shown below in paragraph (a); regardless of the amount of steel required, about which it provides no guidance for tangential and radial spacing, Clause 11.10.3.3 limits the shear resistance to 122.16 kN, for these plates.

(A) Using the standard requirements, Clause 11.10.3.2. gives the factored shear resistance as:

$$V_r = V_c + V_s \quad (35)$$

The V_r value is limited to

$$V_{r,max} = 0.6 \cdot \lambda \cdot \phi_c \cdot \sqrt{f_c'} b_o d = 122.16 \text{ kN} \quad (36)$$

V_c is computed as

$$V_c = 0.2 \cdot \lambda \cdot \phi_c \cdot \sqrt{f_c'} b_o d = 40.72 \text{ kN}$$

Since the applied load is higher than that provided by concrete, i.e., 112.36 kN > 40.72 kN, steel reinforcement was provided, as shown in Figs. 4.1-5, 4.1-6, and 4.1-7.

The steel area was determined considering two kinds of shear reinforcement which were reported to be effective [125]:

(1) vertical "stirrups", Figs. 4.1-5 and 4.1-7 (a);

It was considered that the potential failure surface intercepts both verticals of the stirrups (not likely to have surfaces at steeper angles).

$$V_S = V_S - V_C = 71.6 \text{ kN}$$

Although the V_S value is 71.6 kN, it was assumed, for good engineering practice, that the loading which produces collapse is the maximum between the value obtained multiplying the theoretical load (112.36 kN) by a coefficient, say 1.35 (factored load), and the value tabulated in Table 4.1-1, when the fibres contribution is considered, i.e., 228.92 kN; hence

$$V_S = V - V_C = 188.2 \text{ kN}$$

$$A_V = V_S / \phi_S f_S = 738.04 \text{ mm}^2 \quad (37)$$

$$\begin{aligned} A_{S, \text{provided}} &= 24 \text{ bars of } 6.35 \text{ mm diameter} \\ &= 759.60 \text{ mm}^2 \end{aligned}$$

$$V_{S, \text{provided}} = 193.70 \text{ kN.}$$

$$V_r = V_C + V_{S,provided} = 234.42 \text{ kN} > 122.16 \text{ kN},$$

hence $V_r = 122.16 \text{ kN}$, as prescribed by Clause 11.10.3.2.

(2) bent up bars, $\alpha = 45^\circ$, Figs. 4.1-6 and 4.1-7 (b)

$$A_{vi} = V_S / [(\sin\alpha)\phi_S f_S] = 1043.9 \text{ mm}^2$$

The strength of the shear reinforcement bars is $f_S = 300.00 \text{ MPa}$.

$$\begin{aligned} A_{vi,provided} &= 12 \text{ bars of } 6.35 \text{ mm diameter} \\ &= 379.80 \text{ mm}^2 \end{aligned}$$

$$\begin{aligned} V_{si,provided} &= 68.47 \text{ kN} < 0.3 \cdot \lambda \cdot \phi_C \cdot \sqrt{f'_C} b_o d \\ &= 61.08 \text{ kN}, \text{ as required by Clause} \\ &11.3.6.3. \end{aligned}$$

$$V_r = V_C + V_{si,provided} = 101.80 \text{ kN} < 122.16 \text{ kN}$$

(3) bent up bars, Figs. 4.1-6 and 4.1-7 (c)

$$\begin{aligned} A_{vi,provided} &= 24 \text{ bars of } 6.35 \text{ mm diameter} \\ &= 759.60 \text{ mm}^2 \end{aligned}$$

$$\begin{aligned} V_{si,provided} &= 102.71 \text{ kN} < 0.5 \cdot \lambda \cdot \phi_C \cdot \sqrt{f'_C} b_o d \\ &= 101.80 \text{ kN} \end{aligned}$$

as prescribed by Clause 11.3.6.4. (0.75 in the above formula is required by this Clause, too).

$$V_R = V_C + V_{Si,provided} = 142.52 \text{ kN} > 122.16 \text{ kN},$$

hence $V_R = 122.16 \text{ kN}$.

The shear reinforcement was anchored by hooks around the top bars (6.35 mm in diameter) and the development length was chosen as 200 mm (Clause 12.3.1) - Figs. 4.1-5, 4.1-6.

Table 4.1-2 summarizes these computations.

(B) A more detailed approach was used, based on Joint ACI-ASCE Committee report [125] and Canadian work reported by Regan [129].

It is assumed that shear reinforcement carries all the shear beyond inclined cracking, taken as half the shear resistance of a plate without shear reinforcement. The capacity of the shear reinforcement is considered equal to the yield strength of the shear reinforcement crossing a potential inclined crack at 45° from the perimeter of the loaded area or as the case may be. The shear resistance is taken as the minimum between the concrete shear resistance on a critical perimeter $d/2$ outside the outer perimeter of shear reinforcement (V_{Calc}^c), and the combined capacity of concrete and shear steel, within this critical

perimeter, considering a potential inclined crack at 45° , (V_{calc}), from the perimeter of the loaded area or as the case may be.

(1) Vertical "stirrups"

(i) Failure surface 1, Fig 4.1-7 (a), $c_1^i = 334.35 \text{ mm}$

$$V_{\text{calc}}^i = 16d^2 (c_1^i/d+1) \sqrt{f_c^i} = 301.62 \text{ kN} \quad (38)$$

V_u is given by Eqn. 31 for concrete resistance. The diameter of the shear reinforcement bar is 6.35 mm, and the nominal steel yield stress is taken as $f_s = 300 \text{ MPa}$.

$$\begin{aligned} V_u &= 217.45 \text{ kN} \\ V_{\text{calc}} &= (V_u/2) + V_s, \text{ in which} \\ V_{\text{calc}} &= 222.67 \text{ kN} \end{aligned} \quad (39)$$

Hence

$$V_{\text{predicted}} = \min(V_{\text{calc}}^i, V_{\text{calc}}) = 222.67 \text{ kN}$$

(ii) Failure surface 2, $c_2^i = 484.35 \text{ mm}$

$$V_{\text{calc}}^i = 16 \cdot d^2 (c_2^i/d+1) \sqrt{f_c^i} = 409.78 \text{ kN}$$

$$V_u = 347.83 \text{ kN}$$

$$V_{\text{calc}} = (V_u/2) + V_s = 287.86 \text{ kN}$$

$$V_{\text{predicted}} = \min(V_{\text{calc}}, V_{\text{calc}}) = 287.86 \text{ kN}$$

Between the failure loadings corresponding to failure surfaces (1) and (2) the ultimate loading is chosen as 222.67 kN.

Adjusting the available part of the Canadian work [129], the required area of shear reinforcement was computed as:

$$V_{s1} = V - 0.75 \cdot V_{cu1} \quad (40)$$

$$V_{s2} = V - 0.75 \cdot V_{cu2} \quad (41)$$

$$V_s = V_{s1} + V_{s2} = 2V - 0.75 \cdot (V_{cu1} + V_{cu2}) \quad (42)$$

$$V_{cu1} = 130.38 \text{ kN, see Appendix D}$$

V_{cu2} was computed using the ratio $u_2/u_1 = 350/150 = 2.33$ between the perimeters of the two critical sections; u_1 and u_2 are the pseudo-critical perimeters for the loaded area and at the top end of surface 2. Hence,

$$V_s = 132.22 \text{ kN}$$

and the required reinforcement area was $A_s = 518.51 \text{ mm}^2$, i.e., 17

bars of 6.35 mm diameter. Provided area was 24 bars \cdot 31.65 mm² = 759.60 mm², thus OK.

(2) Inclined bars

The computations are similar to those performed above, therefore just the significant results are shown. The main difference is due to the inclined angle, 45°, of the shear steel bars, which reduces the shear steel reinforcement effectiveness, at least from a theoretical point of view.

(i) Failure surface 1, $c_1' = 17.84$ in., Fig. 4.1-7 (b)

$$V_{\text{calc}}' = 16d^2 (c_1'/d+1)\sqrt{f_C'} = 387.27 \text{ kN}$$

$$V_u = 247.28 \text{ kN}$$

$$V_{\text{calc}} = (V_u/2) + V_s = 204.20 \text{ kN}$$

$$V_{\text{predicted}} = \min(V_{\text{calc}}', V_{\text{calc}}) = 204.20 \text{ kN}$$

If the fibres contribution is considered, $\theta = 45^\circ$ - see Appendix D, point (f), then

$$V_f = 27.41 \text{ kN}$$

$$V_{\text{calc}} = (V_u/2) + V_s + V_f = 231.61 \text{ kN} \quad (43)$$

(ii) Failure surface 1, $c_1^i = 17.84$ in., Fig. 4.1-7 (c)

$$V_{\text{predicted}} = \min(V_{\text{calc}}^i, V_{\text{calc}}) = 204.20 \text{ kN was determined as in point (1).}$$

(iii) Failure surface 2, $c_2^i = 25.71$ in., Fig. 4.1-7 (c)

$$V_{\text{calc}}^i = 16d^2 (c_2^i/d+1)\sqrt{f_c'} = 531.31 \text{ kN}$$

$$V_u = 421.42 \text{ kN}$$

$$V_{\text{calc}} = (V_u/2) + V_s = 291.18 \text{ kN}$$

Between the loadings corresponding to the failure surfaces (2)(ii) and (2)(iii), the ultimate loading is chosen as 204.20 kN.

Adjusting the available part of the Canadian work [129], the required A_s is computed as shown in point B (1) (ii).

The required reinforcement area is

$$A_s = 733.39 \text{ mm}^2, \text{ i.e., 24 bars of 6.35 mm diameter. Provided area is 24 bars} \cdot 31.65 \text{ mm}^2 = 759.60 \text{ mm}^2, \text{ thus OK.}$$

In both cases, illustrated in Fig. 4.1-7 (b) and (c), the theoretical approach showed that this type of reinforcement is not fully effective. It was felt, at the time when these values were computed, that only experimental studies would clarify which type of shear reinforcement was the most effective one.

(c) As mentioned in point (f), plates without shear reinforcement, the ultimate shear strength of a plate is:

$$V_u = V_C + V_S + P_u^i \quad (44)$$

(1) vertical "stirrups", Figs. 4.1-5 and 4.1-7 (a), and $\theta = 45^\circ$,

$$A_v = V_S / \phi_S f_S = 738.04 \text{ mm}^2$$

$$V_S = A_v \cdot \phi_S \cdot f_S = 193.70 \text{ kN}$$

$$V_C = f_t^i \cdot \pi \cdot (B+x \cdot \cot \theta) \cdot x \cdot \sqrt{(1+(\cot \theta)^2)} = 137.59 \text{ kN}$$

$$V_r = V_C + V_S = 331.29 \text{ kN}$$

(2) bent up bars, $\sigma = 45^\circ$, Figs. 4.1-6 and 4.1-7(b), and $\theta = 45^\circ$,

$$V_{si, \text{provided}} = 68.47 \text{ kN}$$

$$V_C = f_t' \cdot \pi \cdot (B+x \cdot \cot\theta) \cdot x \cdot \sqrt{(1+(\cot\theta)^2)} = 137.59 \text{ kN}$$

$$V_r = V_C + V_{si,provided} = 206.06 \text{ kN}$$

The fibre contribution, $V_f = P_u'$, was computed as indicated in Appendix D, point (f).

$$\begin{aligned} V_f &= P_u' = \sigma_{cu} \cdot \pi \cdot (B+x \cdot \cot\theta) \cdot x \cdot \sqrt{(1+(\cot\theta)^2)} \\ &= 27.41 \text{ kN} \end{aligned}$$

$$V_u = V_C + V_{si,provided} + P_u' = 233.47 \text{ kN}$$

(3) bent up bars, Figs. 4.1-6 and 4.1-7(c), and $\theta = 45^\circ$,

$$V_C = f_t' \cdot \pi \cdot (B+x \cdot \cot\theta) \cdot x \cdot \sqrt{(1+(\cot\theta)^2)} = 137.59 \text{ kN}$$

$$V_{si,provided} = 102.71 \text{ kN}$$

$$V_r = V_C + V_{si,provided} = 240.30 \text{ kN}$$

The conventional shear reinforcement contribution has been taken as indicated in the Canadian standard [114].

Although corner reinforcement was used, it did not influence the plates behaviour since they were tested as simply supported along the edges with the corners free to lift.

The theoretically obtained values suggest that:

A P plate reinforced with 10 No. 10 bars/m width of plate (Series I) should fail in punching shear, as predicted by Eqns. 30 vs. 16 and 32 vs. 16 ($81.44 \text{ kN} < 180.43 \text{ kN}$ and $133.08 \text{ kN} < 180.43 \text{ kN}$) or flexure as predicted by Eqns. 25 vs. 16 ($218.02 \text{ kN} > 180.43 \text{ kN}$), Eqns. 28 vs. 16 ($363.20 \text{ kN} > 180.43 \text{ kN}$), Eqns. 31 vs. 16 ($203.88 \text{ kN} > 180.43 \text{ kN}$) and Eqns. 34 vs. 16, 24 ($220.20 \text{ kN} > 180.43 \text{ kN}$).

A FP plate reinforced with 10 No. 10 bars/m width of plate (Series I) would fail in punching shear as predicted by Eqns. 30 vs. 16, 24 ($81.44 \text{ kN} < 311.36 \text{ kN}$), Eqns. 32 vs. 16, 24 ($133.08 \text{ kN} < 311.36 \text{ kN}$), Eqns. 26,27 vs. 16, 24 ($282.47 \text{ kN} < 311.36 \text{ kN}$), Eqns. 33 vs. 16, 24 ($264.07 \text{ kN} < 311.36 \text{ kN}$), Eqns. 31 vs. 16, 24 ($203.28 \text{ kN} < 311.36 \text{ kN}$), and would fail in flexure as predicted by Eqns. 28,29 vs. 16, 24 ($451.87 \text{ kN} > 311.36 \text{ kN}$) and Eqns. 25, 27 vs. 16, 24 ($335.43 \text{ kN} > 311.36 \text{ kN}$).

A P plate reinforced with 6 No. 10 bars/m width of plate and shear reinforcement as shown in Fig. 4.1-7 (a), would fail in flexure as predicted by Eqns. 36, 39 and 44 vs. 16 ($122.16 \text{ kN} > 112.36 \text{ kN}$, $222.67 \text{ kN} > 112.36 \text{ kN}$ and $331.29 \text{ kN} > 112.36 \text{ kN}$); the same plate reinforced with 6 No. 10 bars/m width of plate having shear reinforcement as shown in Fig.

4.1-7 (c) would fail in flexure ($204.20 \text{ kN} > 112.36 \text{ kN}$, and $240.30 \text{ kN} > 112.36 \text{ kN}$) as predicted by Eqns. 39 and 44 vs. 16.

A FP plate reinforced with 6 No. 10 bars/m width of plate and shear reinforcement as shown in Fig. 4.1-7 (b) would fail in punching shear as predicted by Eqns. 36 vs. 16, 24 ($101.80 \text{ kN} < 228.92 \text{ kN}$) or flexure as predicted by Eqns. 39 and 44 vs. 16, 24 ($231.36 \text{ kN} > 228.92 \text{ kN}$ and $233.47 \text{ kN} > 228.92 \text{ kN}$).

It is correct to say that whatever type of failures are likely to occur they are primary failures and are difficult to differentiate them clearly; one type of failure triggers the other one.

The conservativeness of the Code provisions regarding punching shear is present: regardless of the amount and arrangement of the shear reinforcement, all plates are limited by Clause 11.10.3.3 to the same shear capacity. Eventually, the shear reinforcement was provided as shown in Table 6.1-1.

4.2. Mathematical modeling and computer code

Introduction

The forces in the sections of a structure due to the loads on the structure and its deformations can be determined by mathematical or physical models of the structure.

The mathematical modeling can be based on two solutions: differential or variational. In the differential solution, the problem is reduced to the integration of differential equations with partial derivatives, taking into account the boundary conditions, while the variational solution is reduced to finding out those functions which minimize or maximize a functional, taking into account the boundary conditions.

The exact analytical methods are not used on a large scale basis because it is quite difficult to describe the behaviour of the whole structure, or parts of it, using functions. As an alternative, the numerical methods are broadly employed although they are approximate. The most used numerical methods are the Finite Difference Method (FDM) and Finite Element Method (FEM). The former one uses a pointwise approximation whilst the latter one uses a piecewise approximation. The FEM is known as a versatile analytical tool, with broad applicability in different situations, such as material analysis (elastic-inelastic, homogeneous-nonhomogeneous, isotropic-anisotropic); structural

analysis (linear structures, surfaces, volumes); types of loads (static or dynamic); and problem category (equilibrium, eigen values) [132].

When a mathematical model is considered to characterize the reinforced concrete structural behaviour, in most of the situations, it is assumed that the reinforced concrete is elastic, homogeneous and isotropic. The post-elastic behaviour of reinforced concrete elements and/or structures is difficult to model because of the following:

- after cracking, reinforced concrete becomes nonhomogeneous and anisotropic;
- the crack propagation changes continuously the structural topology;
- the physical laws of concrete and steel are nonlinear, and those of concrete subjected to multiaxial state of stresses are not very well known. There are a few known approaches used to represent the constitutive relationship of concrete under multiaxial stress states: linear and nonlinear elasticity theories, perfect and work-hardening plasticity theories, endochronic theory of plasticity, plastic fracturing theories;
- the bond between concrete and steel is not a linear function of loading;

- all these properties are of statistical nature, with a broad scatter.

As Vecchio et al. [133] stated, there is yet no theory able to predict the load-deformation response in an element bounded by rough surfaces (cracks) capable of transmitting shear and compression at the contact locations, but no tension, although there are tensile stresses in the concrete block between the cracks. Besides, the stresses in the reinforcement bars are maximum at the crack locations but vary along the bar length. Therefore, the study of the reinforced concrete bidimensional continuity, due to its complex behaviour, can be suitably solved by means of material techniques or by means of computer simulations using the finite elements.

The modelling of reinforced concrete in FEM depends upon how the concrete cracking and bond are described. In this work, it was assumed that a full bond exists at the concrete-steel interface (the effect of bond is considered by tension-stiffening), and that cracking occurs within a certain volume of the elements. An average reduced shear modulus that takes into account crack interface effects and dowel action was employed too - also known as "smeared cracked approach". The material nonlinearity due to an elasto-plastic response were considered and anisotropy effects are included in the yielding behaviour. The geometrical nonlinearity was taken care of, too.

The nonlinear behaviour of material can be described only if the multi-axial stress-strain relation and the failure criterion of concrete are known. The concrete was modeled by a dual criterion for yield and crushing, in terms of stresses and strains, together with a tension cut-off representation.

Anisotropic degenerate thick shell elements were used together with a layered approach through the thickness of the plate. The rigidity of the anisotropic degenerate thick shell reinforced concrete elements was considered to be formed by the rigidity of both materials, with the steel uniformly distributed as a smeared layer of equivalent thickness and rigidity.

Stresses and strains are investigated at integration points. Using the stress and strain evaluations at these points, cracking, yielding, and crushing patterns are obtained.

The following paragraphs describe a FE computer program developed by Hinton and Owen [97] for reinforced concrete plates and shells which utilizes degenerate thick shell elements. This computer program was used to analyse one of the plates as described in Chapter 6. The needed details are given below; all the other ones are to be found elsewhere [97].

Finite Elements

The most versatile finite element that provides flexibility in the analysis of reinforced concrete members is considered the isoparametric element [134]. Isoparametric elements with independent rotational and displacement degrees of freedom (DOF) are employed, in which the three dimensional (3-D) stress and strain conditions are degenerated to shell behaviour. Difficulties, due to the degeneration process, were encountered when the thickness of the element was reduced. An improvement of this model was achieved by means of the so-called reduced integration technique. Since then, the degenerate concept of formulating general shell elements - for thick or thin structures - was adopted by many investigators to derive different types of elements.

The concept of layered model approach (can handle bending and membrane coupling) was used to model reinforced concrete plates and shells and to simulate concrete cracking through the concrete layers. In this concept, triangular, shallow shell parallelogram and Reissner-Mindlin elements were used; the present computer code uses degenerate thick shell elements employing a layered discretization through the thickness of the structural member.

A solid 3-D element based on a quadratic displacement field is transformed in a quadratic degenerate shell element, Fig. 4.2-1,

using two assumptions: "normals" to the middle surface remain practically straight after deformation and the stress components normal to the shell mid-surface is constrained to be zero in the constitutive equations. Each nodal point has a specified 5 DOF, i.e., 3 displacements of the node and two rotations of the "normal" at the node. To define the degenerate curved shell elements, four coordinate systems are used: global coordinate system (GCS); nodal coordinate system; curvilinear coordinate system; and local coordinate system, Fig. 4.2-2. The nodal coordinates, nodal displacements, as well as the global stiffness matrix and applied force vector are related to GCS. The nodal coordinate system is defined at each nodal point with the origin at the mid-surface. One of the associated unit vector to this system of coordinates defines the direction of the "normal" at the node, whilst the other two unit vectors define the rotations of the "normal" at the node. This mode of defining the nodal coordinate system is important in that there are no gaps or overlaps along the element boundaries.

The curvilinear system is defined as having the origin in the midplane and its coordinate values to vary between -1 and 1 on the respective faces of the element, or in other words, the element is mapped on a curvilinear, general, system of coordinates.

The local coordinate system is defined at those points where the

stresses are to be calculated. The local and GCS are related by the direction cosine matrix [97].

The element geometry is input giving the global coordinates of pairs of points on the top and bottom surfaces. Any point within the element could be defined using the element shape functions applied to the nodal coordinates, because this is isoparametric formulation [97]. The relationship is made up by two parts: one describes the intercept of the "normal" with the mid-surface and the other one describes the position of this point along this "normal".

The element displacement field is described by the 5 DOF of the "normal": 3 displacements of its midpoint and two rotations Fig. 4.2-3. The displacement field for the whole element can be expressed as a relation between the shape function matrix of the degenerate element and the vector of the element variables

$$\underline{u} = \underline{N} \underline{d} \quad (45)$$

This is an important relation because it provides for the field displacement that is used to find out the strains and stresses at that point. The strains and stresses, and their resultants, are conveniently expressed in local coordinate system. There are five strain and five stress components at the node. The strains are related to the nodal variables by the strain matrix

$$\underline{e} = \underline{B} \underline{d} \quad (46)$$

whereas the stresses are related to the change in the strain field by the elasticity matrix

$$\underline{s} = \underline{D}(\underline{e} - \underline{e}_0) \quad (47)$$

The generalized Hooke's law is valid for elastic range of the material. With or without internal symmetry, it is demonstrated [97] that

$$\underline{s} = \underline{D} \underline{e} \quad (48)$$

The general elasticity matrix has among its elements constituent shear correction factors. At layer interfaces, two conditions must exist: the displacements and stress continuity. The first condition is satisfied ("normal" is straight even if the element is deformed) but the second one is not satisfied unless shear correction factors are used; Reference 97 gives all the details of computing these shear correction factors.

An extensive review of the quadratic shell elements and numerical integration is given in Reference 97. In this work, 8-node Serendipity element, Fig. 4.2-4, and reduced integration on the transverse shear strains, as well as on the membrane strains were employed (full integration produces shear and membrane

locking).

Due to the nonlinear behaviour of the compressed concrete, concrete cracking and reinforcement response, a layered approach is recommended to find out the real response of the structure [97]. The layered approach provides for modeling the stress distribution through the thickness by a piecewise constant approximation (each layer contains stress points on its mid-surface). The strain matrix, B , is calculated at the mid-surface of each layer; based on it, the element stiffness matrix, K_e and the internal force vector f_e are determined using Gaussian integration. The stress and strain vectors are evaluated at each of the integration points to determine the onset and development of cracking, yielding, or crushing.

Material properties

The concrete nonlinear stress-strain relations are based on the flow theory of plasticity: the yield criterion, the flow and hardening rule and the crushing condition. The yield condition used in most applications is formulated in terms of the first stress invariant and shear invariant, and two material parameters [97]. Because the stress normal to the middle plane is neglected, the triaxial stress state (due to the transverse shear stresses) is reduced to a biaxial one. The yield criterion is, except for the two material parameters, the same as Huber-Mises

criterion of plastic yield [134]. The material parameters are obtained from uniaxial compression test and the biaxial test under equal compression stresses. It is advantageous to use a relation between biaxial yield strength and the uniaxial yield strength, f'_C , because the yield function, eventually, is function of only one material parameter, i.e., f'_C - the compressive strength.

As mentioned before, a dual criterion is used for yield: the perfectly plastic model and work(strain)-hardening model are presented in Fig. 4.2-5 together with the tensile behaviour. The subsequent increased plastic deformation and a corresponding expansion of the loading surfaces are functions of the hardening parameter defined by the hardening rule expressed in terms of the effective plastic strains. When the maximum strength f'_C is reached, a perfectly plastic response is assumed until crushing surface is developed, Fig. 4.2-6. The flow rule refers to the stress-strain relationship in the plastic range, assuming the normality of the plastic deformation rate vector to the yield surface. This rule defines a plastic strain increment related to a gradient of the current stress function that could be the yield condition or the subsequent loading functions in the strain hardening model that defines its direction perpendicular to the yield surface. The plastic flow vector is defined by the yield function derivatives which can be explicitly formulated, if the yield function is known.

The hardening rule defines the motion of the subsequent yield surface (the loading surfaces) during plastic deformation. This rule determines the relation between the loading surfaces (effective stress) and the accumulated plastic strain (effective plastic strain) and is obtained extrapolating from the uniaxial stress-strain relationship using the conventional "Madrid Parabola" [97].

The crushing condition is a strain controlled phenomenon. This condition, due to the lack of experimental data regarding concrete ultimate deformation capacity, is obtained transforming the yield criterion, expressed in terms of stresses, directly in terms of strains using the strain invariants and ultimate total strain (extrapolated from uniaxial test results). If the material reaches the ultimate strain capacity, the material does not possess any characteristic to withstand further loadings (the material property matrix, \underline{D} , is set to zero).

The principal stress planes at a point can be determined from the stress vector at the point. The response of concrete in tension, is linear up to cracking strength, f_t' . The cracks are assumed to occur in planes perpendicular to the structural plane. After cracking, the elasticity modulus E and Poisson's ratio are reduced to zero. Because concrete is weak in tension, its tensile behaviour does not contribute in great proportion to concrete strength. A convenient concept, suitable for FEM, is

employed: the idea is to consider a smeared representation for cracked concrete (using certain values for G modulus) which implies that the cracks are distributed across a region of the finite element [97]. It is known that the cracked concrete carries between cracks a certain amount of tensile force normal to the cracked plane (tension stiffening concept). Fig. 4.2-7 presents this stiffening behaviour of cracked concrete. If it is considered that the finite element loses its whole stiffness in the direction of the principal tensile stresses, then distorted crack patterns are obtained. To mitigate this problem, either retained shear stiffness in the cracking plane or nonzero degraded tension stiffness (degrading stiffness concept) are considered [132], i.e., the smeared concrete representation means that the cracked concrete is able to carry a tensile stress of

$$f_t = 0.62 f'_c \quad (49)$$

where f_t is the MOR of concrete, which is related to the uniaxial compressive strength of concrete, f'_c .

Cracked concrete is capable of carrying shear stresses across cracks due to the dowel action of the steel bars crossing the section, interlocking of the aggregate and other parameters. In this computer code, the cracked shear modulus of concrete is a function of the tensile strain. The steel bars are considered as steel layers of equivalent thickness; each steel layer has a

uniaxial behaviour resisting only the axial force in the bar direction. A trilinear idealization of the stress-strain elasto-plastic curve is used in this computer code.

Finite Element Solution and Computer Code

The 8-node Serendipity element and reduced numerical integration are employed in the present work. As it was mentioned, a layered approach is used to model and discretize the steel reinforcement and concrete through the thickness. The nonlinear characteristics of the material and geometrical nonlinearities are taken into account too.

The structure of the computer code is given in Fig. 4.2-8. A full 3-D Huber-Mises yield criterion, in which the stress components are modified by introducing anisotropic parameters, is employed.

The tangential and initial stiffness approach to numerical solution is adopted and associated flow rule, in which the plastic potential is assumed to be the anisotropic yield function, is used to define the elasto-plastic incremental constitutive relation.

Although in the present work the same constitutive models were used for both LAC and SFRLAC, except that their own properties

were implemented, probably a better approach would be to investigate and try to apply the results of the nonlinear analysis of SFRC [135] to FEM.

Table 4.1-1: Predicted Ultimate Flexural and Punching Shear Loads of LAC and SFRLAC Plates

Predicted Ultimate Flexural Loads, kN							
	Eqn. 15	Eqn. 16	Eqn. 17				
Series I	184.29	180.43	193.83				
Series II	114.77	112.36	120.71				
Predicted Ultimate Flexural Loads Adding the Fibres Contribution							
	Eqn. 15, 24	Eqn. 16, 24	Eqn. 17, 24				
Series I	318.03	311.36	334.49				
Series II	233.82	228.92	245.92				
Predicted Ultimate Punching Shear Loads, kN, Plates w/o Shear Reinforcement							
	Eqn. 25	Eqn. 26	Eqn. 28	Eqn. 30	Eqn. 31	Eqn. 32	Eqn. 34
Series I	218.02	165.06	361.20	81.44	203.88	133.08	220.20
Series II	184.02						
Predicted Ultimate Punching Shear Loads, kN, Plates w/o Shear Reinforcement, Adding the Fibres Contribution							
	Eqn.25, 27	Eqn.26,27	Eqn.28, 29	Eqn.30	Eqn.31	Eqn.32	Eqn. 33
Series I	335.43	282.47	451.87	81.44	203.88	133.08	264.07
Series II	301.61						

Table 4.1-2: Predicted Ultimate Punching
Shear Strengths of LAC and SFRLAC Plates

Predicted Ultimate Punching Shear Loadings, kN, Plates with Vertical "Stirrups"			
Figure	Eqn. 36	Eqn. 39	Eqn. 44
4.1-7(a)	122.16	222.67 - failure surface 1	331.29
		287.86 - failure surface 2	
Plates with bent-up bars			
4.1-7(b)	101.80	204.20 - failure surface 1	206.06
		(231.61) - failure surface 1	(233.47)
Plates with bent-up bars			
4.1-7(c)	122.16	204.20 - failure surface 1	240.30
		291.18 - failure surface 2	

Note: The number in parentheses include the fibre contribution.

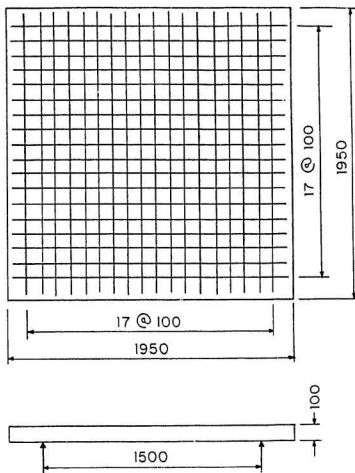


Fig. 4.1-1 Bottom reinforcement - 10 #10 bars/m
(All dimensions in mm)

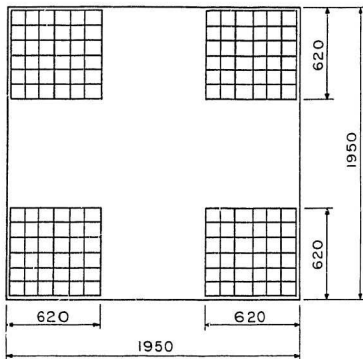


Fig. 4.1 - 2 Top reinforcement (All dimensions in mm)

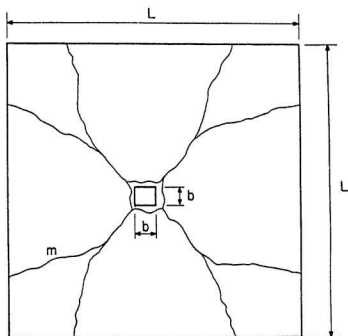


Fig.4.1-3 Assumed yield-line mechanism
(Reference 127).

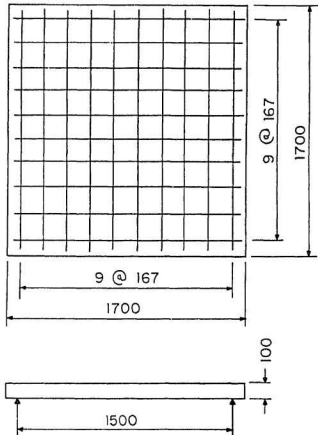


Fig. 4.1-4 Bottom plate reinforcement - 6 #10 bars/
unit width (All dimensions in mm)

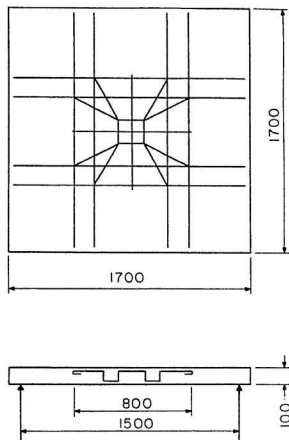


Fig. 4.1-5 Shear reinforcement : vertical stirrups (all dimensions in mm)

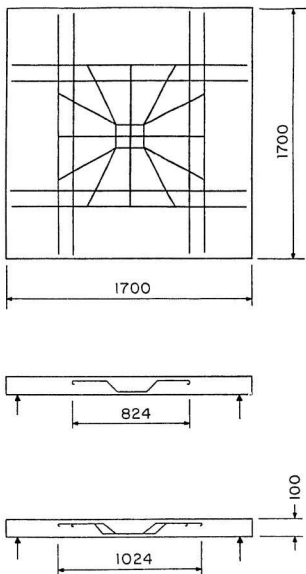
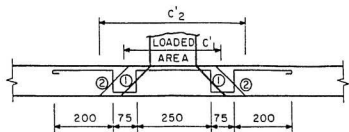
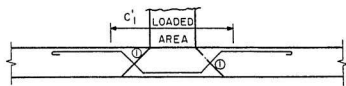


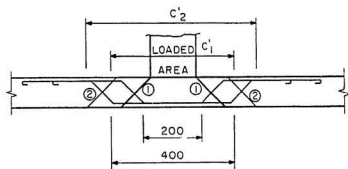
Fig. 4.1-6 Shear reinforcement: single and double shear head. (all dimensions in mm).



(a)

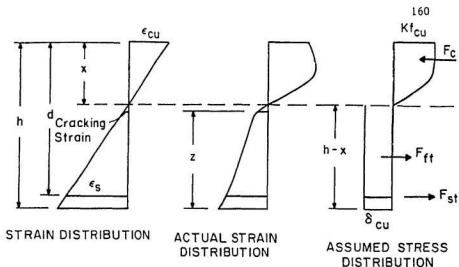


(b)

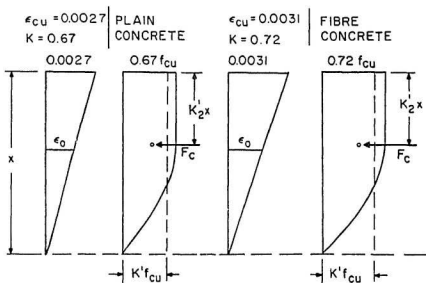


(c)

Fig. 4.1-7 Computational details for shear resistance.



(a) STRESS AND STRAIN DISTRIBUTION AT FAILURE



(b) MODIFIED STRESS BLOCK FOR LIGHTWEIGHT FIBRE CONCRETE

Fig. 4.1-8. Strain and stress distribution at failure (from reference 91)

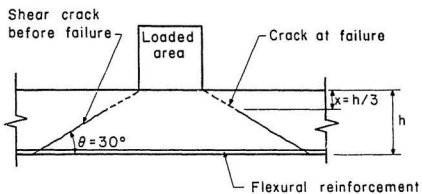


Fig. 4.1-9 Failure model for punching failure in slabs
(Reference 91)

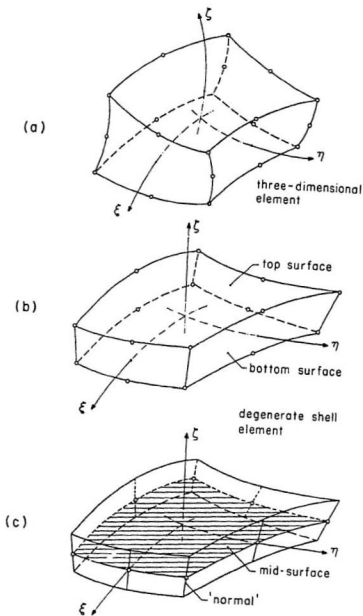


Fig. 4.2-1 (a) Quadratic solid three-dimensional element, (b) and (c) the corresponding degenerate shell element (from reference 97).

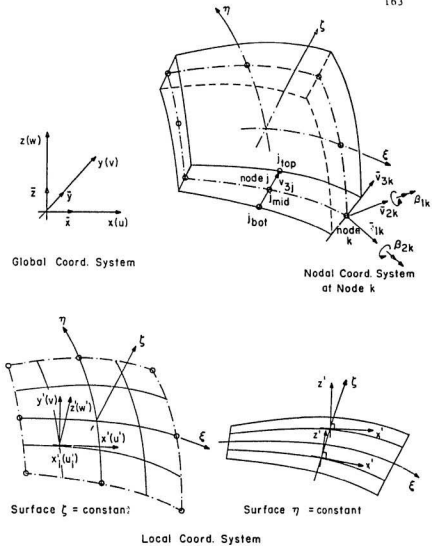


Fig. 4.2-2 Coordinate systems: (a) nodal and curvilinear systems, (b) local system of axes. (reference 97)

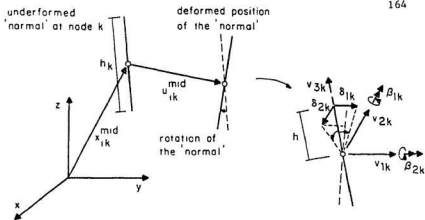


Fig.4.2-3 Displacements of a point on the "normal" at node k (reference 97)

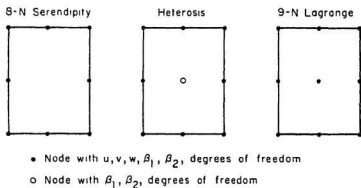


Fig.4.2-4 Nodal configuration of the three quadratic shell elements (reference 97)

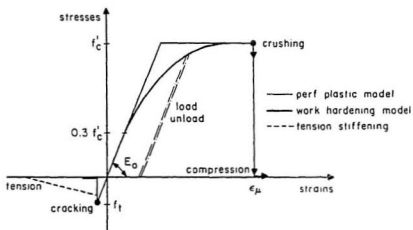
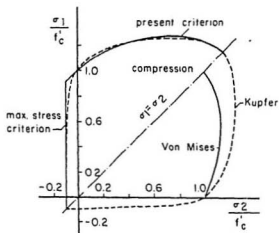


Fig.4.2-5 One-dimensional representation of the concrete constitutive model (reference 97).

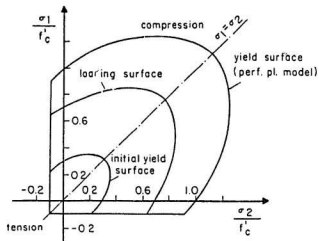


Fig.4.2-6 Two-dimensional stress space representation of the concrete constitutive model (reference 97)

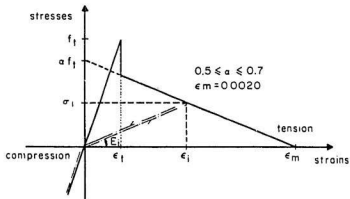
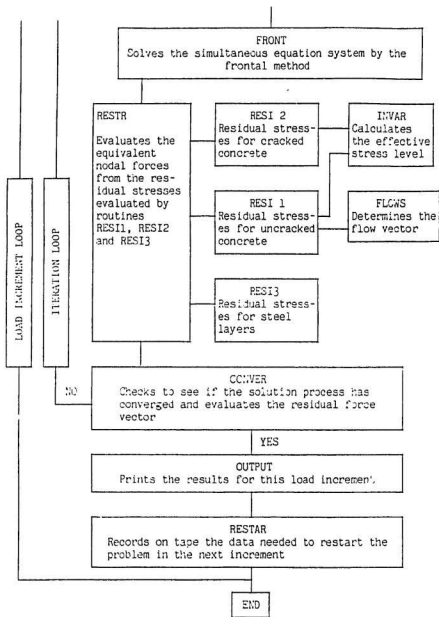


Fig.4.2-7 Loading and unloading behavior of cracked concrete illustrating tension stiffening behaviour (reference 97)

Fig. 4.2-8 (continued)



CHAPTER 5. EXPERIMENTAL STUDY: LAC AND SFRLAC PLATES

5.1. Test Set-up

The plates were tested as simply supported along the edges with the corners free to lift. Each plate was supported along the edges on a round steel bar welded to a steel plate fixed to the upper face of the supporting frame. The supporting frame was placed on eight columns so arranged as to give enough space for a person to enter under the plate, obtain the cracking pattern, and take the readings, Fig. 5.1-1. A layer of mortar was laid on the top of the concrete columns supporting the concrete frame, thus ensuring a horizontal position of the supporting frame and consequently of the plate. A steel protective grid was used under the plate to protect the person doing the above described operations, (please see Fig. 6.2-29).

The columns and supporting frame were cast in the laboratory; dense concrete was used for this purpose. This test set-up was used for all the experiments without any incident. A steel frame, shown in Fig. 5.1-2 (a) and (b), was erected to hold and provide support to the actuator of the testing machine; thus the loading could be applied downward upon the top surface of the plate.

5.2. Instrumentation

The loading was applied through a 667.2 kN (150 kips) actuator using a MTS testing machine, Fig. 5.1-2 (a) and (b). The actuator calibration was checked before starting each test. In those tests where controlled increasing deformation mode of loading was used, the built-in-transducer in the actuator provided for the feed back signal. The loading was applied in predetermined increments; the loading and displacements values were read from the MTS machine front panel. The vertical displacements of the middle plate bottom surface were taken using a LVDT, supplied with power by a Daytronic Power Supply; its signals were read from a multimeter connected to the LVDT. Thereafter the readings on the multimeter were processed using the LVDT calibration factor. The vertical displacements at the plate corners and the midside of the top plate surface atop support lines were also monitored, using dial gages with a one-hundredth of a millimetre precision, Figs. 5.1-2 (a) and (b), 5.2-1 and 5.2-2.

The load-displacement curves were obtained, using a X-Y Hewlett & Packard plotter connected to the MTS machine. The strains were measured on top and bottom concrete surfaces at predetermined locations, see Fig. 5.2-1 (plates P4, P5, FP4, FP5) and Fig. 5.2-2 (plates P6, P7, FP6, FP7), and on reinforcing bars, as shown in Fig. 5.2-3.

The concrete electrical resistance strain gages used, which were glued on the concrete surfaces, were Showa foil strain gages, 60 mm long, 120 Ω resistance with a gage factor of $2.12 \pm 1 \%$.

The steel electrical resistance strain gages, glued on reinforcing bars, were carefully mounted as shown in the fabricator's manual. The protection against humidity was ensured by a heat shrink tube waxed at its ends. The steel electrical resistance strain gages were 10 mm long, 120 Ω resistance with a gage factor of $2.04 \pm 0.5 \%$.

The gages were connected, using 4-26-DEV wires, to BHL Electronics Model 1225 switching and balancing units (Wheatstone bridge circuit). The readings, in microstrains, were taken from two BHL Electronics 1200 Portable Digital Indicators, one for concrete gages and the other for the steel gages respectively.

5.3. Methodology

In all, fourteen square plates [presented later on in Table 6.1-2], with uniformly distributed flexural reinforcement bars equal in both directions, were tested. The initial plate dimensions, 1.95·1.95·0.10 m, were used for six plates, because they have been initially designed to have a free span of 1.75 meters. Afterwards, it was decided to change the plates dimensions to 1.70·1.70·0.10 m, with a free span of 1.50 m. Eventually, in all

experiments, regardless of the plate dimensions and in order to obtain comparable results, the free span was 1.5 m in either direction. Following the removal from the curing environment, strain gages were glued on the concrete top and bottom surfaces in two different arrangements, as shown in Figs. 5.2-1 and 5.2-2, respectively. At the testing moment, the plates were set on the test set-up arrangement shown in Fig. 5.1-1. Between the plates and the supporting round steel bar along the edges, thin rubber pads were introduced to remove any unevenness of the contact surfaces. The vertical displacements of the rubber pads were monitored by dial gages mounted as shown in Fig. 5.2-1 (D2 and D5) and Fig. 5.2-2 (D5 and D6), and those readings were subtracted from the vertical readings taken by the LVDT in order to obtain the real midplate vertical displacements at the bottom of the plate.

As shown in Figs. 5.1-2 (a) and (b), the concentrated loading was applied at the center of the plate, on the top surface, by a round rigid and thick steel plate having an area of 22500 mm². The applied loading was considered the least advantageous for the plate behaviour; an increased size of the loading area could increase the ultimate load value and change the failure pattern [124]. Between the steel plate and the concrete plate, a thin rigid rubber pad was introduced to create an uniform pressure distribution under the steel plate.

The loading was applied in two ways: controlled increasing load or deformation modes. When the tests were carried out in controlled increasing load mode, the loading was applied in increments of 4.5 kN. The controlled increasing deformation mode tests were completed such that the increasing displacement increments corresponded to a 4.5 kN increase in loading; the test was continued after the maximum plate capacity was reached, in order to obtain the energy absorption capacity of the plates [please see Figs. 6.2-9 to 6.2-12].

Following each load or displacement increment, the following readings were noted: concrete strains, steel strains, vertical displacements at the middle bottom surface of the slab, corners, and midside top surface of the slab. The cracking pattern was monitored for each plate; in addition, the maximum load, behaviour at failure, and cracking patterns after the collapse were also taken [please see Figs. 6.2-13 to 6.2-21].

The stress-strain curves for the steel reinforcing bars are given in Fig. 5.3-1 for No. 10 bar, and Fig. 5.3-2 for 6.35 mm bar. These diagrams were used to interpret the results.

The concrete properties required in the theoretical presentation, in Chapter 6, were determined on standard specimens cured in the same conditions as the plates to which they relate, as presented in Chapter 2.

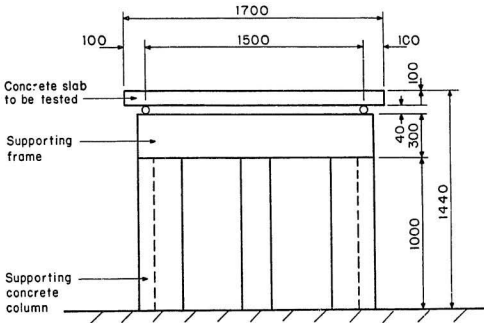


Fig. 5.1-1 Test set up



Fig. 5.1.2(a) Test set up

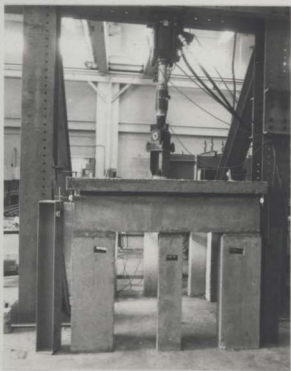


Fig. 5.1-2(b) Test set up

Fig. 5.1-2(b) Test set up

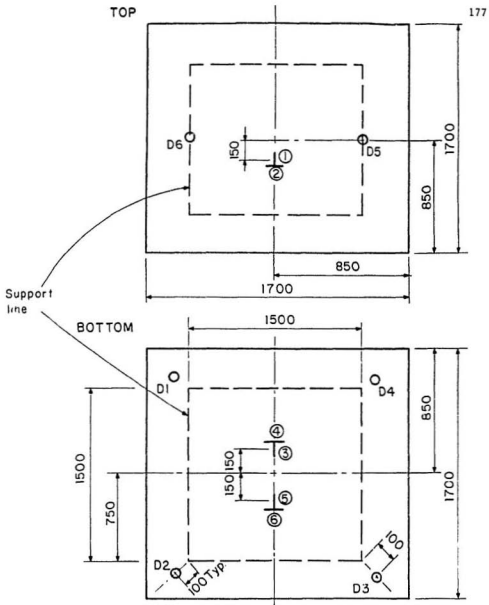


Fig. 5.2-2 Plate instrumentation: concrete strain gage locations in plates P6, P7, FP6 and FP7.

(Not to scale)

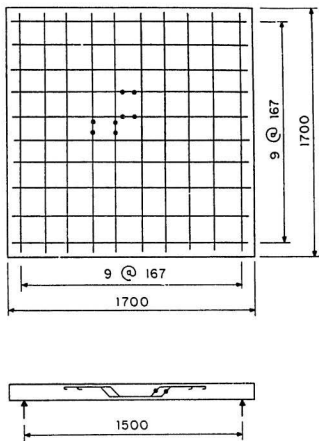


Fig. 5.2-3 Steel gages locations
(All dimensions in mm)

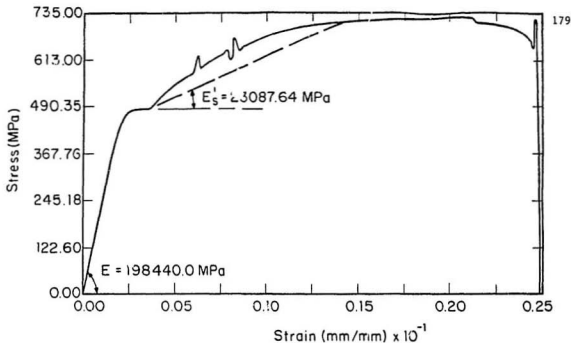


Fig. 5.3-1 Stress-strain curve for steel reinforcing bar #10

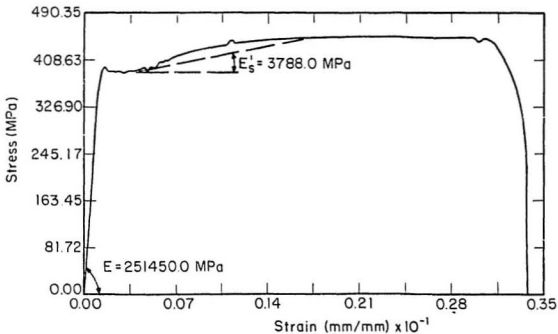


Fig. 5.3-2 Stress-strain curve for steel reinforcing bar 1/4" dia.

CHAPTER 6. RESULTS: LAC AND SFRLAC PLATES

6.1. Introduction

A synopsis of the experimental results of the plates used in this work is given in Table 6.1-1. The plates without or with fibres are marked as P or FP plates, respectively. A few rheological and hardened state properties of concrete, for each plate, are given in Table 6.1-2. As it is shown in Table 6.1-1, two types of flexural reinforcement were used for the plates, Series I and II, having 10 No. 10 and 6 No. 10 steel reinforcing bars per unit width respectively. Plates P1, FP1, P2, FP2, P3 and FP3 were tested in the controlled increasing load mode; the rest of the eight plates were tested under controlled increasing deformation mode to obtain the post-failure behaviour, and thereby to assess the ductility and energy absorption capacities of the plates.

First, the shear capacity of the plates was investigated, P1 being designed to fail in punching shear mode. The effect of the fibres addition on the punching strength of the plate without shear reinforcement was then looked at, FP1 being designed to fail also in punching shear. The fibres addition increased the punching shear strength of the plate by 32 percent, and changed its mode of failure.

Then, as always required in good engineering practice, and to answer one of the question raised in section 1.6, the plates were designed to fail in flexure, and to prevent the sudden punching, as encountered in P1 test. The flexural reinforcement was reduced by 40 percent, and shear reinforcement was provided in two arrangements regardless of the fibres presence (with the exception of FP2) in accordance with the computations completed in section 4.1.

The first arrangement was provided for P2 - vertical "stirrups", Figs. 4.1-5 and 4.1-7 (a). Its pair, FP2, had only fibres as shear reinforcement, and it had good ductility prior to failure. The surprising aspect was the high load capacity of FP2, i.e., 60 percent more than P2.

The second arrangement consisted of providing as conventional shear reinforcement, inclined (bent up) bars, in two arrangements, Figs. 4.1-6 and 4.1-7 (b) and (c): P3, had two rows of inclined (bent up) shear reinforcement bars; FP3 had a single row of inclined (bent up) bars and fibres to supplement the shear capacity, see Tables 4.1-1 and 4.1-2.

It was assumed that this second arrangement of shear reinforcement would probably provide the required type of failure (confirmed by the tests on FP3, while P3 was accidentally punched), and all the other plates were

manufactured as P3 and FP3. At the same time, maintaining the same flexural and shear reinforcement arrangements and pattern of loading, the COE effect on the behaviour of the plates would also be investigated.

6.2. Experimental Results and Discussions

Deflections Measurements

The load-deflection curves are given in Fig. 6.2-1 for eight of the plates tested in this investigation. These deflections were obtained under the controlled increasing displacement mode of testing, using the readings from the LVDT, see also section 5.3. To avoid its damage, the LVDT was removed when it was necessary and the whole curves were monitored by the X-Y plotter connected to the MTS machine, Figs. 6.2-9 to 6.2-12. Thus the whole behaviour after failure was monitored in order to assess the energy absorption capacity of the plates and their ductility. Regardless of the curing environment, fibre reinforced plates (FP) show, with the exception of FP4, at all loading stages (shown in the Fig. 6.2-1), less deflection for the same load compared with the plain concrete plates (P plates), more clearly shown after the first crack occurred (initial cracking stage). These curves would suggest an increased plate stiffness of the FP plates compared to the P plates, shown mainly after the initial cracking stages. The plates began to behave nonlinearly at

relatively low stages of loading, as the cracking loads show, Table 6.2-1 (higher for FP). The maximum reduction in deflection after cracking occurred for FP4.

The average corner displacements are compared with the central deflection, Table 6.2-1, at first crack loading and ultimate loading stages. Also the concrete and steel strains, as measured, are given at the same loading stages.

Concrete Strains

The concrete strains were picked up at a few locations shown in Figs. 5.2-1 and 5.2-2. The measured concrete strain values at two important loading stages are given in Table 6.2-1. The observed strains on the bottom surface of the plates are plotted in Figs. 6.2-2 and 6.2-3, for two strain gages perpendicular to each other and parallel to the plate edges. Some of the given values are obviously too high for concrete regardless of the fibres presence; that is because following cracking, as observed by naked eye, the strain gages continued to pick up strains until the crack was large enough to destroy the strain gage.

The strains in the central region of top surface of the plate, in the vicinity of the loading area, are given in Figs. 6.2-4 and 6.2-5. The concrete strains, for the FP plates (Fig. 6.2-5), reached almost in all cases over 3000 microstrains, or over 0.003

and close to 0.004, while for the ordinary reinforced concrete plates (Fig. 6.2-4), the maximum observed value was a little over 3000 microstrains or 0.003 (P6 plate). As expected, the FP plates, are capable of carrying more loads than the plain concrete plates, fact confirmed by the concrete strains measurements, Figs. 6.2-4 and 6.2-5.

The concrete strain gage perpendicular to the loading edge area, P_{c1} or fp_{c1} , indicated at strains ranging from 68 to 86 percent and 73 to 84 percent of the ultimate load for P and FP plates, respectively, smaller strains than in the immediately previous load step. It is assumed that these changes indicated the occurrence of the diagonal cracking within the perimeter on which the strain gage was glued, and from these readings the diagonal crack loading could be obtained using Figs. 6.2-4 and 6.2-5; they are listed in Table 6.2-2, column 3.

The measured concrete strains were not used in assessing the plate capacities; they were replaced by the realistic values of compressive strains as determined on standard cylinders following ASTM C 39, and listed in Table 6.1-2.

Steel Strains

The measured strains on the flexural tension reinforcement at the locations shown in Fig. 5.2-3, are given in Figs. 6.2-6 and 6.2-

7. The steel strain values at the first crack loading and in the proximity of the ultimate loading are given in Table 6.2-1. According to the experimentally obtained stress-strain curve of Fig. 5.3-1, a flexural steel tension bar starts to behave nonlinearly at about 1600 microstrains, and begins to yield at about 2471 micro-strains. Hence the steel strain values listed in Table 6.2-1, close to the ultimate loads indicate that the flexural reinforcement has yielded (localized yielding has already occurred). When assessing the plate capacities, these values are useful as they relate through the stress-strain curve of Fig. 5.3-1 to the steel stresses in the flexural bars. At about 62 to 88 percent of the ultimate load, due to the crack widths, a marked increase in strain took place, confirming that diagonal cracking occurred, Figs. 6.2-6, 6.2-7 and Table 6.2-2, column 4. The FP plates, except FP6, show at the same level of steel strain in the flexural reinforcement greater loads than the P plates mainly around the final loading steps. At these ultimate loading stages, the fibres contributed more to the whole plate strength, bridging the existing cracks, increasing the steel strains in the flexural reinforcement (strain hardening), therefore increasing the stresses in the flexural bars.

Although it is difficult to conclude, it seems that the COE created conditions which lowered the steel strains; for example P4, FP4, and P5 have less strains in the flexural reinforcement

than P6, FP6 and P7.

The measured strains on shear reinforcement bars are given in Fig. 6.2-8 and Table 6.2-3; the experimental stress-strain curve, Fig. 5.3-2, indicates that the steel yields at about 1193 microstrains. It seems that the shear reinforcement carried loads mainly after the diagonal cracking occurred (evident for FP plates), and the values are indicating the yielding of the shear reinforcing bars, Table 6.2-3 (except FP7 plate).

Complete Load-deformation Curves

Figs. 6.2-9 to 6.2-12 show the complete load-central deflection curves (pre- and post-failure) as obtained during the tests; these curves are used, as shown later on in this section, to assess the energy absorption capacity of the plates; the residual strengths of the plates, Table 6.2-4 were determined too.

The difference between the load-displacement curves, shown in Fig. 6.2-1 and Figs. 6.2-9 to 6.2-12, exists because the vertical displacements of the bottom of the plate were measured by the LVDT up to a few steps before failure (shown in Fig. 6.2-29), and then removed to avoid its damage, whereas Figs. 6.2-9 to 6.2-12 give the load-displacement plots taken by the load and displacement transducers in the MTS machine. A few punching cones (failure surfaces) were cut out and examined, too, Figs.

6.2-27 and 6.2-28.

Cracking

As mentioned in section 5.3, the cracking of the plates was monitored (by naked eye) to obtain more information about the plate behaviour.

A typical case of cracking is given in sequential snapshots in Figs. 6.2-29. The first cracks appeared, as expected, on the bottom surface of the plate, under the perimeter of the loaded area (the region of maximum forces, i. e. moment and shear), Figs. 6.2-29 (2) to 6.2-29 (5), at loads varying from 13 to 27 percent of the maximum loads, Table 6.2-2. The plates cured in COE cracked at an average 23.12 percent, while the plates cured in LBE cracked at an average of 16 percent of the maximum loading, respectively. The first crack load was slightly improved by the fibres presence, as the results indicate, although the plates behaved similarly regardless of the fibres presence with respect to the cracking process.

More cracks occurred, starting from the central bottom region of the plate, under the loaded area, mainly as ramifications of the previous ones, developing along a narrow area in the direction of the diagonals; at the same time, radial cracks occurred, Fig. 6.2-29 (12). The cracks continued to develop in length in the

direction of the diagonals, Figs. 6.2-29 (14) to 6.2-29 (22), as the load was increased. At higher loading stages, the well defined cracked perimeter on the bottom of the plate, approximately under the perimeter of the loaded area, increased its width, with the cracks along diagonals developing even more in lengths and width, especially in the middle area of the plate, Figs. 6.2-29 (23) to 6.2-29 (29); the cracking pattern seemed to be identical with the cracking pattern shown in Fig. 4.2-3. The corners were lifted, at this moment, well above the support perimeter, consequently cracks were formed at the corners on the lateral surface of the plate as deep as the plate depth, forming the corner pivots. As the load increased, the cracks began to spread all over the bottom surface of the plate in radial directions; however, the existing cracking pattern was suggestive of a flexural yield mechanism, well defined in length and width (well developed diagonal cracks splitting in the corner region); up to the maximum (failure) loading, the existing cracking pattern did not change except that the widths of the cracks were continuously increasing, as the applied load increased. The whole plate bent such that it looked like a dinner plate. Eventually, the punching of the plate occurred, Fig. 6.2-29 (31), with an extended region being pushed downward (cone formed bodies, Figs. 6.2-27 and 6.2-28) and with the loaded area imprinted in the top surface of the plate, Figs. 6.2-13 (a), 6.2-14 (a), 6.2-16 (a), 6.2-19 (a), and 6.2-20 (a). Prior to punching, on the top surface of the plate, a circular crack

occurred - close to the supports region and cutting the corners - Figs. 6.2-13 (a), 6.2-14 (a), 6.2-16 (a), 6.2-19 (a), and 6.2-20 (a).

Modes of Failure

The three observed modes of failure are presented in Table 6.1-1 as: sudden punching - P1, ductile punching shear - FP1, and flexure-punching shear, for example FP4.

The punching failure occurred suddenly (P1) when the maximum load had been attained, just a few cracks in radial directions being present (not well developed in length and width) on the bottom surface of the plate; the loaded area punched through at the maximum load, forcing a cone formed body, Fig. 6.2-27, to separate from the plate. The extent of the base area of the cone formed body was reduced when fibres were present, Figs. 6.2-14 (b) vs. 6.2-19 (b), Figs. 6.2-16 (b) vs. 6.2-18, and Figs. 6.2-13 (b) vs. 6.2-17; see also Fig. 6.2-28 for FP1.

The sudden punching failure (present in P1) was changed into a ductile one, termed as ductile punching shear failure, by the reduction of the flexural reinforcement and the presence of vertical "stirrups" as shear reinforcement (P2), distributed as shown in Figs. 4.1-5 and 4.1-7 (a), or by the added fibres, distributed in the whole volume of the plate (FP1 and FP2). In

this case, the extent of the cracks on the bottom surface of the plate was about the same as in the first type of failure (sudden punching), with larger vertical displacements.

FP3, P4, FP4, P5, FP5, P6, FP6, P7 and FP7 failed in flexure-punching shear. The cracking occurred as already described, in the sub-section on "Cracking". In addition, a circle like crack occurred close to the maximum (failure) loads on the top surface of the plates, Figs. 6.2-13 (a), 6.2-14 (a), 6.2-16 (a), 6.2-19 (a) and 6.2-20 (a); these cracks, together with the cracked patterns on the bottom of the plates, lends the idea that the plates failed in flexure. At this moment, probably the "membrane effect" has been developed (it takes place after the yield lines are formed); due to this phenomenon, the load carrying capacity of the plates was increased [136]. The top surface crack occurred at 155.68 kN for P5, 182.37 kN for P6, and 173.47 kN for FP7, representing 97.22, 84.0 and 85.0 percent of the maximum loads, respectively. Eventually, the plates failed in punching. A few details after failure are given in Figs. 6.2-15 (b), 6.2-21, 6.2-23, 6.2-24, 6.2-25 and 6.2-26.

Experimentally Obtained Maximum Strength

Comparing two plates which failed in punching P1 and FP1 (Series 1), it seems that the fibres increased the maximum punching shear strength by 32 percent and changed the sudden type of failure

into a ductile one, see Table 6.1-1.

Reducing the flexural reinforcement of a plate without fibres by 40 percent, the plate strength decreased by 22 percent, but the mode of failure was changed into a ductile one, if shear reinforcement was provided (P1 vs. P2 with vertical "stirrups"); the plate with fibres, FP2, lost a surprisingly small 0.7 percent of punching shear strength of FP1, and also changed the mode of failure.

The addition of the inclined (bent up) bars as shear reinforcement for FP plates, decreased the shear capacity by almost 8.0 %, 14.86 %, and 20.0 % for LABE and by 14.84 % and 20.0 % for COE (FP2 vs. FP3, FP6, FP7, FP5 and FP5), respectively, but changed the failure mode from ductile punching shear to flexure-punching shear.

The change from the vertical "stirrups" to inclined (bent up) bars as shear reinforcement for P plates, increased the shear punching capacity of the plates by 13.89 % and 5.6 %, for LABE and by 2.8 % or maintain the same punching shear strength for COE (P2 vs. P6, P7, P4 and P5); the modes of failure were changed from ductile punching shear to flexure-punching shear.

The plates within each curing environment, LABE or COE, proved to have almost the same failure loads. The COE lowered the failure

loads of P plates, without affecting the FP plates. It seems that although the concrete itself became weak (P6 and P7 vs. P4 and P5) the fibres supplied the difference.

The variation of punching shear strength with age could be studied just for LABE (other parameters were kept the same). For P plates there is an increase of 13.88 % over a period of 64 days, and for FP plates a decrease of 7.5 % over a period of 56 days. The effect of increased compressive strength on punching shear strength is given in Fig. 6.2-30 (a) and (b).

It is important to include completely the coarse LA within the concrete mass, otherwise it seems that the LA is subjected to damage caused by COE; this effect was noticed only for one plate, Fig. 6.2-22.

The change in testing mode from controlled increasing load to controlled increasing deformation mode lowered the maximum loads with 7.5, 13.2, 7.5 and 13.2 percent (FP3 vs. FP4, FP5, FP6 and FP7).

Post-failure Behaviour

After the failure occurred, the loading of the plates was continued in the controlled increasing deformation mode of testing as far as was practical in the actual arrangement, i.e.,

as far as the displacement range of the actuator allowed, Figs. 6.2-9 to 6.2-12.

The ductility was determined as the ratio between the maximum loading displacement and ultimate displacement and the first crack load displacement, respectively. Up to the maximum and ultimate load displacements, the ductility was, almost in all the cases, greater for the FP plates, Table 6.2-4, columns 7 and 8.

The areas under the load-central deflection curves were computed and based on their values, the energy absorption capacity of the plates were determined. The results are presented in Table 6.2-4. The energy absorbed up to the maximum load and up to the ultimate load, is less for the P plates than for the FP plates, from 9.0 to 49.0 percent, and from 4.0 to 55.0 percent, respectively; this fact proves that the FP plates would withstand dynamic loads better than the P plates and preserve their structural integrity.

6.3. Computation of the Ultimate Loading of the Plates

The theories available for conventional reinforced concrete used to calculate the maximum (failure) load of the plates were presented in section 4.1, as they apply to this work. In this section, the necessary calculations were done using the actual (measured) material properties. The fibres addition,

materialized in the improved strength of the plates (see maximum load values and steel and concrete strains), was considered as a contributor to the plate capacity, too.

(a) Flexural Strength

Using Eqns. 15, 16, and 17 of section 4.1, the maximum flexural load was calculated for each plate; the results are listed in Table 6.3-1 (a) and (b). No major changes were done with respect to the theory presented in section 4.1, except that the actual concrete compressive strength and strains as determined on standard cylinders corresponding to each plate, and steel stresses (via stress-strain curves) replaced the design values in calculations. The calculated values listed in Table 6.3-1 (a) correspond to the maximum measured flexural steel strain values, while in Table 6.3-1 (b), the average measured flexural steel strain values (this approach was considered more appropriate to the real situation) were used. The calculations were carried out using the computer program shown in Appendix E - "Calculation of Flexural Strength".

Eqn. 16 gave the most appropriate results, Tables 6.3-1 (a) and (b), to the experimental ones; it gave good predictions of the maximum strength and mode of failure for the P plates but it was less precise for the FP plates. The values listed in Table 6.3-1 (b) are used for the shear strength of the plates computations.

(b) Punching Shear Strength

The punching strength values, as obtained using different methods presented in section 4.1, are given in Table 6.3-2. The main modification was done in Moe's Eqn., which has different forms for design and analysis (experimental checking). The fibres contribution was taken into account when it was necessary (FP plates), and if the theories provided for proper hypotheses. The calculations for P3, FP3, P4, FP4, P5, FP5, P6, FP6, P7, and FP7 were carried out using the second computer program - "Calculation of Shear Strength" - shown in Appendix E. A realistic value of the depth of the concrete compressive block has been used as determined in Appendix E, the first program. This second computer program gives the results for Eqns. 39 and 44 of Chapter 4. The angles of failure surfaces with the horizontal plane were taken as the average experimental ones: 30° and 40°, for LAC and SFRLAC respectively - see Figs. 6.2-27 and 6.2-28.

For the plates without shear reinforcement, except P2 (P1, FP1, P2 and FP2), Eqn. 25 overestimates the punching shear strength; even Eqn. 28 gives overestimates.

The Eqns. of the Code [114], i. e., Eqn. 30 (also Eqn. 36), were used to compute the punching shear strength of FP3, P4, FP4, P5, FP5, P6, FP6, P7 and FP7, using two assumptions: the limitations

imposed by the Clauses (11.3.6.3, 11.3.6.4 and 11.10.3.3) of the Code were applied or not, the results being listed in column 6, above or under the bar line respectively. In column 6, the results obtained using the modified Eqn. 39 (modified Moe's Eqn.) are listed. The Eqns. of the Code [114] underestimate the punching shear strength of the plates; more appropriate values to the experimental ones, are obtained when using Eqn. 44- especially for FP_i plates. Eqn. 39 gives overestimates. The steel contribution, V_s , has been calculated considering the same stress in all the bars of the shear head, though it had been measured just on one of the shear reinforcement bars. This could be too approximate because the steel contribution to the shear reinforcement of the plates is an important term and could change the results quite a bit.

(c) Computer code results

The computer code described in section 4.2 was used to analyse one plate (P4), with the discretization as shown in Fig. 6.3-1. This required changes in the original computer code. At the beginning, the concrete modulus of elasticity and compressive strength, steel tensile strength and modulus of elasticity employed, were those determined in the experimental tests; the computer code yielded results quite different from the expected values (high cracking and maximum loads at significantly lesser displacements as obtained in the test). Consequently, different

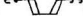
parameters were varied (Versions 1 to 4): the modulus of elasticity (20000.0 and 24000.0 MPa), the compressive strengths (from 34.5 to 55 MPa), and the loading. The steel parameters (tensile strength and modulus of elasticity) were maintained unchanged. Table 6.3-3 lists the maximum experimental load and the corresponding values as given by the computer code; also the steel stresses at cracking and ultimate loads as measured during the tests and as obtained using the computer code are presented in the same table. The displacement vs. load curves are presented in Fig. 6.3-2. A few observations are to be made:

- the computer code gave higher cracking and maximum loadings, but the deformability of the plate is well described;
- probably a different mesh size would influence the results given by the computer code; because of the excessive CPU time needed to run a FE program, the results were considered satisfactory.
- the accuracy with which the structural behaviour may be predicted by the computer code depends on the accuracy with which the elastic modulus was estimated, because E influences significantly the deformation of the structure, i.e., the deflections; the modulus of elasticity could be different for the plate (in bending) than as determined on cylinders (compression); however, the modulus of elasticity value has been given two values: 20000.0 and 24000.0 MPa;
- possible difference between the concrete compressive

strength of the plate and that one determined on cylinders could exist, therefore the values of the compressive strength were varied from 34.5 to 55 MPa, although the influence of the concrete compressive strength variation alone on the plates behaviour was not significant;

- the computer code prediction of the maximum load is higher than the experimental value, and
- keeping in mind that the results are subject to further possible improvements, the Finite Element Code is considered a convenient means for analyzing concrete plates.

Table 6.1-1 Synopsis of Experimental Results

Series	Plate	Fibre Volume %	Curing Environment	Reinforcement		Behaviour at Failure			Mode of Testing
				Flexural	Shear	Deflection (mm)	Failure Load (kN)	Mode of Failure	
1	2	3	4	5	6	7	8	9	10
I	P1	-	L	10 # 10	-	9.82	195.71	Sudden punching	Controlled
	FP1	.815			-	14.13	258.00	Ductile punching	
II	P2	-	B	6 # 10		20.21	160.13	Ductile punching	increasing loading
	FP2	.815			-	22.11	256.00	Ductile punching	
	P3	-	E			2.75	45.00	Accidental punching	Flexure-punching shear
	FP3	.815				22.50	235.74		
	P4	-	C			27.66	164.57	Controlled increasing deformation	
	FP4	.815				23.76	218.00		
	P5	-	E			27.12	160.13		
	FP5	.815				26.42	204.61		
	P6	-	L			32.06	182.37		
	FP6	.815				28.10	217.95		
	P7	-	B			26.31	169.02		
FP7	.815			26.43	204.61				

Accidental punching - sudden punching due to overloading of the plate - human error.

Table 6.1-2 Properties of Concrete Used for the Plates

Plate	Age (days)	Curing Environment	Fibres Content % by Volume	Air Content %	Slump (mm)	Concrete Unit Weight (Kg/m ³)	Compressive Strength (MPa)	Compressive Strain x10 ⁶	Splitting Tensile Strength (MPa)	Modulus of Elasticity (MPa)
1	2	3	4	5	6	7	8	9	10	11
P1	42		-	7.25	65.00	1873.0	47.00	2920	5.41	21278.0
FP1	44	L	.815	8.00	55.00	1931.0	44.00	2780	5.23	20089.0
P2	28	A	-	6.75	50.00	1959.0	40.28	2640	5.01	19954.0
FP2	32	B	.815	5.70	75.00	2031.0	38.70	2570	4.91	18963.0
P3	31	E	-	7.25	85.00	1853.0	40.70	2840	5.03	21253.0
FP3	30		.815	6.25	62.50	1959.0	39.21	3050	4.94	23955.0
P4	156	C	-	6.50	90.00	1807.0	55.00	2940	5.85	22624.0
FP4	154	O	.815	5.00	50.00	1858.0	53.23	2794	5.76	21353.0
P5	131	E	-	8.50	80.00	1815.0	53.72	2513	5.78	20970.0
FP5	125		.815	8.00	70.00	1831.0	57.56	2658	5.97	24009.0
P6	92	L	-	6.50	70.00	1791.0	50.56	2743	5.61	22651.0
FP6	86	A	.815	6.00	60.00	1873.0	51.22	3472	5.65	21735.0
P7	85	B	-	5.85	67.50	1796.0	53.42	3039	5.77	19025.0
FP7	84	E	.815	6.00	50.00	1866.0	49.24	3072	5.54	23433.0

Table 6.2-1 Measured Displacements, Loads and Strains

Plate	First Crack Loading, kN					Proximity of Ultimate Load				
	Load [kN]	Central Deflection [mm]	Corner Displacement [mm]	Concrete Strain $\times 10^6$	Steel Strain $\times 10^6$	Loading [kN]	Central Deflection [mm]	Corner Deflection [mm]	Concrete Strain $\times 10^6$	Steel Strain $\times 10^6$
1	2	3	4	5	6	7	8	9	10	11
P4	44.48	.63	.30	246	230	155.68	27.66	7.80	2598	10591
FP4	47.15	.33	.56	161	340	213.50	23.76	13.51	3000	19449
P5	35.58	.915	.43	287	331	155.68	27.12	8.00	2600	14549
FP5	44.48	1.26	.66	258	468	188.82	26.42	9.63	3945	19541
P6	31.32	1.82	.66	128	275	177.92	32.06	9.30	3157	18799
FP6	35.58	1.24	1.16	220	536	195.71	28.10	8.75	3866	21739
P7	22.24	1.13	1.20	60	165	164.58	26.31	9.54	2480	15906
FP7	35.58	1.38	0.77	196	295	191.26	26.43	8.20	3787	17874

Table 6.2-2 Details of Measured Loads and Strains

Plate	Curing Environment	First Crack Loading [kN]	Diagonal Cracking Loading, kN		Failure Load [kN]	Col. 2/5	Col. 3/5	Col. 4/5
			Concrete Strains	Steel Strains				
1	2	3	4	5	6	7	8	9
P6	L	31.32	156.27	141.26	182.37	.17	.86	.78
FP6	A	35.58	163.09	134.44	217.95	.16	.75	.62
P7	B	22.24	132.38	113.97	169.02	.13	.78	.67
FP7	E	35.58	112.26	161.74	204.61	.17	.68	.79
P4	C O E	44.48	149.44	144.68	164.57	.27	.73	.88
FP4		47.15	183.57	161.74	218.00	.22	.84	.74
P5		35.58	118.23	120.8	160.13	.22	.74	.75
FP5		44.48	156.27	137.85	204.61	.22	.76	.67

Table 6.2-3 Measured Loads, Deflections and Strains at Failure

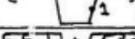
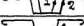
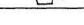
Plate	Curing Environment	Shear Steel Strain Gages	Behaviour at Failure		Steel Strains Microstrains $\times 10^6$	
			Deflection [mm]	Failure Load [kN]	1	2
					6	7
1	2	3	4	5	6	7
P4	C		27.66	164.57	1330	1600
FP4			23.76	218.00	10800	-
P5	E		27.12	160.13	1207	445
FP5			26.42	204.61	2190	-
P6	L		32.06	182.37	2024	1660
FP6			28.10	217.95	3903	-
P7	B		26.31	169.02	2303	429
FP7	E		26.43	204.61	799	-

Table 6.2-4: Salient Results Obtained from Experiments

Plate	Cracking Deflection (mm)	Maximum Load Deflection (mm)	Ultimate Deflection (mm)	Loading After Failure (kN)	Maximum Col. 1 Col. 2 Col. 3 Col. 4 Col. 5 Col. 6	Col. 1 Col. 2 Col. 3 Col. 4 Col. 5 Col. 6	Ultimate Ductility as Unity Loading for P7	Energy Absorption					
								Up to Max. Loading kN · m	Up to Ultimate kN · m	As Unity For P Plates up to Ultimate Load			
1	2	3	4	5	6	7	8	9	10	11	12	13	14
P6	1.82	42.61	50.63	134.25	182.37	23.41	33.31	.74	1.22	6.206	7.768	1.00	1.00
FP6	1.24	37.89	55.56	134.25	217.95	30.56	51.25	.61	1.88	6.783	8.061	1.09	1.04
P7	1.13	30.78	30.78	-	169.02	27.24	27.24	-	1.00	3.938	3.938	1.00	1.00
FP7	1.38	32.36	45.00	90.16	204.61	23.45	32.61	.44	1.22	5.240	6.115	1.33	1.55
P4	0.63	32.41	39.41	90.16	164.57	51.44	82.55	.54	2.30	3.844	4.489	1.00	1.00
FP4	.33	25.69	32.41	90.16	238.00	77.85	89.21	.41	3.60	4.509	5.177	1.16	1.15
P5	.42	52.00	40.00	90.16	160.13	32.79	43.71	.56	1.60	3.199	4.064	1.00	1.00
FP5	1.00	32.75	42.75	50.16	204.61	24.44	33.93	.44	1.24	4.765	5.684	1.49	1.40

Table 6.3-1 (a): Theoretical Predictions Using Measured Maximum Steel Strains

Plate	Failure Loading kN	Eqn. 15	Eqn. 16	Eqn. 17	Col 2 — 1	Col 3 — 1	Col 4 — 1
1	2	3	4	5	6	7	8
P4	164.57	193.29	189.23	203.29	1.17	1.15	1.23
FP4	218.00	268.32	262.69	282.20	1.23	1.21	1.29
P5	160.13	201.56	197.33	211.98	1.26	1.23	1.32
FP5	204.61	269.86	264.20	283.83	1.32	1.29	1.39
P6	182.37	202.50	198.25	212.98	1.11	1.09	1.17
FP6	217.95	267.83	262.21	281.69	1.23	1.20	1.29
P7	169.02	202.23	198.00	212.70	1.20	1.17	1.26
FP7	204.61	266.72	261.13	280.53	1.30	1.28	1.37

Table 6.3-1 (b): Theoretical Predictions Using Measured Average Steel Strains

P4	164.57	161.02	157.64	169.35	0.98	0.96	1.03
FP4	218.00	245.04	239.90	257.72	1.12	1.10	1.18
P5	160.13	189.53	185.55	199.34	1.18	1.16	1.24
FP5	204.61	269.86	264.20	283.83	1.32	1.29	1.39
P6	182.37	198.83	194.66	209.12	1.09	1.07	1.15
FP6	217.95	267.83	262.21	281.69	1.23	1.20	1.29
P7	169.02	191.82	187.80	201.75	1.13	1.11	1.19
FP7	204.61	250.11	244.36	263.05	1.22	1.20	1.29

Table 6.3-2: Computed Punching Strength Using Available Methods

Plate	Failure Loading (kN)	Eqn. 25	Eqn. 26	Eqn. 28	Eqn. 30	Eqn. 31	Eqn. 32	Eqn. 39	Col. $\frac{3}{2}$	Col. $\frac{4}{2}$	Col. $\frac{5}{2}$	Col. $\frac{6}{2}$	Col. $\frac{7}{2}$	Col. $\frac{8}{2}$	Col. $\frac{9}{2}$
1	2	3	4	5	6	7	8	9	10	11	12	13	14	15	16
P1	195.71	227.40	202.43	247.96	85.20	213.03	139.21	-	1.16	1.03	1.27	0.43	1.09	0.71	-
FP1	258.00	362.51	241.38	272.77	109.54	237.38	163.55	-	1.40	0.94	1.06	0.42	0.92	0.63	-
P2	160.13	-	-	-	120.60	-	-	140.16	-	-	-	0.75	-	-	0.87
FP2	256.00	317.69	221.50	237.32	103.76	221.56	128.71	-	1.24	0.86	0.93	0.40	0.87	0.50	-
			Eqn.36	-	Eqn.39	-	Eqn.44	-							
FP3	235.74	-	99.10	109.18	-	240.35	164.73	-	0.42	0.46	-	1.02	-	0.70	-
P4	164.57	-	140.85	151.69	-	238.25	192.50	-	0.86	0.92	-	1.45	-	1.17	-
FP4	218.00	-	115.47	116.83	-	259.48	166.59	-	0.53	0.54	-	1.19	-	0.76	-
P5	160.13	-	117.22	117.22	-	245.73	206.28	-	0.73	0.73	-	1.53	-	1.29	-
FP5	204.61	-	102.28	102.28	-	261.37	153.65	-	0.50	0.50	-	1.28	-	0.75	-
P6	182.37	-	135.05	150.00	-	240.98	222.27	-	0.74	0.82	-	1.32	-	1.22	-
FP6	217.95	-	113.27	114.54	-	265.05	171.45	-	0.52	0.53	-	1.22	-	0.79	-
P7	169.02	-	121.07	121.07	-	249.21	215.93	-	0.72	0.72	-	1.47	-	1.28	-
FP7	204.61	-	133.29	133.29	-	233.28	141.69	-	0.65	0.65	-	1.14	-	0.69	-

Table 6.3-3: Comparison of Experimental and Finite Element Analytical Values

	Version 1	Version 2	Version 3	Version 4	Experimental
Modulus of Elasticity, MPa	20,000.00	20,000.00	24,000.00	24,000.00	22,624.00
Compressive Strength, MPa	34.50	45.00	45.00	55.00	55.00
FEM Predicted Ultimate Load, kN	186.00	204.00	216.00	216.00	164.57
FEM Predicted Maximum Displacement, mm	29.60	28.40	34.00	36.00	27.66
FEM Cracking Load, kN	60.00	60.00	60.00	72.00	44.48
Concrete Stress during first crack (MPa)	11.07	10.73	11.06	13.33	5.60
Steel Stress at the above load, MPa	173.30	137.60	123.80	148.20	66.20
FEM Loading (Closer to Ultimate Load), kN	186.00	192.00	204.00	210.00	155.68
Concrete Stress at the above load, MPa	38.55	52.10	47.22	49.00	47.83
Steel Stress at the above load, MPa	722.60	664.50	794.50	826.70	696.22

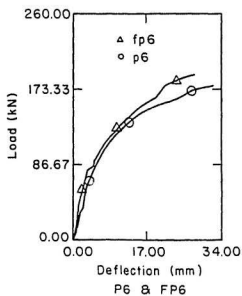
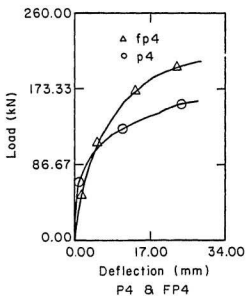
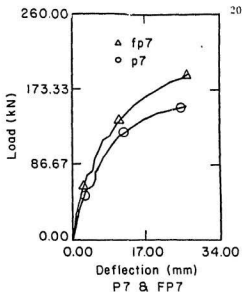
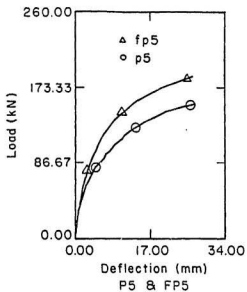


Fig. 6.2-1 Load - deflection curves

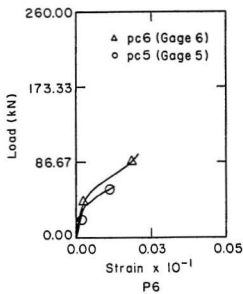
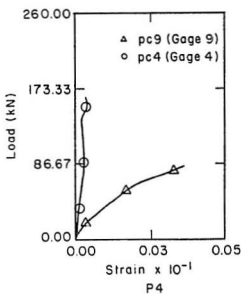
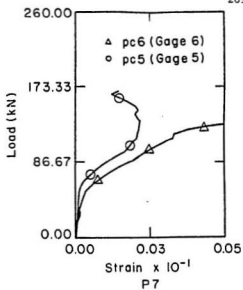
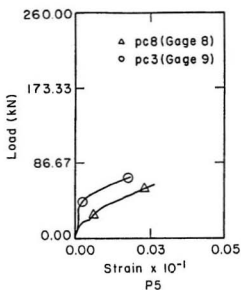


Fig. 6.2-2 Bottom concrete strains vs. load

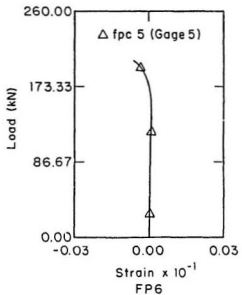
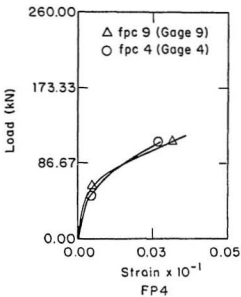
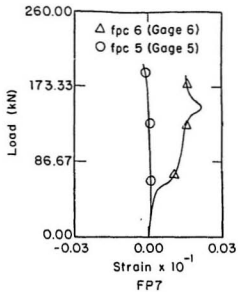
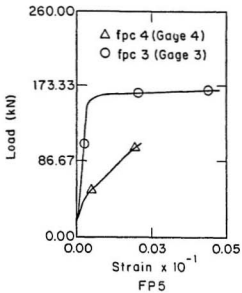


Fig. 6.2-3 Bottom plate concrete strain vs. load

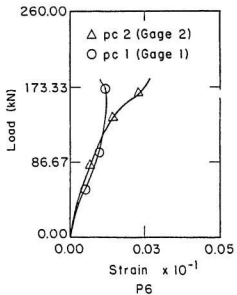
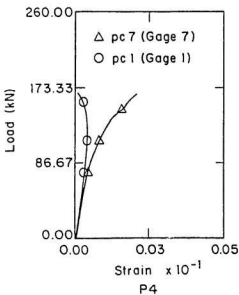
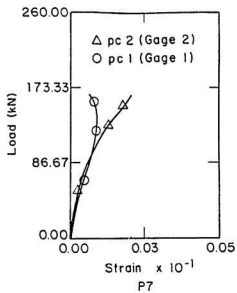
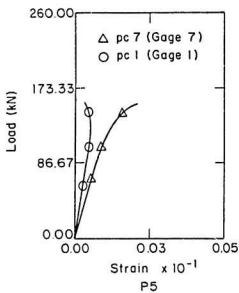


Fig. 6.2-4 Top plate concrete strains vs. load

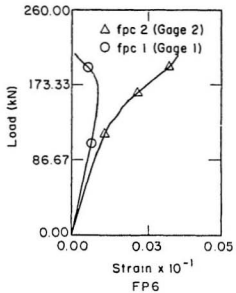
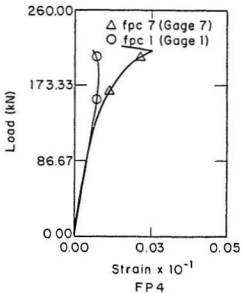
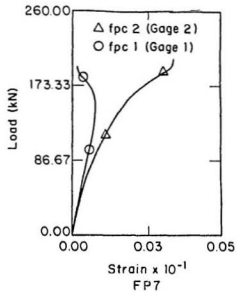
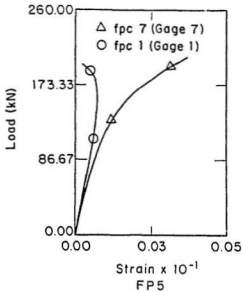


Fig. 6.2-5 Top plate concrete strain vs. load

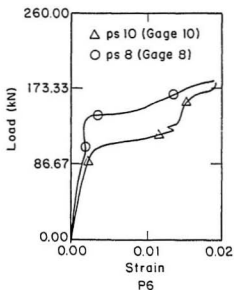
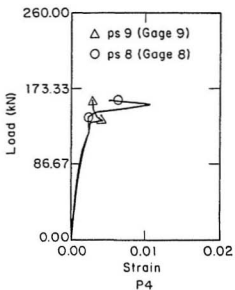
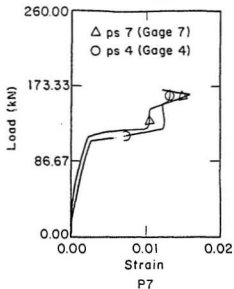
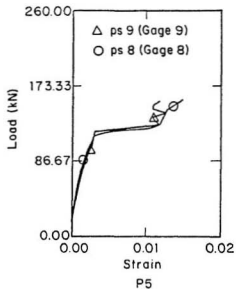


Fig. 6.2-6 Flexural steel strain vs. load

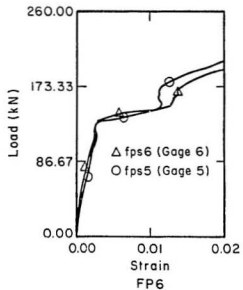
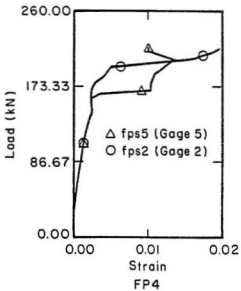
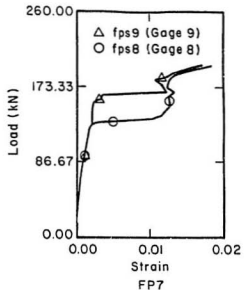
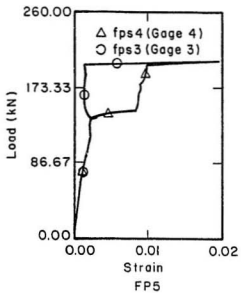


Fig. 6.2-7 Flexural steel strain vs. load

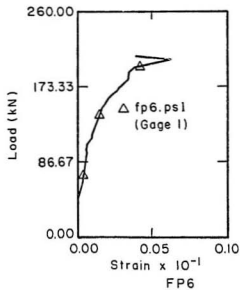
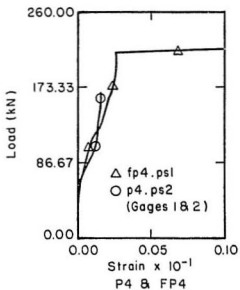
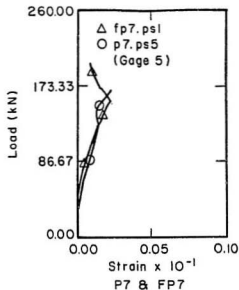
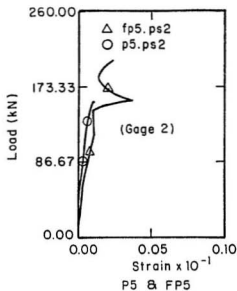


Fig. 6.2-8 Shear steel strain vs. load

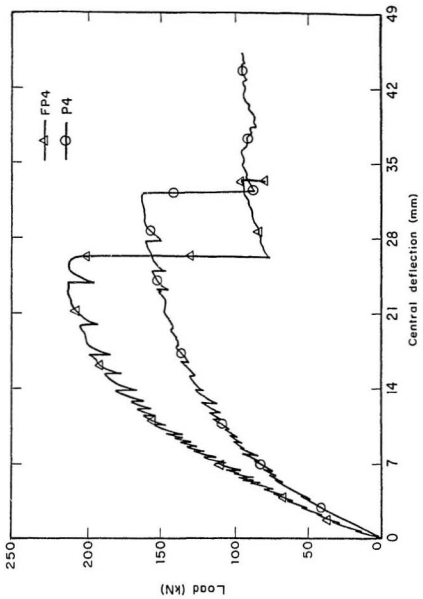


Fig. 6.2-9 Load - central deflection curves

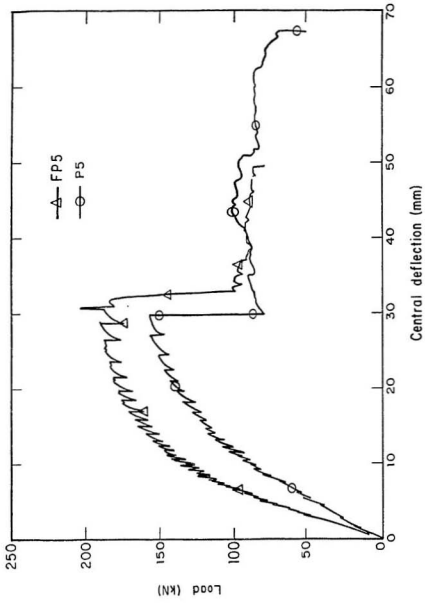


Fig. 6.2-10 Load - central deflection curves

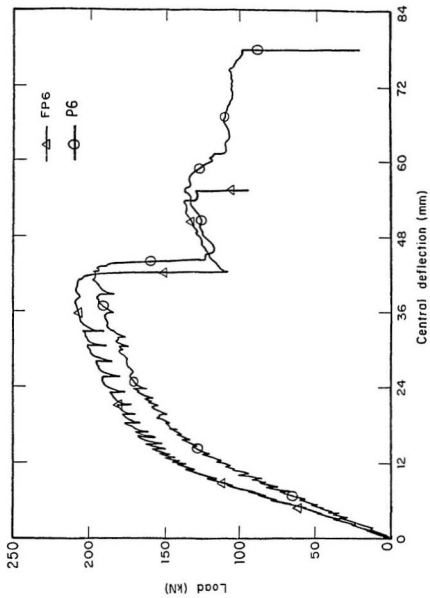


Fig. 6.2-11 Load - central deflection curves

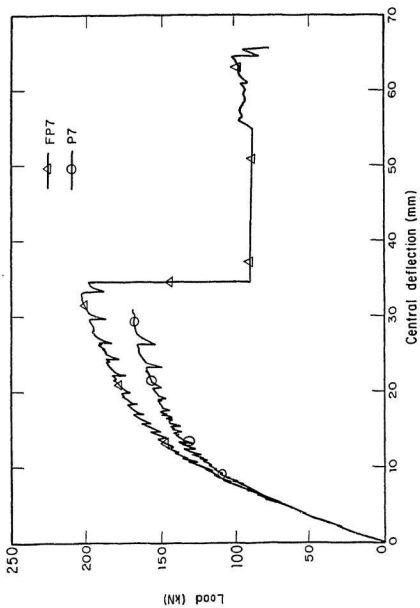


Fig. 6.2-12 Load - central deflection curves

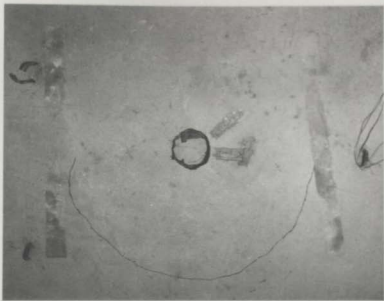


Fig. 6.2-13(a) Failure pattern P4: top surface

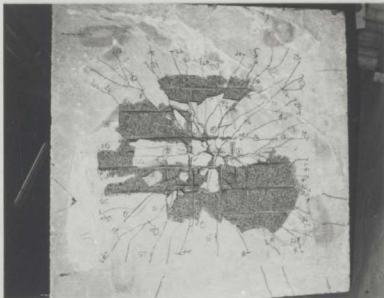


Fig. 6.2-13(b) Failure pattern P4: bottom surface



Fig. 6.2-14(a) Failure pattern P5: top surface

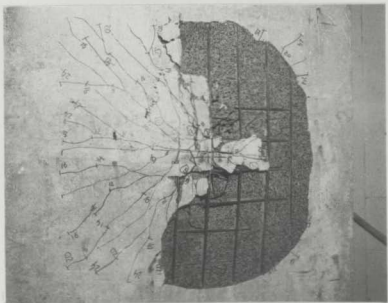


Fig. 6.2-14(b) Failure pattern P5: bottom surface

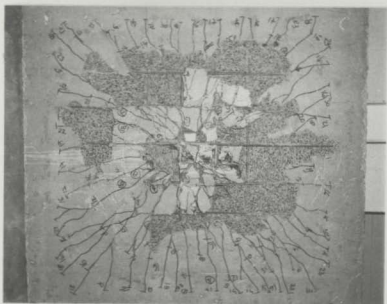


Fig. 6.2-15(a) Failure pattern P6: bottom surface



Fig. 6.2-15(b) Plate P6: bottom surface, failure detail

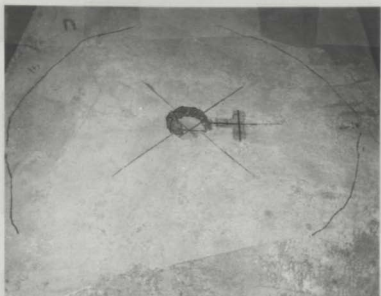


Fig. 6.2-16(a) Failure pattern P7: top surface

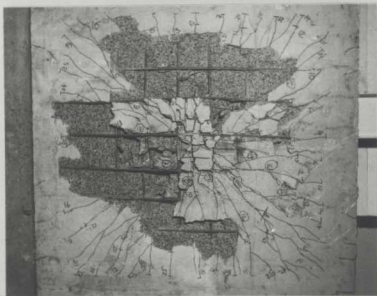


Fig. 6.2-16(b) Failure pattern P7: bottom surface

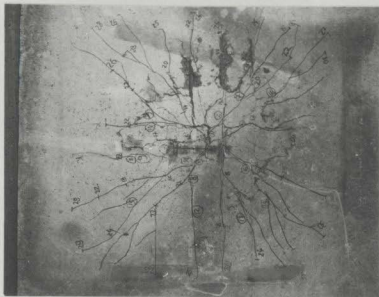


Fig. 6.2-17 Failure pattern FP4: bottom surface

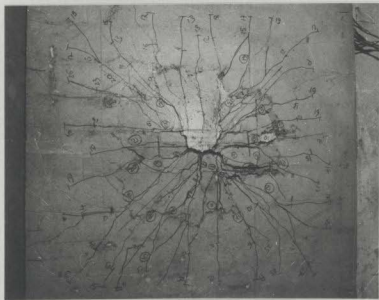


Fig. 6.2-18 Failure pattern FP6: bottom surface

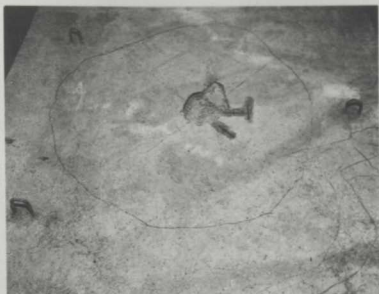


Fig. 6.2-19(a) Failure pattern FP5: top surface

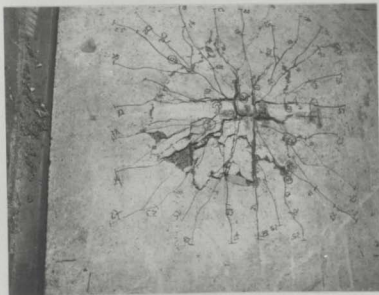


Fig. 6.2-19(b) Failure pattern FP5: bottom surface



Fig. 6.2-20(a) Failure pattern FP7: top surface

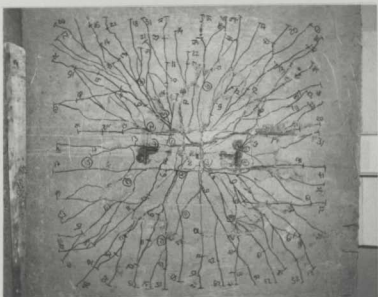


Fig. 6.2-20(b) Failure pattern FP7: bottom surface



Fig. 6.2-21 Plate P5: bottom surface, failure detail



Fig. 6.2-22 Plate P5: concrete surface exposed to COE



Fig. 6.2-23 Plate FP5: bottom surface, failure detail



Fig. 6.2-24 Plate FP6: bottom surface, failure detail

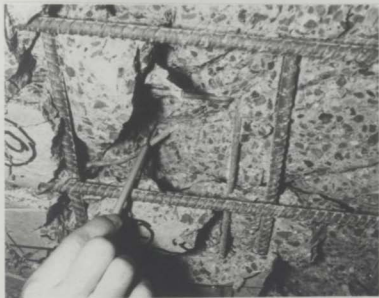


Fig. 6.2-25 Plate P7: bottom surface, failure detail

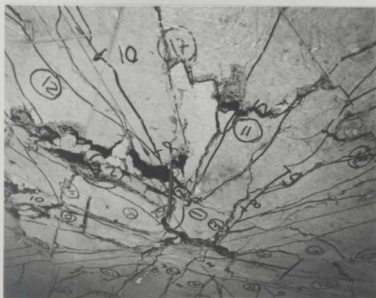


Fig. 6.2-26 Plate FP6: bottom surface, failure detail



Fig. 6.2-27 Plate without fibres: punching cone



Fig. 6.2-28 Plate with fibres: punching cone



Fig. 6.2-29(1) Plate FP7: before cracking



Fig. 6.2-29(2) Plate FP7: loading step no. 8



Fig. 6.2-29(3) Plate FP7: loading step no. 9



Fig. 6.2-29(4) Plate FP7: loading step no. 10



Fig. 6.2-29(5) Plate FP7: loading step no. 11



Fig. 6.2-29(6) Plate FP7: loading step no. 12



Fig. 6.2-29(7) Plate FP7: loading step no. 13



Fig. 6.2-29(8) Plate FP7: loading step no. 14



Fig. 6.2-29(9) Plate FP7: loading step no. 15



Fig. 6.2-29(10) Plate FP7: loading step no. 16



Fig. 6.2-29(11) Plate FP7: loading step no. 17



Fig. 6.2-29(12) Plate FP7: loading step no. 18



Fig. 6.2-29(13) Plate FP7: loading step no. 19



Fig. 6.2-29(14) Plate FP7: loading step no. 20



Fig. 6.2-29(15) Plate FP7: loading step no. 21



Fig. 6.2-29(16) Plate FP7: loading step no. 22



Fig. 6.2-29(17) Plate FP7: loading step no. 23



Fig. 6.2-29(18) Plate FP7: loading step no. 24



Fig. 6.2-29(19) Plate FP7: loading step no. 25



Fig. 6.2-29(20) Plate FP7: loading step no. 26



Fig. 6.2-29(21) Plate FP7: loading step no. 28



Fig. 6.2-29(22) Plate FP7: loading step no. 29



Fig. 6.2-29(23) Plate FP7: loading step no. 36



Fig. 6.2-29(24) Plate FP7: loading step no. 37



Fig. 6.2-29(25) Plate FP7: loading step no. 38



Fig. 6.2-29(26) Plate FP7: loading step no. 39



Fig. 6.2-29(27) Plate FP7: loading step no. 40



Fig. 6.2-29(28) Plate FP7: loading step no. 41



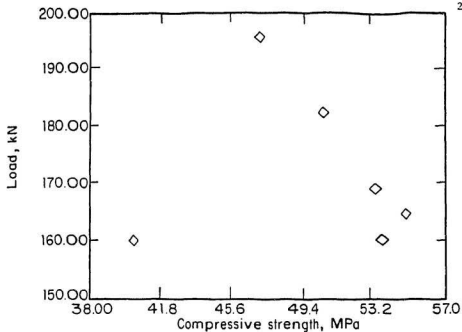
Fig. 6.2-29(29) Plate FP7: loading step no. 42



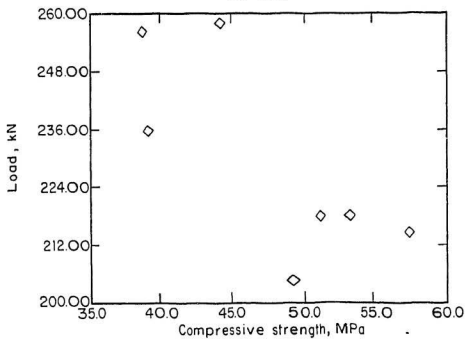
Fig. 6.2-29(30) Plate FP7: loading step no. 43



Fig. 6.2-29(31) Plate FP7: loading step no. 44



(a) LAC



(b) SFRLAC

Fig. 6.2-30 Failure load variation with the compressive strength

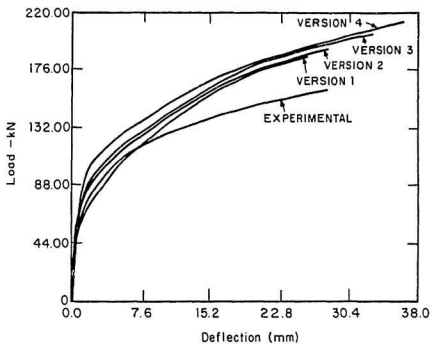


Fig. 6.3-2 FEM predicted vs. experimental load-deflection curves - P4

CHAPTER 7. CONCLUSIONS AND RECOMMENDATIONS

On the basis of the limited results of the experimental and theoretical studies carried out as a part of this thesis work, the following salient aspects have been noted. The study included investigations on the influence of steel fibres and expanded shale lightweight aggregate (coarse), MEL-lite, on the compressive and flexural strengths of the LAC and the load carrying and deformation characteristics of square concrete plates. The influence of the cold ocean environment on the strength and deformation characteristics were also investigated.

- (1) The Weight Method [101] used to proportion the mixture of LAC, using expanded lightweight shale aggregate (MEL-lite), as coarse lightweight aggregate, and the mixing method were reliable for this type of aggregate, yielding uniform rheological properties, close to the specified ones;
- (2) A volume of 0.815 % or 64 Kg/m³ steel collated fibres with deformed ends (hooked ends), Dramix 50/0.5, were properly incorporated in the expanded shale lightweight aggregate concrete, MEL-lite, as described in Chapter 2. The quantity of incorporated fibres was obtained by a trial-and-error method because the available studies did not help to determine it; the fibres were added to the LAC recipe, so

that the influence of the fibres could be thoroughly investigated. The time of mixing was chosen such that the fibres attained their maximum aspect ratio. Although the results given by inverted slump cone test (ISCT) are difficult to be interpreted, the method is recommended for future use, because of the ease with which it can be carried out;

- (3) Careful workmanship was required to compact SFRLAC in order to obtain the continuity and isotropy of the fibre-aggregate skeleton. Future research should develop standard methods for checking the uniformity and compacting of SFRC, including SFRLAC;
- (4) The 28-days air-dried unit weight of LAC and SFRLAC has been determined, using ASTM 567, as 1856 Kg/m³ and 1914 Kg/m³, respectively;
- (5) The compressive strength at 28-days of age of LAC and SFRLAC were determined as 47.73 MPa at 0.002560 to 0.002730 strains, when continuously immersed in water (except a maximum of 3-4 days required for capping), and as 45.57 MPa at 0.002600 to 0.002760 strains, when air-dried in laboratory. There is an increase in compressive strength with age, though no relationship was established. The maximum compressive strength was observed at 158 days of age

as 64.0 MPa for LAC and 62.56 MPa for SFRLAC in LABE, and 58.70 MPa for LAC and 60.38 MPa for SFRLAC in COE;

- (6) The uncontrolled fibres distribution and orientation, related to the mixing and compaction procedures, respectively, determined the variability and scatter of a few results, especially for MOR;
- (7) The fibres addition lowered slightly the compressive strengths for both environments, LABE or COE;
- (8) The fibres addition did not change the elastic limit of LAC;
- (9) The static secant (chord) modulus of elasticity in compression, E, had been determined using ASTM C 469; the E values ranged from around 20000.0 MPa to 24000.0 MPa, at all ages, but there is no well-defined development with respect to age as for the compressive strength;
- (10) The fibres addition created larger variability in E values for the SFRLAC subjected to COE than SFRLAC subjected to LABE;
- (11) The modulus of rupture (MOR) has been determined using ASTM C 78 for LAC and SFRLAC and ASTM C 1018 for SFRLAC. The MOR values computed as recommended in ASTM C 78 are higher for

SFRLAC than LAC, as they should be, though the remarks made in point (3), this chapter, are applicable; there was an increase of MOR values with respect to age both for LAC and SFRLAC regardless of the curing environment. At an increased strain rate of loading, the MOR values of SFRLAC did not change significantly;

- (12) The 72 hours absorption of SFRLAC in fresh water was found as 5.4 percent;

- (13) The flexural reinforcement reduction by 40 %, from Series I to Series II, decreased, as expected, the maximum load carrying capacity of the plates regardless of the presence of steel fibres and/or shear reinforcement. Within Series II, the shear reinforcement was changed to provide an effective punching shear strength of the plates. The inclined (bent-up) bars were more efficient than the vertical "stirrups" in providing punching shear strength, changing also the mode of failure from ductile punching shear to flexure-punching shear;

- (14) The fibres, used alone as shear reinforcement, increased or decreased (flexural reinforcement was reduced by 40 % in this case) the maximum load carried by the plate by 32 % or 0.8 %, respectively. It is assumed that the enhanced shear capacity was based on the reinforcing effect of the close

spaced fibres, and after the cracking occurrence, on the work required to debond, pull-out and overcome the shear-friction;

- (15) The use of steel fibres and shear steel bars (inclined bars) lowered the maximum load carried by the plate having just fibres (FP2) by an average of 15.54 % regardless of the curing environment. A change in the failure mode occurred too: from ductile- to flexure-punching shear;
- (16) At the same failure pattern, i. e., flexure-punching shear, the FP plates, having fibres and one row of inclined bars as shear reinforcement, attained higher maximum loads than the P plates - having two rows of inclined bars as shear reinforcement;
- (17) The addition of fibres alone changed the sudden punching failure to a ductile punching shear (Series I). When both fibres and inclined bars as shear reinforcement were used (FP plates), the ductile punching shear failure was changed into flexure-punching shear failure. The latter situation occurred also when two rows of inclined bars were used as shear reinforcement (P plates) vs. vertical "stirrups" (P2). Consequently, well detailed shear reinforcement can induce ductile flexural failures;

- (18) Based on the values of the first crack loads and on the load-deflection curves, it seems that the FP plates had greater stiffness compared with the P plates at all loading stages, much more so after cracking. The FP plates enhanced the cracking, deformation and strength behaviour;
- (19) At 0.815 percent fibre volume addition, the ductility with respect to maximum and ultimate loads are respectively increased by an average of 10.44 % and 27.17 %, compared with the plates without fibres;
- (20) The change in the testing mode, from controlled increasing load mode to controlled increasing deformation mode, provided for the estimations of the energy absorption capacity of the plates. At 0.815 percent fibre volume addition, the energy absorption capacity with respect to maximum load and up to ultimate load are respectively increased (characteristic of SFRLAC) by an average of 26.75 % and 28.50 %, compared to the plates without fibres;
- (21) The change in testing mode, as described in point 20, lowered the maximum loads carried by the plates;
- (22) The modified conventional reinforced concrete theory for bending or shear - the effect of fibre addition was included as a uniform tensile stress, σ_{cu} , and SFRLAC compressive

strength replaced the compressive strength of ordinary concrete - provided acceptable results for SFRLAC. This is in accordance with the provisions of ACI Committee 544 for SFRC design [137];

- (23) Recently, the ACI Committee 544 issued a report including a synopsis of the design considerations for SFRC [137]. The report gives a detailed review of the design applications for shear in beams; the concise review of the design applications for shear in plates or slabs does not recommend any precise method. One of the intents of this study was to supply a proposed method to compute the shear strength of LAC and SFRLAC plates, and check it against the full scale tests. The proposed Equations regarding the shear capacity of the plates underestimate the shear strength of the plates with fibres by an average 26.2 percent; for the plates without fibres, the proposed Equations give overestimates - an average of 24 percent;
- (24) The computer code [97] proved to be a useful, good and convenient tool for assessing the plate behaviour under load. It is also powerful in visualizing the displacement and stress fields all over the plate surface. The only constraint which arose was the CPU time required for the analysis. More appropriate predicted results could be provided by this program if the LAC and SFRLAC are properly

modelled - this being beyond the intent of this study. A future effort in this direction would be supplemented by the existing experimental results;

- (25) It seems that the COE lowered the failure loads of P plates and the steel strains, too;
- (26) Based on the properties observed in the tests and behaviour under COE, SFRLAC is found to be a suitable material for Arctic or sub-Arctic applications.

REFERENCES

1. Gerwick, B. C., "Prestressed Concrete Ocean Structures and Ships," Magazine of Concrete Research, Vol. 28, September 1976, p. 54
2. Fjeld, S. and Morley, C. T., "Offshore Concrete Structures," Handbook of Structural Concrete, Pitman Books Limited, 1983
3. ----, "Structural Lightweight-aggregate Concrete for Marine and Offshore Applications," Concrete Society Technical Report No. 16, The Concrete Society, May 1978.
4. Valenchon, C. P., Jardinier, R. C., Sparks, C. P. and Manesse, J. P., "The Concrete Floating Production Platform "Nekton 8000"," Proceedings of the Sixth International Symposium on Offshore Mechanics and Arctic Engineering, V 1., Houston, March 1-6, 1987, pp. 77-84
5. Kronen, H., Andersen, J. H., "Concrete Exposed to Cryogenic Temperature," Nordisk Betong, No. 6, 1982, pp. 13-16
6. Clarke, J., "Concrete Offshore Structures - the Next Ten Years," Concrete International, March 1983, pp.36-38
7. Hoff, G. C., "The Challenge of Offshore Concrete Structures," Concrete International, August 1985, pp. 12-22
8. Ozawa, A., Kato, M. and Unoki, K-I., "Development Study on a Hybrid-Type Guyed Tower with a Concrete Base," Offshore Technology Conference, Houston, Texas, April 27-30, 1987, pp. 485-494
9. Kobayashi, H., Hirakawa, S. and Suzuki, T., "Experimental Study on a New Type of Oil Production Platform," Offshore Technology Conference, Houston, Texas, April 27-30, 1987, pp. 465-473
10. Sparks, C. P., et al., "PLTB 1000, a Concrete Tension Leg Platform," Proceedings of the Fourth International Symposium on Offshore Mechanics and Arctic Engineering, V 1., Dallas, Feb. 17-22, 1985, pp. 14-21
11. Radjy, F. F. and Loeland, K. E., "Microsilica Concrete: Properties and Applications," Civil Engineering in the Arctic Offshore, Proceedings of the Conference Arctic '85, San Francisco, California, March 25-27, 1985, pp. 680-688
12. Neville, A. M., Properties of Concrete, John Willey & Sons,

New York, 1975

13. ACI Committee 357, "Guide for Design and Construction of Fixed Offshore Structures," ACI 357.R-84 Report, September 1985
14. Holm, T. A., "Performance of Structural Lightweight Concrete in a Marine Environment," ACI Publication SP-65, American Concrete Institute, Detroit, 1980, pp. 589-609
15. Federation Internationale de la Precontrainte, Manual of Lightweight Aggregate Concrete, Second Edition, John Wiley & Sons, 1983
16. Federation Internationale de la Precontrainte, "Design and Construction of Concrete Sea Structures," Fourth Edition, Telford, London, 1985
17. Tachibana, D., Imai, M. and Okada, T., "Qualities of High-Strength Lightweight Concrete Used for Construction of Arctic Offshore Platform," OMAE, Tokyo, 1986, pp. 361-367
18. Fagerlund, G., "Frost Resistance of Concrete with Porous Aggregate," CBI Forskning Research, 1978, p. 189
19. Litvin, A. and Fiorato, A. E., "A Lightweight Concrete for OTEC Cold Water Pipes," Concrete International, March 1981, pp. 48-55
20. Kong, F. K., Evans, R. H., Cohen, E. and Roll, F., "Fiber Reinforced Concrete," Handbook of Structural Concrete, McGraw-Hill Book Company, 1983
21. -----, "Concrete Island Towed to Arctic," Concrete International, March 1982, pp. 57-59
22. ACI Committee 213, "Guide for Structural Lightweight Aggregate Concrete," Reported by ACI Committee 213, ACI Manual of Concrete Practice, 1987, Vol. 1, p. 30
23. Bagon, C. and Frondistau-Yannas, S., "Marine Floating Concrete Made with Polystyrene Expanded Beads," Magazine of Concrete Research: Vol. 28, No. 97: December 1976, pp. 225-229
24. -----, "Lightweight Concrete," New Zealand Concrete Construction, Vol. 24, February 1980, pp. 5-12
25. Levi, F., Constantino, M., Perlazzene, Sonzogno, G. and Marioni, A., "Prestressed Concrete Floating Drydock with a Lifting Capacity of 100,000 t," Proceedings to the FIP Symposium - Concrete Sea Structures, Tbilisi, Sept. 1972,

pp. 31-35

26. Jensen, J. J., "Impact of Falling Loads on Submerged Concrete Structures," Proceedings of the International Symposium on Offshore Structures held at COPPE, Federal University of Rio de Janeiro, Brasil, October, Vol. 1, pp. 215-231
27. Carino, N., "Offshore Concrete Structures in the Arctic: Research Needs," US Department of Commerce, National Bureau of Standards, April 1984
28. ACI Committee 357, "State-of-the-Art Report on Offshore Concrete Structures for the Arctic," ACI 357.1R-85 Report, April 1986
29. Fitzpatrick, J. and Stenning, D. G., "Design and Construction of Tarsiut Island in the Canadian Beaufort Sea," Proceedings to Fifteenth Annual OTC, Houston, Texas, May 2-5, 1983, pp. 51-59
30. Gerwick, B. C., Construction of Offshore Structures, John Wiley & Sons, Inc., 1986
31. -----, "MAI - Mobile Arctic Island," Arctic Offshore Technology Conference and Exposition, Calgary, Alberta, Canada, November 6-9, 1984
32. Wetmore, S. B., Borchardt, D. R., "The Design, Construction and Deployment of A Concrete Island Drilling System The Glomar Beaufort Sea 1," Arctic Offshore Technology Conference and Exposition, Alberta, Calgary, November 6-9, 1984
33. Knudsen, A., Jakobsen, B., "Concrete Gravity Platforms for the Bering Sea," Arctic Offshore Technology Conference and Exposition, Calgary, October 28-31, 1986
34. -----, "Sonat Hybrid Arctic Drilling Structure - SHADS," Arctic Offshore Technology Conference and Exposition, Alberta, Calgary, November 6-9, 1984
35. American Petroleum Institute, API 2N, "Planning, Designing, and Constructing Fixed Offshore Structures in Ice Environments," Dallas, 1982
36. ACI Committee 318, "Building Code Requirements for Reinforced Concrete (ACI 318-83)," and "Commentary on Building Code Requirements for Reinforced Concrete (ACI 318M-83)," American Concrete Institute, Detroit, 1983
37. Kobayashi, K., "Development of Fibre Reinforced Concrete in

- Japan," *The International Journal of Cement and Composites and Lightweight Concrete*, Vol.5, No. 1, February 1983, pp. 27-40
38. ACI Committee 212, "Admixtures for Concrete," ACI 212.1R-81, ACI Manual of Concrete Practice, Vol. 1, 1987, p. 23
 39. Det Norske Veritas, "Rules for the Design, Construction and Inspection of Offshore Structures," Oslo, 1977, Reprint (1981), p. 67
 40. ----, "Concrete Sea Structures in Arctic Regions," Proceedings of the FIP/CPCI Symposia, Calgary, Canada, August 25-31, 1984
 41. RILEM Technical Committee 32-RCA, Subcommittee "Long-Time Studies", "Resistance of Concrete to Chemical Attacks, Seawater Attack on Concrete and Precautionary Measures," *Matériaux et Constructions*, Vol. 18, No. 105, 1985, pp. 223-226
 42. Mehta, K., "Durability of Concrete in Marine Environment-- A Review," *International Conference on Concrete in Marine Environment*, ACI Publication SP-65, Detroit, 1980, pp. 1-19
 43. Federation Internationale de la Precontrainte, "State of the Art Report - Special Concretes," May, 1982, p. 68
 44. Federation Internationale de la Precontrainte, "A State-of-the-Art Report from FIP: Thin-walled Concrete Units," *Concrete International*, March 1985, pp. 66-68
 45. Wells, R. A., "Future Developments in Fibre-Reinforced Cement, Mortar and Concrete," *Composites*, April 1982, pp. 169-172
 46. Barab, S. and Hanson, D., "Investigation of Fiber Reinforced Breakwater Armor Units," *International Symposium on Fiber Reinforced Concrete*, ACI Publication SP-44, Ottawa, 1973, pp. 415-434
 47. Kormeling, H. A., Reinhardt, H. W. and Shah, S. P., "Static and Fatigue Properties of Concrete Beams Reinforced With Continuous Bars and With Fibers," *Journal of the American Concrete Institute*, January-February, 1980, pp. 36-43
 48. Anderson, W. E., "Proposed Testing of Steel-Fibre Concrete to Minimize Unexpected Service Failures," *RILEM Symposium on Testing and Test Methods of Fibre Cement Composites (Sheffield, 1978)*, Construction Press, Lancaster, 1978, pp. 223-232

49. ACI Committee 544, "Guide for Specifying, Mixing, Placing, and Finishing Steel Fiber Reinforced Concrete," Report No. ACI 544.3R-84, ACI Journal, March-April 1984, pp. 140-147
50. Jamroz, Z., "Lightweight Aggregate Concrete with Steel Fibre Admixture," Proceedings, RILEM Symposium on Testing and Test Methods of Fibre Cement Composites (Sheffield 1978), Construction Press, Lancaster, 1978, p. 121-127
51. Ritchie, A. G. B. and Al Kayyali, O. A., "The Effects of Fibre Reinforcement on Lightweight Aggregate Concretes," RILEM Symposium on Fibre Reinforced Cement and Concrete (September 1975), Construction Press, Lancaster, V.1, 1976, pp. 247-256
52. Swamy, R. N., Mangat, P. S. and Rao, C. V. S. K., "The Mechanisms of Fiber Reinforced of Cement Matrices," International Symposium on Fiber Reinforced Concrete, ACI Publication SP-44, American Concrete Institute, Detroit, 1974, pp. 1-28
53. Kobayashi, K. and Cho, R., "Flexural Characteristics of Steel Fibre and Polyethylene Fibre Hybrid-Reinforced Concrete," Composites, April 1982, pp. 164-168
54. Ramakrishnan, V., Coyle, W. V., Kulandaisamy, V. and Schrader, E. K., "Performance Characteristics of Fiber Reinforced Concrete with Low Fiber Contents," Journal of the American Concrete Institute, September-October 1981, pp. 388-394
55. Gopalaratnam, V. S. and Shah, S. P., "Properties of Steel Fiber Reinforced Concrete Subjected to Impact Loading," Journal of the American Concrete Institute, January-February 1986, pp. 117-126
56. ACI Committee 544, "State-of-the-Art Report on Fiber Reinforced Concrete," Report No. ACI 544.1R-82, Concrete International, May 1982, pp. 9-30
57. Edgington J., Hannant, D. J. and Williams, R. I. T., "Steel Fibre Reinforced Concrete," Current Paper No. CP 69/74, Building Research Establishment, Garston, Watford, 1974, p. 17
58. Proceedings, RILEM Symposium on Fiber Reinforced Cement and Concrete (September 1975), Construction Press, Lancaster, 1976
59. Proceedings, RILEM Symposium on Testing and Test Methods of Fibre Cement Composites (Sheffield 1978), Construction Press, Lancaster, 1978, p. 545

60. Hannant, D. J., *Fibre Cements and Fibre Concretes*, John Wiley & Sons, New York, 1978
61. Hibbert, A. P., "Impact Resistance of Fiber Concrete," Ph. D. Thesis, University of Surrey, Department of Civil Engineering, Guilford, UK, July 1979, p. 261
62. Hoff, G. C. (Editor), *Fiber Reinforced Concrete-International Symposium*, ACI Publication SP-81, American Concrete Institute, Detroit, 1984
63. Knoblauch, H., "Manufacture and Properties of SFRC and Mortar with Increasing Fiber Content," *Betonwerken und Fertigteil-Technik*, Heft 10, 1979, pp. 588-594
64. Patton, M. E. and Whitaker, W. L., "Effects of Fiber Content and Damaging Load on Steel Fiber Reinforced Concrete Stiffness," *Journal of the American Concrete Institute*, January-February 1983, pp. 13-16
65. Hibbert, A. P. and Hannant, D. J., "Toughness of Fibre Cement Composites," *Composites*, April 1982, pp. 105-111
66. ACI Committee 544, "Measurement of Properties of Fiber Reinforced Concrete," ACI Report No. 544.2R-78 (revised 1983), *Fibre Reinforced Concrete - International Symposium*, ACI Publication SP-81, Detroit, 1984, pp. 433-439
67. Raouf, Z. A. and Hussain, A. A., "Technical Notes: Some Properties of Steel Fibre Concrete at Early Ages," *The International Journal of Cement and Composites and Lightweight Concrete*, Vol. 6, No. 2, May 1984, pp. 117-121
68. Raju, N. K., Basarajiah, B. S. and Rao, K. J., "Compressive Strength and Bearing Strength of Steel Fibre Reinforced Concrete," *Indian Concrete Journal*, June 1977, pp. 183-188
69. Swamy, R. N. and Jojagha, A. H., "Impact Resistance of Steel Fibre Reinforced Lightweight Concrete," *The International Journal of Cement Composites and Lightweight Concrete*, Volume 4, Number 4, November 1982, pp. 209-220
70. Schrader, E. K., "Impact Resistance and Test Procedure for Concrete" *Journal of the American Concrete Institute*, March-April 1981, pp. 141-146
71. Balaguru, P. N. and Ramakrishnan, "Freeze-Thaw Durability of Fiber Reinforced Concrete," *Journal of the American Concrete Institute*, May-June 1986, pp. 374-382
72. Liu, T. C. and McDonald, J. E., "Abrasion-Erosion Resistance

- of Fiber-Reinforced Concrete," Cement, Concrete, and Aggregates, CCAGDP, Vol. 3, No. 2, Winter 1981, pp. 93-100
73. Schupack, M., "Durability of SFRC Exposed to Severe Environments," Steel Fiber Concrete US-Sweden Joint Seminar, Swedish Cement and Concrete Research Institute, Stockholm, 1985, pp. 479-496
 74. Lankard, D. R. and Walker, A. J., "Status Report on Laboratory and Field Investigations of the Durability of Wire and Concrete Exposed to Various Service Environments," Battelle Development Corporation, June 1978, p. 26
 75. -----, "Long Term Saltwater Corrosion Test of Fibrous Concrete Beams," Australian Wire Industries PTY. Ltd., May 1981, p. 4
 76. Hannant, D. J. and Edgington, J., "Durability of Steel Fiber Reinforced Concrete," RILEM Symposium on Fibre Reinforced Cement and Concrete (September 1975), Construction Press, Lancaster, V.1, 1976, pp. 159-169
 77. Mangat, P. S. and Guruswamy, K., "Steel Fibre Reinforced Concrete for Marine Applications," Behaviour of Offshore Structures, Elsevier Science Publishers B. V., Amsterdam, 1985, pp. 867-879
 78. Schrader, E. K., "Material Properties (Mixing, Transportation, Handling, Finishing) Specifications Mix Design", 1979 World of Concrete, Session B-16 Fibrous Concrete, p. 27
 79. Zollo, R. F., "Fibrous Concrete Flexural Testing-Developing Standardized Techniques," Journal of the American Concrete Institute, September-October 1980, pp. 363-368
 80. Cabrera, J. G. and Wooley, G. R., "A Study of Twentyfive Years Old Pulverized Fuel Ash Concrete Used in Foundation Structures," Proceedings, Institution of Civil Engineers, Part 2, 79, March 1985, pp.149-165
 81. Swamy, R. N. and Jojagha, A. H., "Workability of Steel Fibre Reinforced Lightweight Aggregate Concrete," The International Journal of Cement Composites and Lightweight Concrete, Volume 4, Number 2, pp. 103-109
 82. Swamy, R. N. and Lankard, D. R., "Some Practical Applications of Steel Fibre Reinforced Concrete," Proceedings, Institution of Civil Engineers, Part 1, 56, August 1974, pp. 235-256
 83. Pomeroy, C. D., "An Assessment of the Commercial Prospects

- for Fibre-and Polymer-modified Concretes," Magazine of Concrete Research: Vol. 28, No. 96: September 1976, pp. 121-130
84. Craig, R. J., "Structural Applications of Reinforced Fibrous Concrete," Concrete International, December 1984, pp. 28-32
 85. Vanderberghe, M. P. and Nemegeer, D. E., "Industrial Flooring with Steel Fiber Reinforced Concrete," Concrete International, March 1985, pp. 54-57
 86. Jamrozy, Z. and Swamy, R. N., "Use of Steel Fibre Reinforcement for Impact Resistance and Machinery Foundations," The International Journal of Cement and Composites and Lightweight Concrete, Vol. 1, No. 2, pp. 65-75
 87. Henager, C. H., "Steel Fibrous Ductile Concrete Joint for Seismic Resistant Structures," Symposium on Reinforced Concrete Structures in Seismic Zones, ACI Publication SP-53, 1974 ACI Annual Convention, pp. 371-386
 88. Roberts, T. M. and Ho, N. L., "Shear Failure of Deep Fibre Reinforced Concrete Beams," The International Journal of Cement Composites and Lightweight Concrete, Volume 4, Number 3, August 1982, pp. 145-152
 89. Nielsen, M. P., Braestrup, M. W., Jensen, B. C. and Bach, F., "Concrete Plasticity, Beam Shear - Shear in Joints-Punching Shear," Danish Society for Structural Science and Engineering Special Publication, Technical University of Denmark, Copenhagen, October 1978, p. 129
 90. Swamy, R. N. and Al-Ta'an, S. A., "Deformation and Ultimate Strength in Flexure of Reinforced Concrete Beams Made with Steel Fibre Concrete," Journal of the American Concrete Institute, Vol. 78, No. 5, September-October 1981, pp. 395-405
 91. Swamy, R. N., "Steel Fibre Concrete for Bridge Deck and Building Floor Applications," The Structural Engineer, Vol. 64A, No. 6, June 1986, pp. 149-157
 92. Ghalib, M. A., "Moment Capacity of Steel Fiber Reinforced Small Concrete Slabs," Journal of the American Concrete Institute, July-August 1980, pp. 247-257
 93. Swamy, R. N. and Brian, K., "Some Practical Structural Applications of Steel Fiber Reinforced Concrete," ACI Publication SP-44, International Symposium on Fiber Reinforced Concrete, Ottawa, 1973, pp. 319-336

94. Hannant, D. J., "Steel Fibers and Lightweight Beams," The Journal of the Concrete Society, Vol. 6, No. 8, August 1972, pp. 39-40
95. Paillère, A. M. and Serrano, J. J., "Use of Metal Fibres in Lightweight Aggregate Concrete," RILEM Symposium on Testing and Test Methods of Fibre Cement Composites (Sheffield 1978), Construction Press, Lancaster, 1978, pp. 205-222
96. Nemegeer, D., "Flexural Strength of Lightweight Concrete Reinforced with Steel Wire Fibres," Dramix Project, N. V. Bekaert S. A., Zwevegem, August 1977, p. 7
97. Hinton, E. and Owen, D. R. J., Finite Element Software for Plates and Shells, Pineridge Press Limited, Swansea, UK, 1984
98. Petroleum Directorate, "Offshore Installations: Guidance on Design and Construction," Regulatory Provisions, Petroleum Directorate, Government of Newfoundland and Labrador, St. John's, Newfoundland, 1982
99. MEL-lite, Leaflet supplied by Avon Aggregates Limited, New Brunswick, 1985
100. Pfeifer, D. W., "Sand Replacement in Structural Lightweight Concrete - Freezing and Thawing Tests," Journal of the American Concrete Institute, Nov. 1967, pp. 735-743
101. ACI Committee 211, "Standard Practice for Selecting Proportions for Structural Lightweight Aggregate Concrete" ACI 211.2-81, ACI Manual of Concrete Practice, Vol. 1, 1987, p. 18
102. Gröbl, P., "Mix Design of Lightweight Aggregate Concrete for Structural Purposes," International Journal of Lightweight Concrete, Vol. 1, No. 2, 1979, pp. 63-69
103. Stefanescu-Goanga, A., Incercarile mortarului, betonului si materialelor componente, Editura Tehnica, Bucuresti, 1983
104. Drinkgern, G., "Particle Strength of Lightweight Aggregate Conforming to DIN 4226," Betonwerk und Fertigteil-Technik, Heft 6/81, pp. 349-353
105. Kothari, N. C. and Bonel, E. A., "Strength Properties of Concrete Reinforced with Epoxy-Coated Steel Fibers," Journal of the American Concrete Institute, October 1978, pp. 550-553
106. Hughes, B. P. and Fattuhi, N. I., "Fibre Bond Strengths in Cement and Concrete," Magazine of Concrete Research: Vol.



